Performing in-cylinder heat flux measurements for HCCI combustion

Leroy de Ruijsscher, Anthony Eelbode

Supervisors: Prof. dr. ir. Sebastian Verhelst, Prof. dr. ir. Michel De Paepe
Counsellor: Ir. Stijn Broekaert

Master's dissertation submitted in order to obtain the academic degree of
Master of Science in Electromechanical Engineering

Department of Flow, Heat and Combustion Mechanics
Chairman: Prof. dr. ir. Jan Vierendeels
Faculty of Engineering and Architecture
Academic year 2013-2014

UNIVERSITEIT GENT

Performing in-cylinder heat flux measurements for HCCI combustion

Leroy de Ruijsscher, Anthony Eelbode

Supervisors: Prof. dr. ir. Sebastian Verhelst, Prof. dr. ir. Michel De Paepe
Counsellor: Ir. Stijn Broekaert

Master's dissertation submitted in order to obtain the academic degree of
Master of Science in Electromechanical Engineering

Department of Flow, Heat and Combustion Mechanics
Chairman: Prof. dr. ir. Jan Vierendeels
Faculty of Engineering and Architecture
Academic year 2013-2014

UNIVERSITEIT GENT

Ghent, 2nd of June 2014

The authors

Leroy de Ruijsscher Anthony Eelbode

Preface

As two real petrolheads there was no doubt about the subject of our master's dissertation. Since we are both passionate about cars and everything around it, it was clear that we would chose a thesis involving internal combustion engines. It was a pleasure for us to do research on something we both are passionate about. For this reason we would like to thank our supervisors prof. dr. ir. S. Verhelst and prof. dr. ir. M. De Paepe. They gave us the opportunity to perform this research. We would like to thank prof. dr. ir. S. Verhelst in particular for the regular follow-up and advice, which really gave direction to our thesis.

In particular, we would like to thank our counsellors ir. S. Broekaert and ir. T. De Cuyper for the time and effort they have devoted to us and for the pleasant chats in between the moments of work. Whenever we had a question or a problem, they helped us immediately with answers and advice. Especially the help concerning the TFG sensor is very much appreciated.

Next, we would also like to thank K. Chielens for all the time and work he put into our engine setup, and for all the times we stood in his office with a question to fix a problem. Also the restoration of the fuel cabinet is very much appreciated. In addition, we also like to thank P. De Pue for the fusebox and controllers he installed on our engine setup and all the times we asked for his help.

Further, we thank our fellow students for the support, funny moments and time we spent together. Also our girlfriends, parents and friends, we thank for their support and for giving us the courage to successfully complete this thesis.

Finally we would like to thank each other for the intense, smooth and efficient cooperation, but also for the unforgettable and joyful moments we spent together in this fascinating year.

Leroy de Ruijsscher and Anthony Eelbode

Performing in-cylinder heat flux measurements for HCCI combustion

by

Leroy de Ruijsscher and Anthony Eelbode

Supervisors: prof. dr. ir. Sebastian Verhelst, prof. dr. ir. Michel De Paepe

Counsellor: ir. Stijn Broekaert

Master's dissertation submitted in order to obtain the academic degree of

Master of Science in Electromechanical Engineering

Department of Flow, Heat and Combustion Mechanics

Chairman: Prof. dr. ir. Jan Vierendeels

Faculty of Engineering and Architecture

Ghent University

Academic year 2013-2014

Summary

In this thesis a study on the HCCI combustion process is performed. The lack of knowledge to control the start of combustion demands for a software tool that encompasses all the characteristics of HCCI combustion. In that regard, heat flux measurements are a key in the development of a successful heat transfer model. This thesis contributes for a small part to this research. Chapter 2 includes a discussion on the principles of HCCI, the benefits and drawbacks, the various parameters that influence HCCI combustion and some recent developments. Chapter 3 describes the adaptations we made to the CFR engine setup. In chapter 4 the principle and usefulness of a heat release analysis is explained. In the final chapter, the results are given. These include the methodology of achieving the first HCCI measurement, a discussion on the influence of different engine parameters, the determination of the load and temperature limits of the setup and finally a comparison of the heat flux measurements with existing heat transfer correlations.

Keywords

Homogeneous Charge Compression Ignition, Heat transfer, *Thin Film Gauge* sensor, Heat release analysis

Performing in-cylinder heat flux measurements for HCCI combustion

Leroy de Ruijsscher and Anthony Eelbode

Supervisor(s): Sebastian Verhelst, Michel De Paepe and Stijn Broekaert

Abstract—**Homogeneous Charge Compression Ignition (HCCI) combustion can be described as the controlled auto-ignition of a lean mixture. Since the start of combustion is strongly dependent on chemical kinetics [7], the in-cylinder thermal conditions dictate the characteristics of the combustion. Heat flux to the cylinder walls has a large influence on the thermal conditions. Understanding the effects of wall heat fluxes on the combustion timing, is an essential step in fully controlling and understanding HCCI combustion. Existing heat transfer correlations have already been constructed for Spark Ignition (SI) and Compression Ignition (CI) engines. Their use on HCCI engines has not been fully proven. The heat transfer correlations of *Woschni* [1], *Annand* [2], *Assanis* [3] and *Hohenberg* [4] are tested for HCCI combustion on a single cylinder CFR engine. The results are compared with heat flux measurements, done with a single-layer Thin Film Gauge sensor.**

Keywords—**CFR engine, HCCI, auto-ignition, heat flux, thin film gauge, heat transfer correlation**

I. Introduction

TODAY , automotive industry must face the severe requirements to develop clean technologies in order to achieve a lower fuel consumption and cleaner exhaust emissions for green house gas reduction and ambient air quality improvement. The last couple of years an old combustion technique is being reinvented and reconsidered in this regard. The principle of HCCI combustion is already known for decades. It was first introduced by *Onishi et al.* [5] in 1979. HCCI can be seen as a combination of SI (Spark Ignition) and CI (Compression Ignition) engine principles. As in SI engines, a homogeneous mixture of air and fuel (and exhaust gases if Exhaust Gas Recirculation (EGR) is applied) is brought into the combustion chamber. As in CI engines, the mixture is exposed to high enough temperatures and pressures for auto-ignition to occur. The combination of both types of combustion methods makes it possible to combine the benefits of both. Diesel-like efficiencies and low to zero emissions of soot and NO_X are the result. On the other hand, relatively high CO and HC emissions, a limited operating range and above all the control of the start of combustion (SOC) are challenging problems which prohibit the HCCI concept to be commercialized. The idea of HCCI has been pushed to the background at the time, since no real breakthrough was ever made. Because of the recent advent of electronic sensors and controls and driven by cleaner technology requirements, HCCI has become again a matter of interest. HCCI combustion is achieved by controlling the temperature, pressure and air-to-fuel ratio for auto-ignition to occur. This is far more challenging than the control of classic SI or CI engines. Thanks to new technology this challenge is reconsidered.

Research over the last three decades has shown the great potential of HCCI for achieving high efficiencies and low emissions. Most publications on HCCI present only experimental results. Researchers have been mainly focusing on the effect of different kinds of parameters like compression ratio, inlet temperature, air-to-fuel ratio and use of EGR. Their experimental results give a better understanding of the combustion process of HCCI and their influence on the start of combustion, but still there is no consensus on how to control the start of combustion in the right way. The variety of parameters that can be changed, make it hard to design and optimize a control strategy. Simulation software could offer a breakthrough in this regard. Today, simulation software is used that is designed for classical SI and CI engines. In these models fluid dynamics play an important role because of the flame propagation and in-cylinder injection phenomena that needs to be taken into account. Research has revealed that these models do not fully meet the HCCI concept [6]. *Najt and Foster* [7] showed that the response of the HCCI combustion process to changes in operating parameters can be explained in terms of known chemical kinetics. An HCCI model is therefore needed. Chemical kinetics are mainly influenced by the concentration of the reactants and the temperature. The temperature is dependent on the cylinder wall heat transfer. Consequently, a good heat transfer model is an essential part of developing an HCCI simulation tool.

Using a single-layer Thin Film Gauge sensor, heat flux measurements are performed on a single cylinder CFR engine. The heat flux correlations of *Annand*, *Woschni*, *Assanis* and *Hohenberg* are compared with these heat flux measurements.

II. Correlations

THE heat flux correlations of *Annand*, *Woschni* and *Hohenberg* are originally designed for SI and CI engines, but are also proposed for HCCI engines by several researchers [6], [3]. The heat flux correlation of *Assanis* is a modified version of the *Woschni* correlation, that is fitted on his heat flux measurements for HCCI combustion. In what follows, these correlations will be evaluated for HCCI combustion in a CFR engine using a single-layer TFG heat flux sensor. All the mentioned heat flux correlations use the Reynolds analogy:

$$Nu = \frac{h_c \cdot L}{k} = aRe^b Pr^c \tag{1}$$

The *Annand* correlation is a direct expression of equation 1. For the correlations of *Woschni*, *Assanis* and *Hohenberg* assumptions are made concerning the gas properties in order to calculate the convection coefficient as a function of only the cylinder bore, the characteristic velocity, the cylinder pressure and temperature. Equation 1 can then be transformed to equation 2 for the convection coefficient:

$$h_c(t) = \alpha_s L(t)^{-j} P(t)^k T(t)^{-l} v(t)^m \tag{2}$$

The correlations only differ in exponents (j, k, l and m), the characteristic length L and the characteristic velocity v. To cal-

culate the convection coefficient, only the pressure needs to be measured. The other parameters can be derived from the engine geometry or are predefined.

III. Results

In figure 1 the measured wall heat flux and the calculated wall heat flux from the correlations is shown as a function of crank angle for an inlet temperature of $180°C$, a CR of 13:1 and a λ of 4.53.

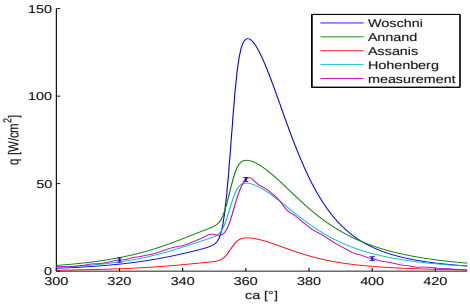

Fig. 1. Wall heat flux as a function of crank angle for $\lambda = 4.53$; $T_{in} = 180°C$ and CR 13:1

From this figure it can be seen that *Woschni* and *Assanis* differ the most from our measurement. *Woschni* underestimates the heat flux during compression and overestimates it during combustion and expansion. *Assanis* underestimates the heat flux during the whole cycle. The *Hohenberg* and *Annand* correlation come closest to the measurement. The *Hohenberg* correlation comes close, but still deviates from the measured heat flux, especially during the expansion stroke. The *Annand* correlation overestimates the heat flux during the whole cycle. Seeing these results, it can be concluded that none of the heat flux correlations are able to estimate the measured wall heat flux accurately. This could be due to wrongly determined exponents, a wrong scaling factor, a wrong characteristic length, a wrong characteristic velocity or a combination of these errors. It is possible to adapt the scaling factors of the correlations in order to get better results, as can be seen in figure 2.

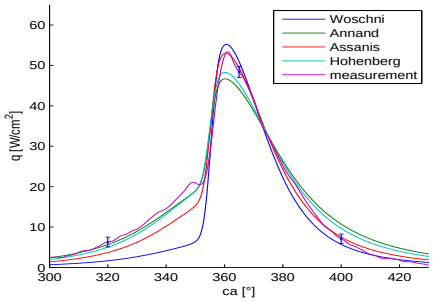

Fig. 2. Wall heat flux for optimized scaling factors as a function of crank angle for $\lambda = 4.53$; $T_{in} = 180°C$ and CR 13:1

The scaling factor of each correlation is optimized using the minimum mean square error method, in order to fit the measured heat flux. Although the error is minimized for the correlations, the estimated heat flux from the correlations can still deviate a lot from the measured heat fluxes in some parts of the cycle. This can be seen from the *Hohenberg* correlation. Although the error is very small, the heat flux resulting from this correlation fails to estimate the peak heat flux and overestimates the heat flux during expansion. The same goes for the *Annand* correlation. When looking at the graphs, one could say that *Assanis* follows the measured heat flux the best, since it is able to predict the heat flux well during combustion and expansion. However, during compression the heat flux is underestimated, which results in a larger error for the *Assanis* correlation. Take note that the compression stroke is the most critical part of the cycle for HCCI combustion. For HCCI it is important to control the SOC, which is very dependent on the pressure and temperature build-up during the compression stroke. When the heat transfer is overestimated, the gas temperature will be underestimated which ultimately results in a SOC that is predicted later in the cycle than should be. The opposite holds for an underestimation of the heat transfer during compression. If we only consider the compression stroke, the *Annand* and *Hohenberg* correlation give the best results. A good correlation should be able to predict the wall heat flux correctly during the whole cycle and not only during some parts of it. This is not the case for any discussed correlation. They all follow the same trend, but none of them is completely correct.

IV. Conclusions

From the results shown above, it can be concluded that none of the heat flux correlations is able to estimate the wall heat fluxes accurately. Therefore, it is believed that structural changes need to be made to the correlations. A new heat flux correlation should be established, based on the characteristics of HCCI. It is possible to optimize the scaling factor for each correlation, but it is rather unsatisfactory to adjust the coefficients of the correlations substantially for every HCCI engine. A good correlation should be applicable on different engine geometries and for different fuels and should be able to predict the heat flux every moment in the cycle.

Acknowledgements

The authors would like to acknowledge the suggestions of all their supervisors and technical staff.

References

[1] P.M. Najt and D.E. Foster, "Compression-ignited homogeneous charge combustion," *SAE Technical Paper 830264*, 1983.

[2] G. Woschni, "A universally applicable equation for the instantaneous heat transfer coefficient in the internal combustion engine," *SAE Technical paper 670931*, 1967.

[3] W.J.D. Annand, "Heat transfer in the cylinders of reciprocating internal combustion engines," *Proceedings of the Institution of Mechanical Engineers 177*, pp. 973–996.

[4] D. Assanis, Z. Filipi, O. Guralp, and J. Chang, "New heat transfer correlation for an HCCI engine derived from measurements of instantaneous surface heat flux," *SAE Technical Paper 2004-01-2996*, 2004.

[5] G. Hohenberg, "dvanced approaches for heat transfer calculations," *SAE Technical Paper 790825*, 1979.

[6] S. Onishi, S. Jo, K. Shoda, and P. Jo et al., "Active thermo-atmosphere combustion (ATAC) - a new combustion process for internal combustion engines," *SAE Technical Paper 790501*, 1979.

[7] H. S. Soyhan, H. Yasar, H. Walmsley, B. Head, G. T. Kalghatgi, and C. Sorusbay, "Evaluation of heat transfer correlations for HCCI engine modeling," *Applied Thermal Engineering 23 (2-3)*, pp. 541–549, 2009.

Contents

Nomenclature

Abbreviations

AE	Absolute Error
AFR	Air to Fuel Ratio
ATDC	After Top Dead Center
BDC	Bottom Dead Center
BTDC	Before Top Dead Center
ca	crank angle
CFR	Cooperative Fuel Research
CHR	Cumulative Heat Release
CI	Compression Ignition
COV	Coefficient of Variation
CR	Compression Ratio
DAQ	Data Acquisition
DI	Direct Injection
ECU	Engine Control Unit
EGR	Exhaust Gas Recirculation
EVC	Exhaust Valve Close
EVO	Exhaust Valve Open
FIR	Finite Impulse Response
HC	Hydrocarbons
HCCI	Homogeneous Charge Compression Ignition
HFM	Heat Flux Microsensor
HRR	Heat Release Rate
IGN	Ignition Timing
imep	indicated mean effective pressure
IVC	Intake Valve Close
IVO	Intake Valve Open
MM	Molar Mass
NTC	Negative Temperature Coefficient
ON	Octane Number
PID	Proportional Integral Derivative
PFI	Port Fuel Injection
PM	Particulate Matter
RE	Relative Error
RH	Relative Humidity
RON	Research Octane Number
rpm	revolutions per minute
RTD	Resistance Temperature Detector
ROHR	Rate of Heat Release

sfc	specific fuel consumption
SI	Spark Ignition
SOC	Start of Combustion
TFG	Thin Film Gauge
TDC	Top Dead Center
VCR	Variable Compression Ratio
VVT	Variable Valve Timing
WOT	Wide Open Throttle

Greek symbols

α	thermal diffusivity	$[\frac{m^2}{s}]$
γ	specific heat ratio	[-]
θ	crank angle	$[^\circ]$
λ	excess air ratio	[-]
μ	mean value	[-]
η	efficiency	[-]
σ	standard deviation	[-]
ϕ	equivalence ratio	[-]

Subscripts

comb	combustion
cyl	cylinder
i	indicated
in	inlet
ss	steady state
trans	transient
w	wall

Roman symbols

A	area	$[m^2]$
B	diameter combustion chamber	$[m]$
c_p	specific heat capacity	$[\frac{J}{kgK}]$
h_c	convection coefficient	$[\frac{W}{m^2K}]$
H_u	Lower heating value	$[J/kg]$
L	characteristic length	$[m]$
m	mass	$[kg]$

N	speed	$[rpm]$
p	pressure	$[Pa]$
Q	heat	$[J]$
P	power	$[W]$
q	heat flux	$[\frac{W}{m^2}]$
R	specific gas constant	$[\frac{J}{kgK}]$
T	temperature	$[K]$
V	volume	$[m^3]$
v	characteristic velocity	$[m/s]$
W	work	$[J]$
x	distance	$[m]$

Chapter 1

Introduction

Nowadays the world economy is strongly dependent on the oil industry. Oil is primarily used as an energy carrier in the energy sector, in the transportation sector and in the production industry. Since the oil supplies are diminishing, the price is starting to rise. It is becoming harder to find and more difficult to mine. New and/or alternative technology is needed in a future where oil prices will be too high to afford. Very recently, advanced techniques made it possible to mine shale gas. This lowers the prices of oil because the fossil fuel supply gets bigger. The impact on the transportation sector however is not yet very clear. It could allow LPG to compete on a bigger scale with diesel and gasoline. Maybe more important is the influence of man on the greenhouse effect. Burning fossil fuel leads to enormous emissions of CO_2, an important greenhouse gas. Also the quality of the ambient air in large cities and the formation of smog and acid rain due to NO_X, SO_X and PM is becoming alarming. For these reasons national governments, but also international organizations, are imposing stricter rules and regulations concerning the emission of greenhouse gases, especially on CO_2 emissions, and pollutants as NO_X, SO_X and PM.

This also has big consequences for car manufacturers. Two main paths can be distinguished to fulfill these regulations.

The first path is to start using different kinds of technology like electric motors. Usage of renewable electricity leads to zero emissions. The problem however is the storage of electricity in batteries. The energy density of modern batteries is too small for automobile applications. The consequent limited driving range is for most customers too big of a drawback. You also cannot charge your battery as quickly as you could fill your tank with liquid fuel. Charging a battery takes at least a few hours. That is why the driving range of a battery is said to be the driving range in one day. The production cost of batteries,

the lack of sufficient materials to produce them and environmental issues when recycling batteries are also big issues that cannot be neglected. Another possibility is the use of fuel cells. Fuel cells convert hydrogen into electricity with a high efficiency. But like batteries they are very dependent on chemical elements.

The second approach to the problem is clinging to our conventional technologies of internal combustion engines, but enhance them and/or make them suitable for other kinds of energy carriers with a direct or indirect lower or even zero emission of CO_2. Hydrogen for example is still in the running to be the fuel of the future. It has a zero CO_2 emission when making use of the intermittent character of renewable energy sources to store energy in hydrogen [1]. Hydrogen has a lot more potential than for example electric motors and fuel cells due to their higher energy density, much lower dependency on chemical elements and the possibility to build on the existing knowledge and infrastructure of today's internal combustion engine. However, at ambient temperature hydrogen is a gas and the density is some orders of magnitude lower than that of liquid fuels. Storage of hydrogen in cars needs some further research. Another possibility is usage of bio-fuels like alcohol. Alcohols are a liquid at ambient temperature and have an energy density closer to that of gasoline and diesel than most alternative fuels. For the same energy content as one litre of gasoline, one needs 1.6 litres of ethanol and 2.1 litres of methanol. Bio-fuels can be CO_2 neutral when produced in a durable manner. While the crops, from which bio-fuels are extracted, are growing, they can absorb the same amount of CO_2 as they release when they are burnt. So unlike fossil fuels they do not add extra CO_2 to the atmosphere, at least in theory. In practice, bio-fuel crops could increase emissions through land clearance, fertiliser use, and by displacing other crops. If millions of hectares of land are switched from food to bio-fuel crops, food prices will rise and food production is displaced. Nevertheless, methanol and ethanol for example are promising alternatives for current fuels. They have a higher resistance to auto-ignition, a higher latent heat of evaporation and a higher laminar flame speed. These are key elements which can lead to higher engine efficiencies in existing engines.

Next to the use of alternative fuels there has also been a lot of research to improvement of the engines itself by raising efficiencies and reducing emissions. Downsizing has proven to be a successful way of reducing both CO_2 and pollutants in SI engines. Downsizing an engine means making use of a smaller engine while retaining the same power. This is achieved by means of turbocharging. The smaller engine will have to work harder at part-load, this asks for a larger throttle opening, resulting in a better part-load efficiency.

However, at peak power the smaller engine will experience larger pressures which can cause knock, limiting the compression ratio (CR) thus efficiency. Alcohols are interesting in this case because they are more resistant against knock. Other improvements as direct injection, variable valve timing, exhaust gas recirculation (EGR), common rail systems and new after-treatment systems all showed their potential for increasing efficiency and reducing emissions.

The last couple of years an old combustion technique is being reinvented. The principle of HCCI combustion is already known for decades. *Onishi et al.* [2] were the first to conduct experiments on HCCI combustion in 1979. The idea has been pushed to the background at the time, since no real breakthrough was ever made. Since the recent advent of electronic sensors and controls, and driven by cleaner technology requirements, HCCI has become again a matter of interest. HCCI combustion is achieved by controlling the temperature, pressure and air to fuel ratio (AFR) for auto-ignition to occur. This is far more challenging than the control of classic SI or CI engines. Thanks to electronics this challenge is reconsidered. With new technology and lots of acquired experience over the past few years, this concept will be the subject of this thesis.

Research over the last three decades has shown the great potential of HCCI for achieving high efficiencies and low emissions. Most publications on HCCI present only experimental results. Researchers have been mainly focusing on the effect of different kinds of parameters like CR, inlet temperature, AFR, engine speed, type of fuel and use of EGR. Their experimental results give a better understanding in the combustion process of HCCI and their influence on the start of combustion, but still there is no consensus on how to control the start of combustion in the right way. The variety of parameters that can be changed, make it hard to design and optimize a control strategy. Simulation software could offer a breakthrough in this regard. Today, simulation software is used that is designed for classical Spark Ignition (SI) and Compression Ignition (CI) engines. In these models fluid dynamics play an important role because the flame propagation and in-cylinder injection phenomena are taken into account. Research has revealed that these models do not meet the HCCI concept [3]. *Najt and Foster* [4] showed that the response of the HCCI combustion process to changes in operating parameters can be explained in terms of known chemical kinetics. An HCCI model is therefore needed. Chemical kinetics are mainly influenced by the concentration of the reactants and the temperature. The temperature is dependent on the cylinder wall heat transfer. Consequently, a good heat transfer model is an essential part of developing an HCCI simulation model.

The objective of this thesis is to rebuild and equip an existing CFR engine with an EGR system, an air preheater and sensors that make it possible to perform heat flux measurements. The engine setup and heat flux measurements will serve for a doctoral research on the design of an accurate heat transfer model that takes into account all the parameters relevant for an HCCI engine. For measuring the heat fluxes a single-layer *Thin Film Gauge* sensor will be used, a sensor that is recently developed at the *University of Oxford* [5]. Therefore the experience gained during the master's thesis of *S. Broekaert and T. De Cuyper* [6] will be used.

Chapter 2

HCCI

In this chapter, the basic principle of HCCI will be explained, the reason why HCCI is that interesting and which are the disadvantages. Next, some more information on the actual combustion process and which parameters influence the combustion will be given. Further on, there will be a discussion on the problems that are still faced today, some examples of recent developments and the areas that need some further research. Finally, there will be a discussion on wall heat fluxes and the explanation why these are important for a better understanding of HCCI combustion.

HCCI is an abbreviation of Homogeneous Charge Compression Ignition and is already known for decades. The first study on HCCI was performed on a two stroke engine in 1979 by *Onishi et al.* [2]. A few years later, HCCI was implemented on four stroke engines as well. The following years further research was carried out on HCCI, resulting in a better understanding of the concept, but no real breakthrough was ever made. With the demand for more efficient and cleaner engines, together with the recent development of electronics, the HCCI concept is reconsidered as an alternative for the current SI and CI engines.

2.1 The principle of HCCI

HCCI can be seen as a combination of SI and CI engine principles. As in SI engines, a homogeneous mixture of air and fuel (and exhaust gases if EGR is applied) is brought into the combustion chamber. Several fuel introduction strategies can be distinguished. There is port injection (PFI), early in-cylinder injection, late in-cylinder injection and a combination of PFI and in-cylinder injection, called dual fuel injection [7]. In this thesis PFI will be used. As in CI engines, the mixture is exposed to high enough temperatures and pressures for auto-ignition to occur. The combination of both types of engines makes

it possible to combine the benefits of both. These advantages will be highlighted in section 2.2.

The auto-igniting homogeneous charge results in a uniform combustion. This is different from SI engines, whose combustion depends on the propagation of a turbulent flame front. It is also different from CI engines, whose combustion depends on diffusive combustion. The exact implications and consequences of HCCI combustion will be explained more precisely in the following section. A comparison of the different combustion principles between SI, CI and HCCI engines can be found in figure 2.1. The left part is the SI combustion process. You can see the presence of the spark plug, the port fuel injector and the moving flame front. The middle part is the CI combustion process. You can see the fuel injector and the injected spray. The right part is the HCCI combustion process. You can see a port fuel injector but no spark plug or in-cylinder injector. The mixture is ignited by compressing the mixture enough in order to get auto-ignition, so there is no direct control of the start of combustion. You can also notice multiple burning hot spots. This is the mixture burning at several points at the same time because the state of the homogeneous mixture is roughly the same in the whole combustion chamber. It can be said that there is a uniform combustion.

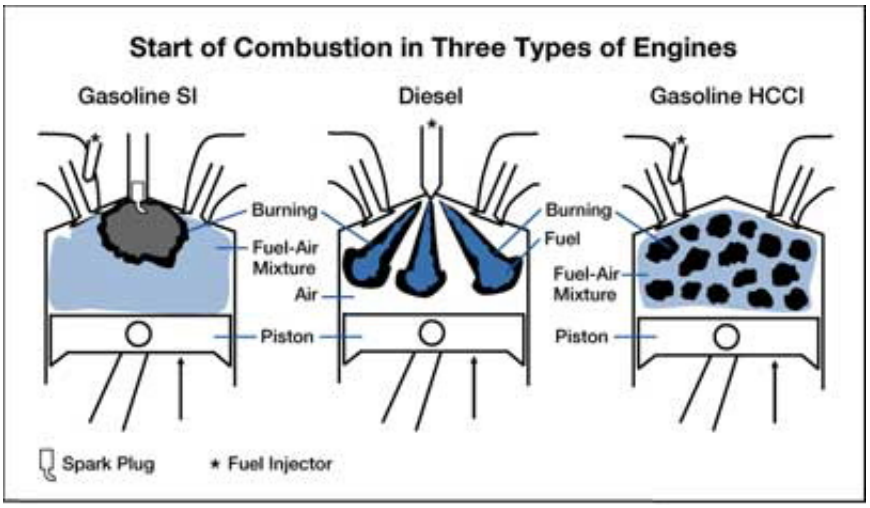

Figure 2.1: Comparison between different types of combustion [8]

2.2 Benefits & Drawbacks

Today's engines do not fulfill the requirements on emissions anymore. Gasoline engines (SI engines) produce high NO_X emissions. Because of the relatively low excess air ratio

(around 1 for stoichiometric combustion) they also produce more CO than diesel engines which rely on a lean combustion. Also hydrocarbons (HC) are left in the exhaust gases due to the mixture getting trapped in crevices and quenching near the cylinder walls. Due to an effective after-treatment however, tailpipe emissions are relatively low. The efficiency of gasoline engines is rather low. At part load, the throttle valve induces pressure losses which lead to low efficiency. The risk of auto-ignition due to high temperatures limits the CR, thus reducing the theoretical efficiency. These low efficiencies imply a relatively high fuel consumption and consequently high CO_2 emissions.

Diesel engines (CI engines) produce a lot of particulate matter (PM) and have NO_X emissions comparable to gasoline engines. Moreover, the rather low exhaust temperatures and the oxygen-rich environment make it difficult to achieve an effective after-treatment. This causes relatively high tailpipe emissions. The part load efficiency however is higher than for gasoline engines, this is mainly due to the lack of a throttle valve. The power control strategy of diesel engines relies on the amount of fuel injected into the combustion chamber. There is no need for a throttle valve so there are no pressure losses. Although a Diesel cycle has a lower theoretical efficiency at the same CR than an Otto cycle, the theoretical efficiency is higher due to the high CR which is needed for high in-cylinder temperatures to allow auto-ignition. These relative high efficiencies imply a lower fuel consumption and consequently lower CO_2 emissions than with gasoline engines.

It can be concluded that gasoline engines have relatively low emissions but a low efficiency (high CO_2 emissions) and diesel engines have relatively high emissions but a high efficiency (low CO_2 emissions).

2.2.1 Benefits

As explained in the introduction, there are recently several technologies introduced which enhance these types of engines. In gasoline engines the efficiency is increased and in diesel engines the emissions are reduced. As mentioned in section 2.1, there is a new type of combustion which combines the benefits of gasoline and diesel engines. HCCI engines combine the high efficiency of diesel engines with the low emissions of gasoline engines.

Efficiency The high efficiency is a consequence of several phenomena which are typical for HCCI engines. First of all, the CR is high as is the case with diesel engines. This high CR is needed for the homogeneous charge to reach temperatures high enough to cause auto-ignition. In other words, the high CR is needed to cause compression ignition. This

high CR results in a high theoretical efficiency. The theoretical efficiency of an Otto cycle is:

$$\eta_{otto} = 1 - \frac{1}{CR^{\gamma-1}} \tag{2.1}$$

with CR the compression ratio and γ the ratio of specific heats. Second, HCCI engines make no use of a throttle valve. SI engines need this valve to regulate the power output, because SI engines cannot be regulated with the amount of injected fuel since it needs a fixed excess air ratio around unity for stoichiometric combustion. HCCI engines on the other hand typically use lean mixtures. If the mixture is too rich, the rate of combustion and the pressure rise rate become too high, which can generate knock related problems, thus damaging the engine. The power is regulated by changing the fuel rate. By avoiding a throttle valve there will be no throttle losses, consequently there will be no negative effect on the part load efficiency. Third, a shorter combustion duration (10-90% heat released) also has a positive effect on the engine efficiency. The short combustion duration is a result of the fact that the homogeneous mixture burns at many points at the same time. There is no flame front that needs to propagate through the entire combustion chamber. The shorter the combustion, the closer the combustion lies to the Otto cycle, where heat is assumed to be added at constant volume. The combustion duration can be as low as 2 to 3°ca (degrees crank angle) [9]. This rapid combustion is the reason why the intake charge cannot be too rich as explained just above. The intake charge therefore needs to be diluted. This can be achieved by a high excess of air (a lean mixture) and/or by the use of EGR. Fourth, lean mixtures result in a higher theoretical efficiency than rich mixtures. The ratio of specific heats depends on the air to fuel ratio [10]. Lean mixtures have a larger ratio of specific heats. This raises the efficiency, as can be seen from equation 2.1. The high efficiency results in a low fuel consumption, thus low CO_2 emissions. One of the first tests on a real production engine showed an increase of part load efficiency from 14 to 34% [11].

NO_X and PM emission As stated before, HCCI engines have both high efficiency and low emissions. With low emissions, low NO_X and PM emissions are meant. However, this comes at a cost. HCCI engines have other kinds of emissions as will be explained later. Low NO_X emissions are the result of the low in-cylinder temperatures in comparison with gasoline and diesel engines. NO_X formation is temperature sensitive, especially above 1800K. The combustion in an HCCI engine occurs simultaneously throughout the

combustion chamber. There is no flame front, as in SI engines, that compresses and heat up the unburned mixture. Because there is no flame front as in gasoline engines, the charge can be very diluted (through lean combustion or by using EGR). There are no local rich areas with local high temperatures as in diesel engines. This uniform lean combustion leads to low maximum temperatures. Mostly, temperatures stay below 1800K depending on the fuel used, while diesel engines reach temperatures up to 1900 to 2100K. Another factor that plays into the formation of NO_X emissions is the duration of the combustion. Because HCCI engines have a short combustion duration, there is also less time for NO_X to form. Research [12] showed that NO_X emissions for HCCI engines can be as low as 1 to 2 ppm, which is extremely low, while SI engines produce a few thousand ppm. The low PM emissions are a consequence of the homogeneous mixture, unlike the very inhomogeneous mixture in diesel engines.

Cycle-to-cycle variations In SI engines, large cycle-to-cycle variations occur. Research [13] has shown that this is because of the variations in fluid flow and charge inhomogeneity during the early flame development. These variations limit the engine performance and give rise to increased emissions. HCCI engines have very little cycle-to-cycle variations since combustion ignition takes place at many points at the same time. There is a uniform combustion, which avoids unstable flame propagation. This results in smooth engine operation.

Cost HCCI engines can be produced cheaper than SI and CI engines. Unlike CI engines there is no need for high pressure injection equipment. The emission control system has the potential to be less costly and less dependent on scarce precious metals than either SI or CI engines.

Fuel flexibility Another advantage of HCCI engines are their fuel flexibility. Tests show that almost any liquid fuel can be used [12]. It is even possible to switch from pure n-heptane (RON0) to pure iso-octane (RON100) with the engine running. To get auto-ignition around TDC, without inlet air preheating, n-heptane required a CR of about 11:1 while iso-octane required 21:1 under the same conditions. It can be concluded that HCCI engines can run at almost any liquid fuel when using an engine with variable CR. Other parameters like inlet temperature and dilution also play a huge role in creating the right conditions for any type of fuel. The most interesting fuels however are those with high Octane Numbers (ON). A higher ON means a higher auto-ignition temperature. Therefore a higher CR is demanded. The higher auto-ignition temperature together with the high

CR results in a higher overall combustion temperature and a shorter combustion duration, resulting in a higher efficiency. That is why a high ON fuel as gasoline (RON98) will be researched in this thesis.

Applicability As a consequence of the fuel flexibility HCCI engines have the potential for normal passenger cars as well as for heavy duty trucks. In fact, it could be scaled to virtually any size-class of transportation engine from small motorcycle to large ship engines. HCCI is also applicable to piston engines used outside the transportation sector such as those used for electrical power generation and pipeline pumping.

2.2.2 Drawbacks

As already said, the principle of HCCI has been known for decades. So there must be some important reasons why HCCI engines are not used worldwide. There is one major drawback that prevents HCCI engines to be produced for commercial purpose.

Control of the ignition timing In SI and CI engines the start of combustion (SOC) is initiated by means of a spark plug or a high pressure injection respectively. There is a direct control of the start of combustion, mostly chosen around TDC. HCCI relies on the auto-ignition of a homogeneous charge. There is no direct control of the SOC. At most, it can be tried to achieve the most ideal climate for the charge to ignite at the right moment. This ideal climate depends on numerous engine settings, the inlet mixture temperature and the CR being the most important. But also inlet manifold pressure, type of fuel, air/fuel ratio, amount of EGR, engine speed and coolant temperature affect the SOC. The precise consequences of these parameters are discussed in the next section.

Limited operating range The intake charge of HCCI needs to be diluted to limit the rate of combustion. Dilution can be achieved by using an excess of air or by using EGR. In other words, the mixture is lean. If the mixture is too rich, the combustion becomes too fast and knock related problems (high pressure rise rates) can cause damage to the engine and lots of noise. HCCI combustion is the same auto-ignition process as knocking combustion. Therefore HCCI engines cannot be used at high loads. If the mixture is too lean, misfire can occur. Almost all the research executed so far show that HCCI engines behave well at low to medium loads, but become unstable at high loads. Several papers mention an upper and lower load limit for HCCI operation [7], [14], [15]. The upper load limit is defined by a pressure rise rate of 10 $bar/°$ca. The lower limit is measured using the Coefficient of Variation (COV) of the imep, which has the upper value of 10%. This is

the same value used for spark ignition engines. For a higher COV_{imep}, a steady operation of the engine is not guaranteed. The COV_{imep} defines the cyclic variability in indicated work per cycle, the calculation can be found in appendix C.

Emission of HC and CO One of the major advantages of HCCI engines is the low emission of NO_X and PM. However, there is a high emission of unburned hydrocarbon and carbon monoxide due to the relatively low temperatures at low and medium load. The oxidation process of the hydrocarbon fuel cannot be completed. Near the cylinder wall the mixture is quenched, resulting in low oxidation of the fuel. As in other engines, crevices are also a source of unburned HC and CO. The low exhaust gas temperatures make it harder for an effective after-treatment like in gasoline engines, where three-way catalysts have proven to be very successful. There are some recent developments to reduce these emissions that will be explained in section 2.4.

Cold start At cold start, it is possible that the mixture refuses to ignite. The intake charge does not receive any heat from the cold intake manifold. During compression, the mixture loses its heat to the cold combustion chamber walls. Several proposals have been made to counter this problem. This will be explained in section 2.4.

2.3 Influence of different parameters

SOC, combustion temperature, combustion duration, pressure rise rate, heat release rate, peak pressure, imep, etc. are some important parameters of the combustion. In an HCCI engine they can be influenced in several ways, which will be discussed in this section. It will give a better understanding of the HCCI process and its properties.

2.3.1 Air to fuel ratio

The homogeneous mixtures used in HCCI engines are usually very lean. Excess air ratios from 2 to 5 are not that uncommon. A lean mixture is used in order to limit the rate of combustion. A homogeneous lean mixture will guarantee a desirable uniform combustion. Since HCCI does not make use of a throttle valve, the air to fuel ratio can be managed by injecting more or less fuel. By using a richer mixture (but still lean overall) more chemical energy is introduced into the cylinder, resulting in a higher heat release. The peak pressure of the combustion will rise, this way heavier load operation can be achieved. A curve of pressure and ROHR (Rate of Heat Release) as a function of crank angle for various air

to fuel ratios can be found in figure 2.2. The experiments to obtain these curves were conducted by *Kumar et al.* [7].

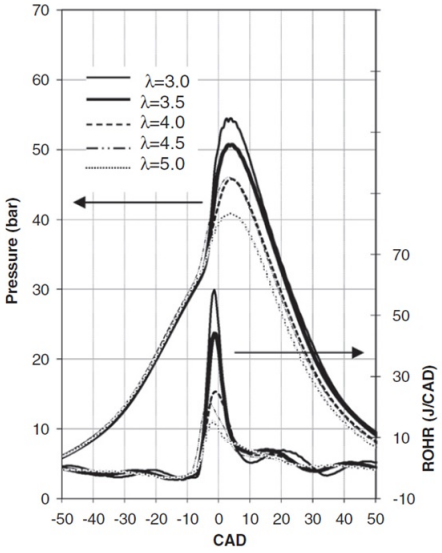

Figure 2.2: Pressure in function of CAD for different lambdas [7]

It can be seen that the peak pressure rises if the mixture becomes richer. The same goes for the ROHR. This can be derived from the fact that more fuel is introduced, thus more energy is available for combustion. The ROHR also indicates a very fast combustion, a consequence of the homogeneous character of the mixture.

2.3.2 Compression Ratio

The CR and inlet temperature are the most important parameters that affect the SOC. When adjusting these two parameters fast and correctly, it would be possible to control the SOC in a wide range. Changing the CR during operation however is quite complex, although several propositions have been made, as will be explained in section 2.4. A high CR is needed for the mixture to be able to auto-ignite. When in operation, and nothing else but the CR is changed, the SOC will shift. When there is a lack of a variable CR system during operation, it is crucial to choose the right CR for the fuel one is using.

2.3.3 Inlet temperature

The inlet temperature has a big influence on the SOC. A higher inlet temperature advances the SOC. This is because the mixture reaches its critical temperature to auto-ignite earlier

in the compression stroke. This earlier combustion results in higher heat release rates and in most cases higher peak pressures. Although preheating can be used in experiments, in commercial applications, the system becomes more complex and expensive.

2.3.4 EGR

In many occasions, exhaust gas recirculation (EGR) is applied when running an engine in HCCI operation. It has many advantages and is easy to install. When EGR is applied, a part of the exhaust gases is introduced at the inlet of the engine. This way a mixture of air, exhaust gas and fuel is ignited in the combustion chamber. Using EGR brings along several interesting properties [9], [16].

Assuming the air and exhaust gas mixture is heated to a specific temperature, the temperature after compression will be lower than when only air is compressed. This is a consequence of the higher heat capacity of the exhaust gas during the compression. This property has an effect on the SOC, because a slower temperature build-up suggests a retardation of the auto-ignition. Exhaust gases also tend to prolong the combustion duration, because of combustion phasing. Since the SOC is delayed, the volume of the combustion chamber is already expanding during combustion, resulting in a lower pressure and temperature during combustion. Consequently the chemical reaction, thus combustion, is slower. This results in smoother and quieter operation of the engine.

Because the exhaust gases are introduced into the inlet of the engine, into the air stream, the air flow is already heated for some part. This is interesting since auto-ignition is greatly dependent on sufficiently high temperatures. Take note that heating up the air also results in a lower density, thus richer mixtures will be obtained for the same fuel rate. This lower density results in a decreased volumetric efficiency. The exhaust gases can also be used to control the AFR to some extent. When exhaust gases are drawn into the combustion chamber, less air will enter. Less air means a lower AFR for the same amount of fuel injected, affecting the pressure and imep.

Using EGR also has some disadvantages. The first problem is higher levels of HC and CO emissions, due to slow oxidation rates and lower flame temperatures. The second problem is the lower engine durability and performance. The low durability is a result of the corrosive and abrasive components (such as sulfur oxide) present in the exhaust gases [16]. The lower performance is due to the heat that is absorbed by the exhaust gases during combustion.

2.4 Recent developments in HCCI

After taking a look at the principle, benefits, drawbacks and characteristics of HCCI engines, this section is dedicated to current and future research and development on HCCI. As mentioned in section 2.2, the biggest problems of HCCI are controlling the SOC, the limited operating range, the emission of HC and CO and cold starting. Several possible solutions for some of these problems will be discussed here.

2.4.1 Speed, load and SOC control

VCR VCR or Variable Compression Ratio is a very important feature that could be implemented on an HCCI engine [17]. VCR allows for the geometric CR of the engine to be changed while in operation. This can be achieved in several ways, e.g. by enabling the cylinder head to vary its position. At the moment, some well-known car manufacturers are also putting research into VCR, even ensuring the CR is controlled as a function of the load and driving demands. A VCR engine in combination with HCCI would be very interesting, allowing another parameter to be changed. It is a way to control the SOC, the operating range, and is considered to come in handy while cold starting. If it is possible to change the CR in fractions of a second, transient operation of the engine would also be simplified. The negative part of VCR is that it makes the engine a lot more complex and raises the cost.

VVT If VVT or Variable Valve Timing is used in an engine, the CR can be changed by varying the timing of the valves [17]. The CR of an engine can be lowered by delaying the closing of the inlet valve during the compression stroke. This way the CR, while in operation, is changed without any geometric changes to the engine and it does not make the engine more complex. VVT also makes it possible to make use of the residual gases. "Re-breathing" can be used as an internal EGR system: by delaying the closing of the outlet valve during the intake stroke, some of the residual gas will be drawn into the combustion chamber, forming a mixture of air, fuel and exhaust gas (as with external EGR). VVT can be seen as an elegant way of controlling the CR and also makes internal EGR possible. Whereas the engine complexity does not change, a complex valve timing controlling system needs to be implemented, which can be seen as a negative part of this system. The most important application of VVT in an HCCI engine is the load, speed and SOC control. It would also benefit the cold-starting capabilities of the HCCI engine.

Turbo- or supercharging Research on turbo- or supercharging in HCCI operation has also been done [18]. Charging the mixture means that the pressure at the inlet is increased. This results in better efficiencies and higher load capabilities.

SI or CI mode The initial concepts to extend the load range of HCCI engines involved switching to SI or CI operation at high loads. This strategy allows to make use of the benefits of HCCI over the most important range, namely part-load, but adds complexity to switch between different modes.

2.4.2 Cold-starting

The biggest problem of cold-starting an HCCI engine is the low temperature of the mixture that is brought into the combustion chamber. If temperatures are too low after compression, no auto-ignition will occur. To cold-start an HCCI engine a few possibilities are available. It is possible to start up an engine as SI or CI engine. When the engine has warmed up, the operation could be switched to HCCI. It is also possible to start up using a high CR, this can be accomplished by VVT or VCR. Another way of starting is to use a glow plug during start-up which heats up the mixture in the combustion chamber [17].

2.4.3 Emissions

HC and CO emissions can be decreased by using a catalyst-type exhaust emission control system. Since high exhaust temperatures are desirable for these catalysts, the low temperatures of HCCI combustion form a problem. Another way to lower these emissions is by using multi-injection strategies which offer a better tradeoff between NO_X, HC and CO emissions. Research has been done [19] using a Direct Injection (DI) injector that creates a stratified charge in the combustion chamber. This results in a higher combustion temperature which results in a higher combustion efficiency and decreased HC and CO emissions at lean operation.

2.4.4 Control strategies

To control the ignition timing in an HCCI engine, a feedback loop can be used. A specific property is measured (e.g. pressure, temperature, heat flux), this info is used to change a certain parameter (e.g. EGR, preheating temperature, λ) which changes the in-cylinder conditions of the engine in order to achieve the demanded SOC. Currently, research is being put into heat flux measurements. Auto-ignition is mainly dependent on temperature and dilution. The dilution grade can be influenced directly by changing the AFR and the

amount of EGR. The temperature is linked to the heat transfer to the cylinder walls. If the heat flux is large, the temperature in the cylinder will be lower, resulting in retarded or no auto-ignition. The contrary holds for small heat fluxes, then the temperature will be high in the cylinder, hence the SOC will be earlier or knock-related problems will occur. General correlations for heat transfer in HCCI engines are being proposed [20]. These correlations could be used to predict the SOC. To develop and test these correlations, appropriate measurements need to be made. For further developments regarding the SOC prediction and HCCI combustion, heat flux measurements can be of great importance. A discussion of the application of heat flux measurements in HCCI engines can be found in section 2.5.

2.5 Heat flux

The biggest problem with HCCI engines is controlling the SOC. This is heavily dependent on in-cylinder thermal conditions. Pressure measurements can be used to determine these conditions. But for calculating temperatures and heat releases, assumptions have to be made, causing the result to deviate from reality. Pressure sensors tend to be very expensive, and since the calculations are computationally intensive, the processing hardware is expensive as well. Therefore, pressure sensors will be difficult to integrate into commercial application.

As mentioned in section 2.4 heat fluxes can also give a great insight into in-cylinder conditions and the SOC in HCCI engines. Because HCCI combustion can be modeled using chemical kinetics, which are dependent on in-cylinder temperature and concentration of the reactants, heat fluxes from the gas to the walls are very important. In this section, heat transfer in HCCI engines is discussed.

2.5.1 Heat flux measurements

In order to carry out heat flux measurements, a heat flux sensor needs to be used. Research for a suitable heat flux sensor is performed at the Department of Flow, Heat and Combustion Mechanics at the Ghent University as well. A brief discussion on several heat flux sensors can be found in the Master thesis of *S. Broekaert and T. De Cuyper* [6].

Coaxial heat flux sensors are used in several heat flux measuring applications like heat losses in SI engines, heat losses during knock and even in heat flux measurements on HCCI engines. The biggest problem is the parasitic lateral effect, making a one dimensional

analysis incorrect. A commercial type of heat flux sensor is produced by Vatell. Since this sensor cannot withstand high pressures, it is not usable in our research where knocking conditions will be studied as well. Another type of sensor is the eroding ribbon sensor. Research has shown that this sensor has an unpredictable behavior.

The type of sensor that is used in our research is the Thin Film Gauge (TFG) sensor, which is reliable and can withstand sufficiently high pressures. This sensor is still under investigation at the Ghent University and the University of Oxford. A full description of the TFG sensor can be found in the master's thesis of *S. Broekaert and T. De Cuyper*. A TFG sensor consists of several Resistance Temperature Detectors (RTD's) whose resistance changes as a function of temperature. They are used to measure the wall temperature of the cylinder. The RTD's are applied on a substrate, which functions as a thermal and electrical insulation for the RTD's. On the other side of the substrate a thermocouple can be applied. This could be used as another boundary condition to determine the heat flux. A TFG sensor can be seen on figure 2.3. Since the TFG has proven its applicability, it is used in our research.

Figure 2.3: A picture of a single-layer TFG sensor.

The resistance of the RTD's is a function of the temperature. Since a current power source is applied, the temperature of the cylinder wall can be derived from the voltage over the resistance. From here on, the heat flux can be calculated from the measured wall temperature using two different techniques. The first one is the Fourier method, which divides the wall temperature into Fourier components and uses the principle of

one-dimensional conduction to calculate the heat flux. The second technique is the FIR-method (Finite Impulse Response). This method assumes that the sensor is a linear time-invariable system. The wall temperature is defined as an input. Using a specific impulse response the transient heat flux will be the output of the system. In order to calculate the steady-state heat flux, the in-depth temperature of the thermocouple can be used. In [6] and in appendix C a thorough description of these techniques can be found.

2.5.2 Heat flux correlations

As mentioned in section 2.4, several heat flux correlations are being proposed. These will come in handy when computer models, for simulation purposes, of HCCI engines are being established. HCCI combustion depends on many parameters, a database of only experimental results would not suffice. Since the simulation of HCCI combustion will only be as good as the underlying computer model, the heat flux correlation and used model for the HCCI engine have to be as accurate as possible. Simulation of HCCI combustion will be of great importance in the HCCI development process.

To this day, several heat flux correlations are being proposed. Most of them are based on SI or CI engines, thus a study on the correctness of these correlations for HCCI is required. *H.S. Soyhan* [3] has executed this study for the most used heat flux correlations for HCCI engines. These are the *Woschni* correlation [21], the modified *Woschni* or *Assanis* correlation [20] and the *Hohenberg* correlation [22]. He had concluded that the *Hohenberg* correlation gave the best results, see figure 2.4. The *Assanis* correlation was good, but overestimated peak pressures. The *Woschni* correlation did not produce any credible results, which is why it is not on the graph. The reason why *Woschni* cannot be used for an HCCI engine can be found in the characteristic velocity. *Woschni* states that the velocity can be divided in a term describing the piston speed and a term describing the speed of the gas introduced by combustion. Since in HCCI a flame front is not present, *Woschni*'s characteristic speed is incorrect for HCCI combustion. *Assanis* and *Hohenberg* use a characteristic velocity that is less dependent of the combustion or is independent of the combustion respectively, which delivers better results. Even though the *Hohenberg* correlation is close to the experimental results, the minor differences could have big consequences in predicting the SOC in HCCI engines. Therefore, better heat flux correlations need to be found by using a different approach in obtaining the correlation. The discussed correlations are constructed using heat flux correlations from SI and CI engines with some empirical modifications to constants. It may be better to start from scratch or to make some structural changes to the existing models that closer represent

the nature of HCCI [3].

Soyhan made his conclusions based on pressure measurements. It would be interesting to evaluate the heat flux correlations using heat flux measurements. This way, no assumptions have to be made which introduce an error.

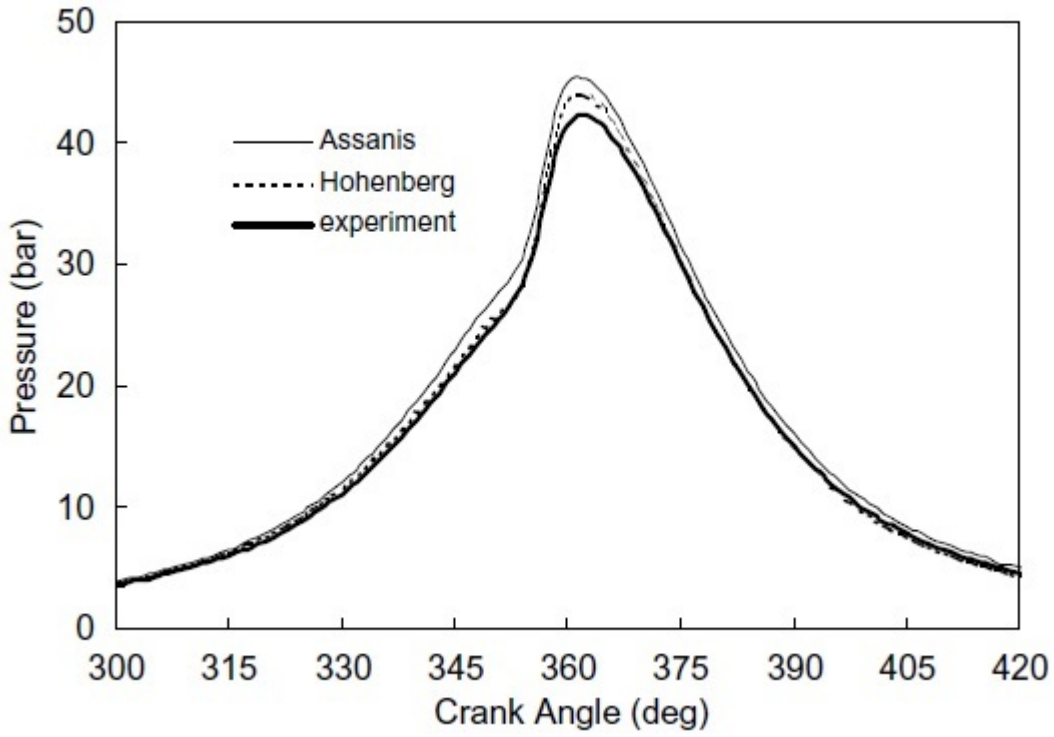

Figure 2.4: Measured and predicted cylinder pressures ($\lambda = 4.5$, 1200rpm, $T_{int} = 523K$ and $P_{int} = 1.026bar$, fuel=unleaded gasoline) [3]

Chapter 3

Test Setup

To conduct the experiments, a Waukesha Cooperative Fuel Research engine is used. In this chapter a summary of its properties and changes that have to be made to the setup are described. The CFR engine was initially designed to develop a gasoline knock test method. To do these experiments, the engine was designed with a variable compression ratio and was suitable for different kinds of fuels. This allows to do tests with different compression ratios or one optimal CR for each fuel.

3.1 CFR Engine

The CFR engine is a standardized, overhead valve, single cylinder, four stroke spark ignition engine. The air flow is regulated using a manually operable butterfly valve and the fuel is injected in the inlet (Port Fuel Injection). This mixture of air and fuel is brought into the combustion chamber where it is ignited using a spark plug. The engine is connected with a belt to an electrical synchronous engine, which keeps the rotational speed at 600 rpm. It is possible to put the belt on a different pulley on the engine, which allows it to achieve speeds of 900 rpm. In this research, the engine will run at 600 rpm.

The ignition timing, the injection timing and the duration of injection are controlled by a programmable MoTeC M4 Pro Engine Control Unit (ECU). Take note that for HCCI operation, the spark plug is not allowed to work. A cross section of the CFR engine can be found in figure 3.1. The most important engine properties can be found in table 3.1.

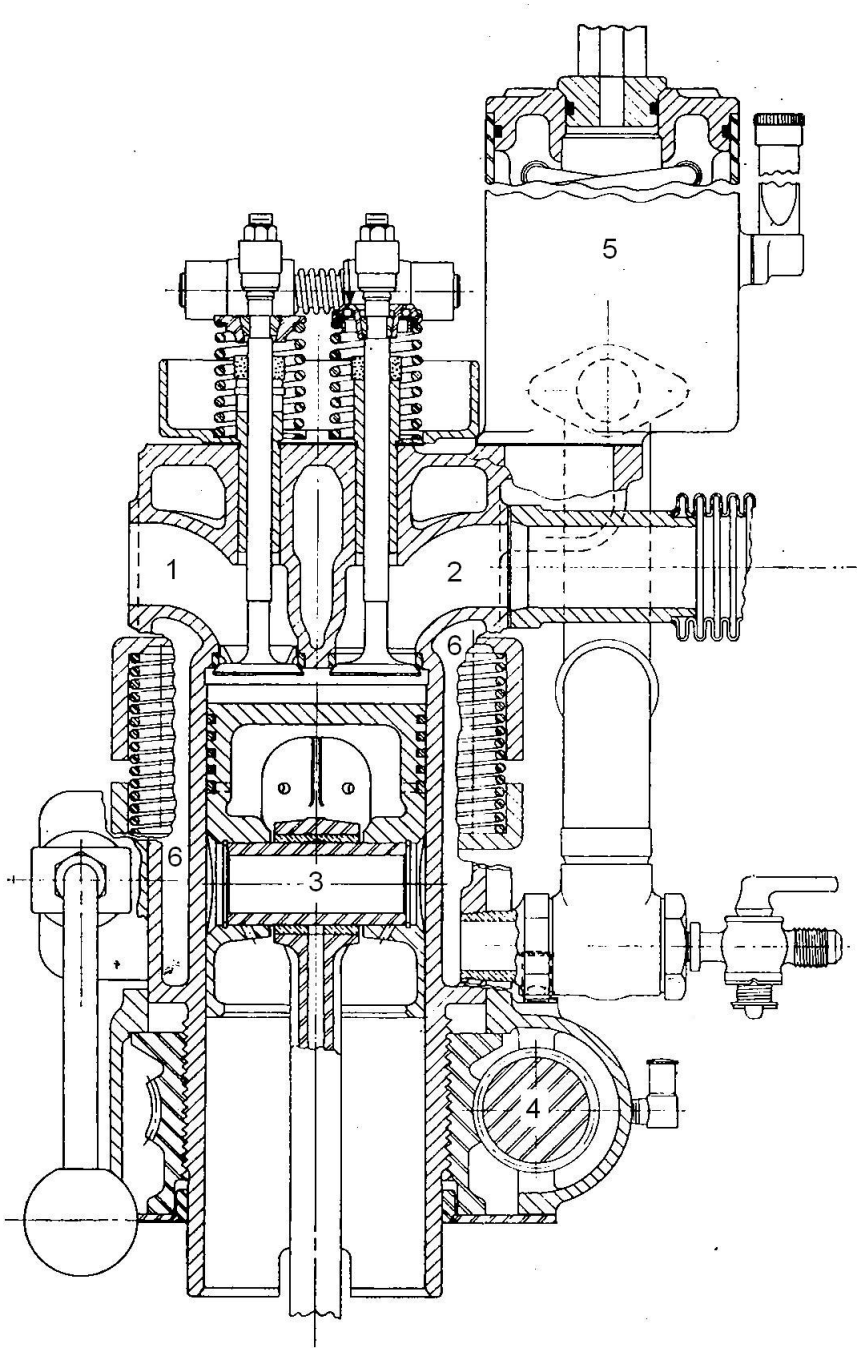

Figure 3.1: Cross section of CFR engine: (1) inlet, (2) outlet, (3) piston, (4) worm wheel, (5) thermosiphon, (6) water jacket

Table 3.1: CFR engine properties

speed [rpm]	600
bore [mm]	83,06
stroke [mm]	114,2
displacement volume [cc]	619
connecting rod length [mm]	254
compression ratio [-]	$4 \sim 18$
IVO [°ca ATDC]	10
IVC [°ca ATDC]	208
EVO [°ca ATDC]	501
EVC [°ca ATDC]	12

Another great attribute of the CFR engine is that there are several openings in the cylinder head to put sensors in. Figure 3.2 shows a cross section of the cylinder head of the engine.

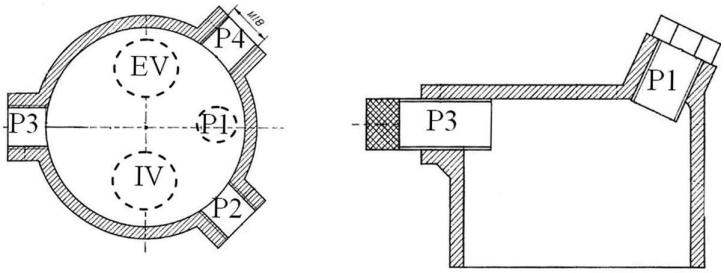

Figure 3.2: Cylinder head of the CFR engine

The top opening P1 is normally used for the spark plug. In opening P2, a Kistler 701A piezoelectric pressure sensor is installed. The other openings (P3 and P4) can be used for other sensors (e.g. heat flux sensor). The inlet and outlet pressure is measured with two Kistler 4075A10 piezoresistive pressure sensors. The pressure in the cylinder is only measured relatively. The absolute cylinder pressure can be calculated by stating that the inlet pressure and cylinder pressure are the same around BDC (Bottom Dead Center) during the intake stroke. The inlet and outlet temperatures are measured with K-type thermocouples. The same type of thermocouples are used to measure the temperature of the oil and cooling water. The air flow is measured using a Bronkhorst F-106BZ mass flow sensor.

The data-acquisition system consists of a PXI-system of National Instruments. It reads data every time the CAM 2614 crank encoder sends a signal. This way there is a sample every $0.1°ca$. A layout of the whole measuring system can be found in figure 3.3

3.2 HCCI-ready CFR engine

As mentioned before, the timing of the SOC in an HCCI engine can be influenced by using an EGR system and/or an air preheater. Since the current setup was not equipped with an air preheater or an EGR system, the setup is completed with both an EGR loop and an air preheater. Figure 3.4 shows a schematic of the engine setup.

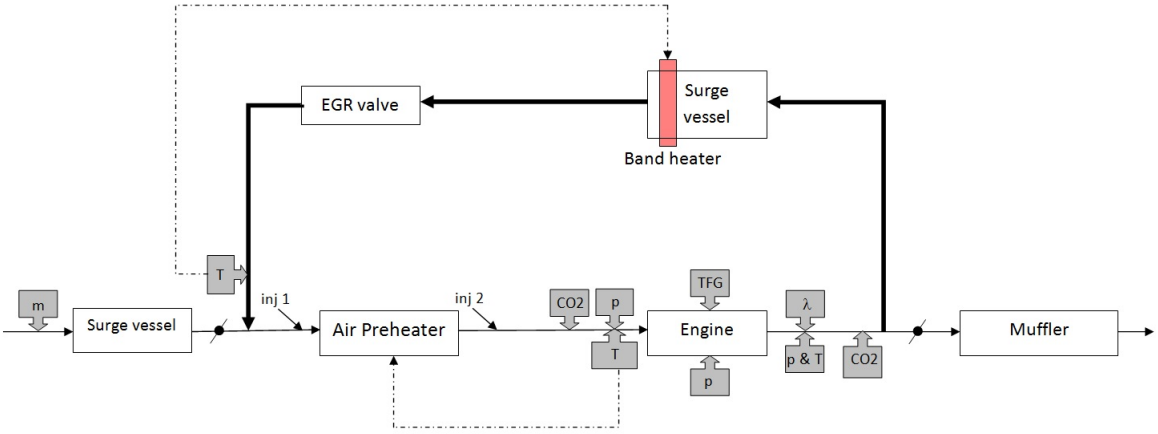

Figure 3.4: A scheme of the engine setup

The EGR loop consists of an EGR valve preceded by a surge vessel with a band heater. The band heater is necessary to avoid condensation in the pipes. Another possibility is to condense all of the water vapor. A cooling battery is then used to condense the vapor in the exhaust gases at a known location. This condensate is then collected. Since in real engines the vapor is still present in the exhaust gases, it is preferred to use a band heater. In that way the water remains in the gases and the results will be closer to reality. The temperature of the band heater is controlled by a simple temperature controller. A PID-controller is not necessary, since an exact temperature control is not needed. The main goal is to keep the exhaust gases above condensation temperature.

The air preheater consists of an element that can heat up the mixture of air, exhaust gas and fuel to a temperature of maximum $400°C$. It is important that this temperature stays

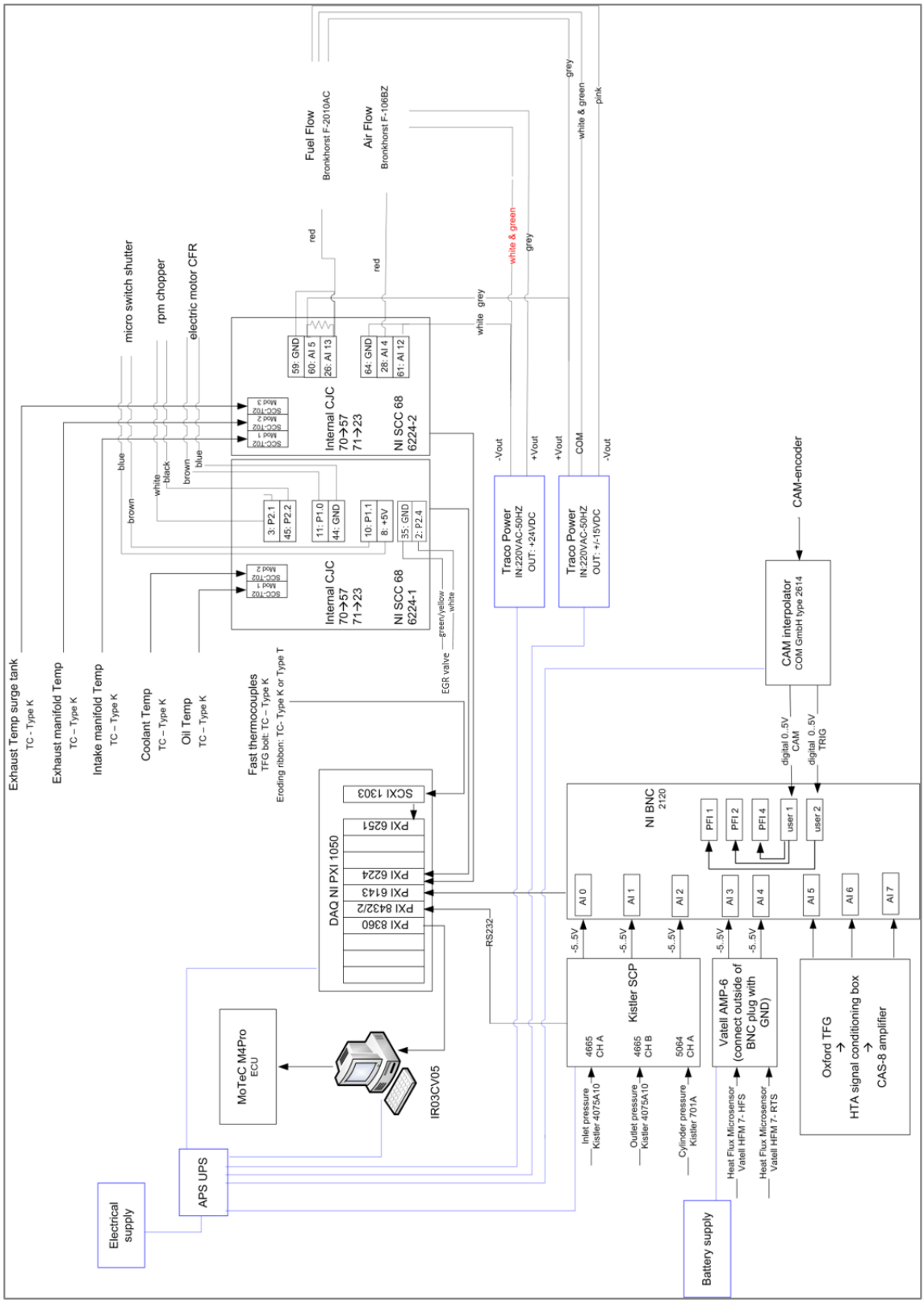

Figure 3.3: Measuring system of the CFR engine

the same during an experiment, therefore a PID-controller is installed. The temperature at the inlet of the engine is used to give feedback to the controller. It was observed during the measurements that the inlet temperature varied only $3°C$ around the set point.

To control and monitor the amount of exhaust gases, some additional sensors are used. In order to avoid condensate in the recirculated exhaust gas, a thermocouple at the end of the EGR loop is installed to monitor the exhaust gas temperature. At the inlet and outlet a branch point that leads to the emission analyser is foreseen to monitor the fraction of CO_2. With these CO_2 concentrations the %EGR can be calculated. However, during the measurements it was observed that when applying EGR, the total mass of air, EGR and fuel that was drawn into the cylinder, dropped quite drastically. When applying EGR it is normal that the volumetric efficiency drops a bit, but not as much as observed. It is believed that the branch point at the inlet is installed too close to the mixing section of fresh air and recirculated exhaust gas. As a consequence, an incorrect fraction of CO_2 is measured at the inlet, leading to a faulty percentage of EGR. Instead, to determine the %EGR, a method based on a volume balance is used. This method assumes that the total mass introduced in the cylinder is independent of the gas properties. This way, two situations can be compared: one with and one without EGR. The difference of air volume flow rate between these two situations then is the EGR volume flow rate. Normally an engine setup does not dispose of an air preheater. Without an air preheater the total mass introduced in the cylinder drops when applying EGR because the temperature of the exhaust gases is higher and the density is lower than that of fresh air. A volume balance then introduces a big error. Since the new setup disposes of an air preheater, the temperature of the entire mixture can be kept constant with and without EGR. The volume balance method is quite accurate in our case but still the calculation of the %EGR with this method is an indication of the real %EGR. The principle of the volume balance method can be found in appendix C.1.4. For accurate measurements in the future, it is recommended to replace the branch point at the inlet further from the mixing section of fresh air and exhaust gas in order to get a better mixing.

Two fuel injectors are installed. One before and one after the air preheater. The injector after the heater will give a good image of a realistic application. To make sure that the mixture that is sent into the cylinder is completely homogeneous, a distance of 180 mm between the injector and the intake valve is chosen. This is also done in other setups [14].

Notice that the preheated air will cool down, since the injected fuel will have to evaporate. With the injector in front of the air preheater the effect of latent heat will not be present,

the air/exhaust gas/fuel-mixture will be heated uniformly. Since the gases have to travel through the heater and pipes, which are located a considerably long distance from the engine inlet, the mixture will certainly be homogeneous. The problem with an injection this far away from the inlet is the engine mapping: if a wrong air to fuel-ratio is measured, the changes in injected quantity will take some time to reach the engine. The engine mapping will have to change in order for this injector to work. In this research, only the injector after the heater is used, which is closest to real application.

3.2.1 EGR

When choosing an EGR valve, several factors need to be taken into account. The temperature and the mass flow through the valve are the most important. It is preferred to use an electromagnetic valve instead of a manually operable butterfly valve. Because our CFR engine only works at 600 rpm, the butterfly valve results in an on/off-regulation which is unwanted. An electromagnetic EGR valve can be used to regulate the rate of EGR by using PWM (Pulse Width Modulation). The EGR valve can be regulated by changing its frequency and duty cycle.

As for temperature, the exhaust gases of an HCCI engine can reach temperatures up to $400°C$. When flowing through the pipes, the temperature will drop and condensation could occur. A band heater will keep the temperature of the gases up to $\pm 100°C$, avoiding condensation. The EGR valves by Pierburg can withstand temperatures up to $560°C$, so temperature will not be an issue.

To control and monitor the exhaust gas recirculation the %EGR is defined as follows:

$$\%EGR = \frac{\dot{m}_{EGR}}{\dot{m}_{EGR} + \dot{m}_{air} + \dot{m}_{fuel}} \tag{3.1}$$

There are three mass flows that need to be measured. The air mass flow is measured with a Bronkhorst F-106BZ mass flow sensor. The fuel mass flow was determined gravimetrically at first. However, it was observed during the measurements that the fuel was heated by the fuel pump to temperatures up to $62°C$. This caused the fuel to evaporate in the measuring cup, which was used to determine the fuel rate gravimetrically. Consequently, a higher fuel rate was measured than in reality. This was confirmed when the air to fuel ratio was calculated with the excess air measured by the emission analyser. Differences in λ of 1.5 were measured between the gravimetrically determined λ and the λ determined from the emission analyser. Therefore it was decided to determine the fuel mass flow with

the measured air mass flow and the λ determined from the emission analyser with the equation of *Brettschneider* [23]. This equation can be found in appendix C.1.3. Because of the measurement error of such emission analysers, there is also an error introduced on the excess air ratio. For this thesis, the excess air ratio λ is only an indication of the real excess air ratio. For further research it is absolutely necessary to control the temperature of the fuel in order to determine the fuel mass flow gravimetrically and consequently the excess air ratio accurately. The EGR mass flow however cannot be measured directly. The high temperatures and chemically aggressive nature of exhaust gases make it difficult to develop a mass flow sensor that can withstand exhaust gases. Nevertheless, *Pierburg* has recently constructed such an exhaust gas mass flow sensor with 2% accuracy that can withstand temperatures up to $300°C$. Unfortunately it could not be purchased because it was still under development at the time the mass flow sensor was needed. Instead, the EGR mass flow is determined as explained earlier, with a volume balance. Figure 3.5 shows the EGR valve.

Figure 3.5: Pierburg EGR valve

3.2.2 Air preheater

The air preheater should be able to heat up the mixture of air, exhaust gas and fuel to temperatures of $400°C$ at a flow rate of 3.06 g/s. The required power of the heater is calculated using the data in table 3.2.

The maximum capacity that is calculated to heat an air/fuel-mixture up to $400°C$ is around 2 kW. This is not taking EGR into account. When EGR is applied, the heat capacity

Table 3.2: Power needed to heat a gas from $20°C$ up to $400°C$.

		dry air	gasoline	methanol	ethanol	EGR (100%)
Heat capacity [J/g.K]	liq.		2.22	2.48	2.43	
	gas	1.02		1.92	1.90	1.234
$T_{autoignition}[°C]$			280	470	360	
Latent heat [J/g]			310	1115	837	
Flow at WOT [g/s]		3.06	0.21	0.48	0.34	3.54
$Power_{20°C \rightarrow 400°C}$[W]		1190	180	900	600	1750

rises, leading to a higher demanded power. Overall this would not change the demanded power that much. Another important issue is the corrosion resistance. Since aggressive exhaust gases will pass through the heater, it must be (highly) corrosion resistant to avoid future problems. Taking these requirements into account, a gas recirculation heater by Osram of 6 kW is used in the setup. The reason why such a high power is chosen, is that for a smaller power the diameter of the heater was too small. This could choke the air stream and lead to pressure drops. Figure 3.6 shows the heater.

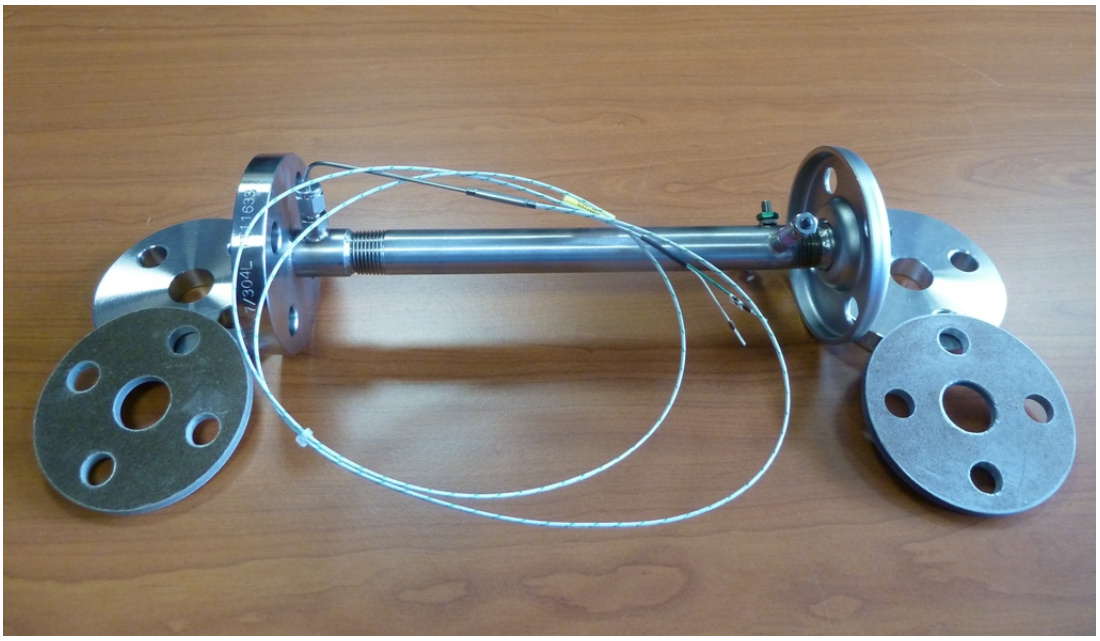

Figure 3.6: The used inline heater by Osram

3.2.3 Final build

With the EGR valve and air preheater selected, the system needs another few adjustments.

pipes All the piping around the CFR engine is renewed. The new pipes are made from the corrosion resistant INOX. The inlet and the exhaust still have the same diameter as in the original setup. The pipes used for the EGR loop also have the same diameter.

In the EGR loop, a flexible part is inserted. This should damp out the vibrations of the engine and also anticipate thermal expansions which could lead to stress in the pipes and system.

surge vessel Because it was too difficult to start the EGR loop from the existing exhaust surge vessel we installed a second exhaust surge vessel in the EGR loop. The volume of a surge vessel for a four stroke engine should be at least 50 times the cylinder volume [24]. The cylinder volume is 619cc so the surge vessel needs to have a volume of 31 liter.

back-pressure valve Back-pressure is necessary to let the exhaust gases stream to the inlet, otherwise they will flow straight to the exhaust. The back-pressure is generated by a manually operable butterfly valve that is resistant against high temperatures. The more the valve is closed, the bigger the possible EGR rate. Attention is needed, since this back-pressure will also have a negative effect on the efficiency of the engine.

A SolidWorks drawing of the whole system, electric parts and wiring not included, can be found in figure 3.7 and in appendix A.

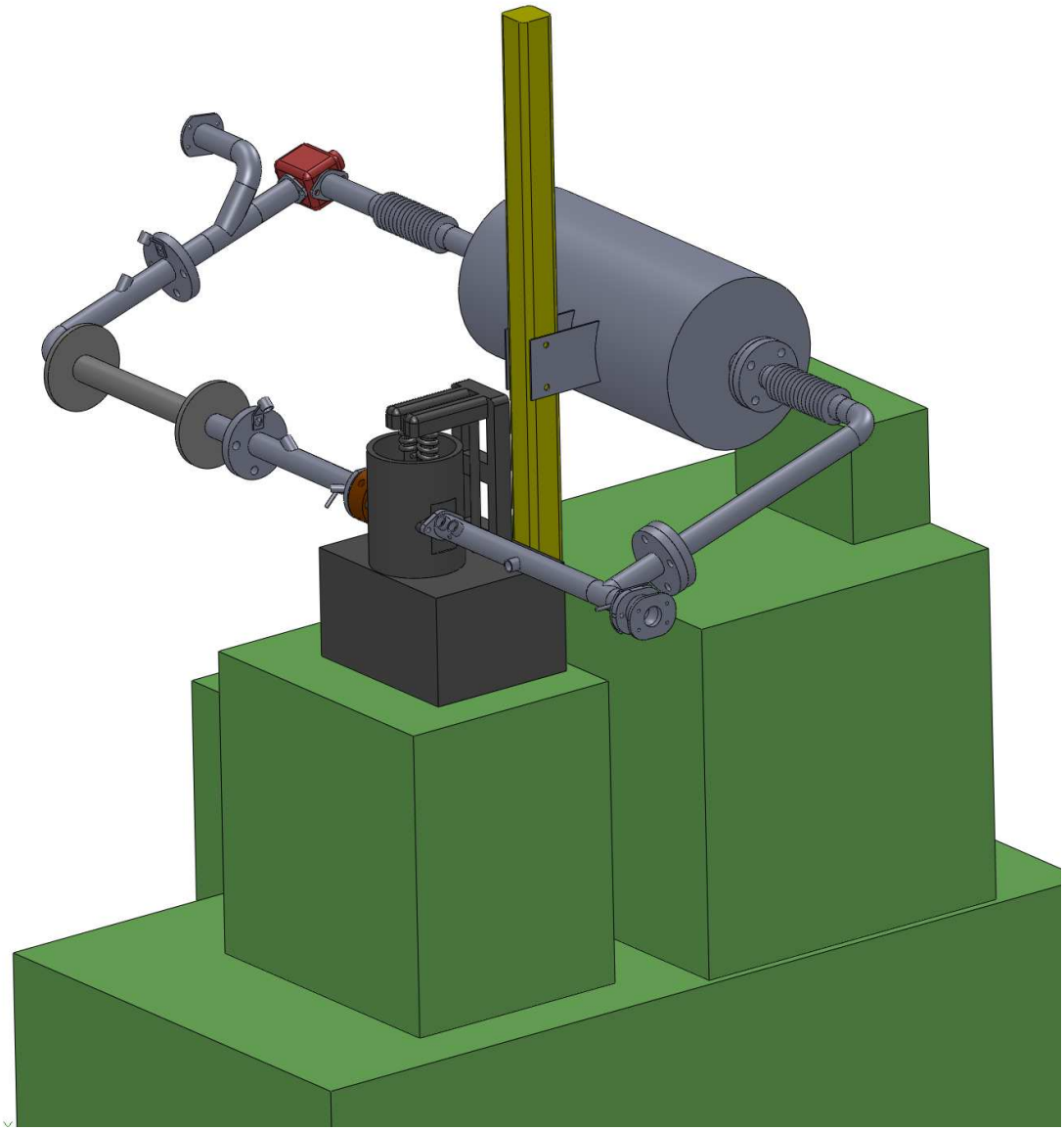

Figure 3.7: Assembly drawing of whole system

Chapter 4

Heat Release Analysis

After the setup is constructed and validated, the CFR engine is able to run in HCCI operation. For the validation of the system, we refer to appendix B. The main objective is to perform heat flux measurements for HCCI combustion. Using a heat release analysis, it is possible to validate the correctness of the heat flux measurements and the assumption that measurements with one heat flux sensor is an acceptable representation for the global heat flux. In this chapter the heat release analysis is explained, this includes the determination of the specific heat ratio and the Heat Release Rate (HRR) in order to calculate the cumulative heat release.

4.1 Heat Release Rate

As already said in the introduction and previous sections, the wall heat transfer is an essential part in understanding the HCCI combustion process because it determines the thermal conditions of the combustion chamber. The thermal conditions and mixture composition determine the timing of the SOC. Temperature is strongly influenced by the wall heat transfer. To determine the wall heat transfer or heat flux, there are two possibilities. You can measure it directly using a heat flux sensor or you can derive it from a pressure trace by performing a heat release analysis. In this thesis the heat flux is measured with a heat flux sensor and checked with a heat release analysis, because that way the assumption of very low spatial variations with HCCI combustion can be validated. The correctness of the heat flux sensor can be checked as well.

To carry out the heat flux measurements only one single-layer TFG sensor will be used, at the cylinder head. One may notice that this will give inaccurate results, because of spatial variations in the cylinder. This holds true for SI and CI combustion, but not for

the HCCI combustion process. The homogeneous character of the mixture and the fact that the combustion starts at multiple locations at the same time results in a uniform combustion and thus little spatial variations. Research has confirmed these low spatial variations [20]. Figure 4.1 shows the heat flux measured at multiple sites of the combustion chamber surface for a homogeneous charge spark ignition engine. Heat flux at the piston side shows a higher peak and faster rise than at the head side. Figure 4.2 shows heat flux traces for HCCI combustion. All head and piston local heat fluxes show similar traces. This is a good indication that the energy release for a premixed HCCI engine is sufficiently homogeneous with no macroscopic flame propagation. With this knowledge we will assume that the heat flux measured at the cylinder head is the averaged heat flux in the cylinder. As a consequence of this assumption, the heat flux coefficient that is calculated from the measured heat flux represents the global heat flux coefficient for the entire cylinder. This hypothesis could be checked by performing a heat release analysis. However, from figure 4.2 it can already be seen that there are some minor differences in the various heat flux traces for HCCI combustion. There will never be a hundred percent homogeneous reaction and wall temperatures at different surfaces in the cylinder will not be exactly the same. Research [20] has shown that a spatially averaged heat flux is a very good assumption to determine the global heat flux. This can be seen from figure 4.3. The heat loss was determined from the spatially averaged heat flux traces from figure 4.2. But of course, to determine a spatially averaged heat flux, multiple heat flux sensors must be placed in the cylinder walls, and in this research, only one TFG heat flux sensor is available.

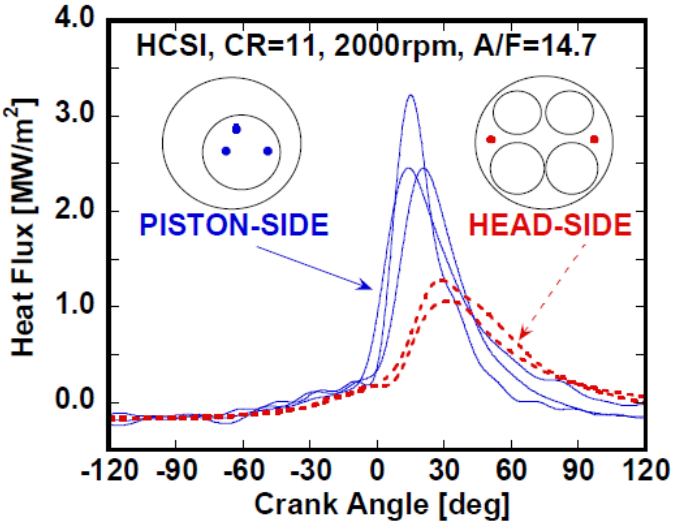

Figure 4.1: Spatial variations of instantaneous local heat fluxes in a homogeneous charge SI engine [20]

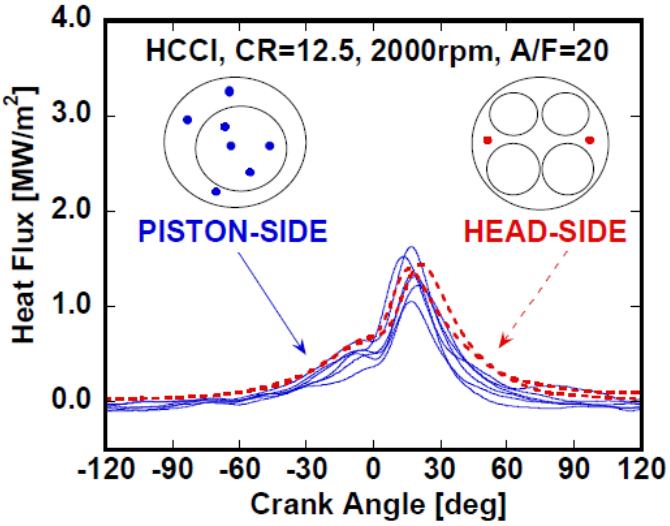

Figure 4.2: Spatial variations of instantaneous local heat fluxes in a premixed HCCI engine [20]

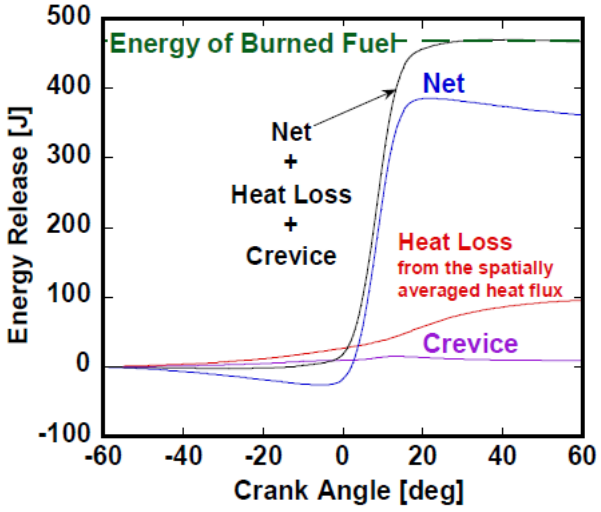

Figure 4.3: Cumulative heat release profile with net heat release calculated from the measured pressure trace and experimentally determined heat transfer [20]

A heat release analysis is frequently used for combustion diagnostics. It is derived from the cylinder pressure trace, which can be a single trace or an average of a large number of cycles. An accurate heat release analysis therefore relies on robust and accurate pressure measurements. A single-zone model will be used to determine the state of the cylinder content in terms of average properties. There is no distinction between burned and unburned gas zones. This is justified by the uniform character of HCCI combustion. On the

other hand, variable gas properties for the mixture as a whole during the combustion cycle will be used, resulting in a variable ratio of specific heats as will be explained in section 4.2.

A heat release analysis itself is an expression of the first law of thermodynamics. The energy that is contained in the fuel is released as work on the piston, sensible heat in the cylinder and heat losses to the wall:

$$\delta Q_{ch} = \delta U_s + \delta W + \delta Q_{ht} \tag{4.1}$$

in which δQ_{ch} is the chemical energy released from the fuel, δU_s is the sensible energy change of the mixture, δW is the work done by piston movement and δQ_{ht} is the heat exchange from the gas to the walls. To be fully correct, you also need to include a term that takes crevice losses into account. This is because the fuel that gets trapped into the crevices does not contribute to the pressure the same way the fuel in the cylinder does. Take note that the volume of the crevices only range to a few percent of the swept volume. This makes it justifiable to neglect these losses. This has already been done for a heat release analysis for HCCI on a CFR engine [25]. In equation 4.1 the first two terms on the right hand side can be described as the net heat release. The net HRR can be written as:

$$\frac{\delta Q_{net}}{dt} = \delta U_s + \delta W = \frac{\gamma}{\gamma - 1} p \frac{dV}{dt} + \frac{1}{\gamma - 1} V \frac{dp}{dt} \tag{4.2}$$

The derivation of this formula can be found in appendix C.

4.2 Variable Specific Heat Ratio

In the previous section, the HRR is calculated using pressure, volume and specific heat ratio. Since the specific heat ratio γ is a function of gas composition and temperature, it changes during the combustion cycle. To calculate the HRR, γ should be known during the closed part of the cycle, from IVC to EVO. During this part, the temperature of the mixture changes and so does its composition, resulting in a changing γ.

The specific heat ratio can be calculated as follows:

$$\gamma = \frac{c_p}{c_v} = \frac{c_p}{c_p - R} \tag{4.3}$$

since,

$$c_p = R + c_v \tag{4.4}$$

Using the right hand side of equation 4.3, γ can be calculated using the specific heat at constant pressure and the specific gas constant of the gas. The variation of these two components causes the γ to change.

4.2.1 Variation of the specific gas constant

The specific gas constant R varies only with the gas composition and is independent of temperature. In our model, the fraction of the mixture that is burned, changes linear during the combustion. This causes the R to be constant before and after the combustion and to change linear during the combustion. An increasing R during combustion, results in an increasing γ. A decreasing R, results in a decreasing γ. The specific gas constant for some important gases is shown in table 4.1. These values are calculated as the ratio of the universal gas constant and the molar mass of the gas. The universal gas constant is equal to 8.3145 $J/mol \cdot K$.

Table 4.1: Specific gas constant for different gases

Gas	R [J/kg.K]
Air	287.1
O_2	259.8
N_2	296.8
H_2O	461.5
CO_2	188.9

4.2.2 Variation of the specific heat

The specific heat of a gas changes with composition and temperature. So during the cycle the temperature and gas composition has to be known for every time step. The gas composition is known before, during and after the combustion. Because the mixture at the inlet is known, the gas composition during and after combustion can be derived from an ideal reaction equation. The temperature can be calculated during the closed part of the combustion cycle, using the ideal gas law 4.5:

$$p \cdot V = m \cdot R \cdot T \tag{4.5}$$

Take note that when the ideal gas law is used to determine the temperature, a single-

zone model is assumed. As already explained, this is an acceptable assumption for HCCI combustion due to its uniform character. Simulation software using multi-zone models for HCCI do also exist, but are beyond the scope of this thesis [26]. In the work of *Heywood* [27] figure 4.4 can be found, which shows the heat capacity for unburned and partially burned mixtures as a function of temperature and equivalence ratio ϕ, which is the inverse of the excess air ratio λ.

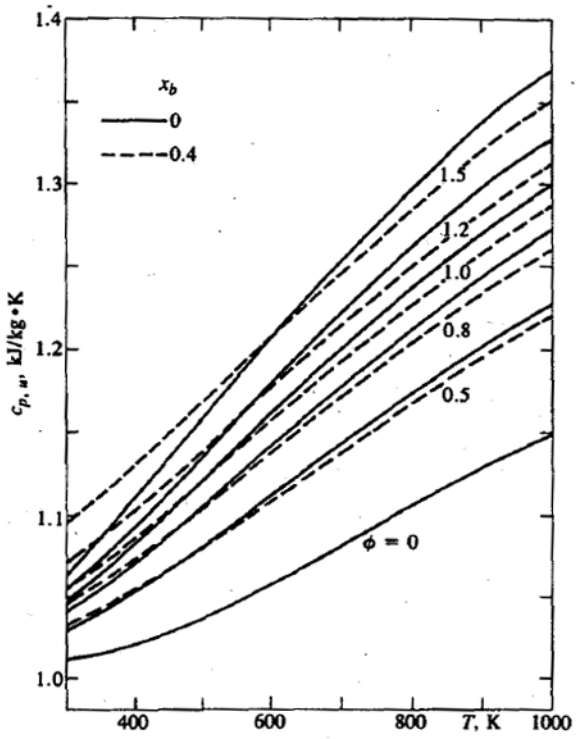

Figure 4.4: Specific heat as a function of temperature, equivalence ratio and burned gas fraction $x_b = 0$ (unburned) and $x_b = 0.4$ (partially burned) [27]

To validate our calculation method, the specific heat during combustion is calculated for SI with gasoline as a fuel and stoichiometric operation. The result can be found in figure 4.5. As can be seen on the figure, the curve follows the same course as in *Heywood* his findings. During the combustion there is a transition from the curve of the specific heat for the unburned mixture to the curve for burned mixture. It can also be concluded that an increasing temperature results in an increasing specific heat. The specific heat of the exhaust gases is higher than that of the unburned gases as expected, but only for low temperatures. For high temperatures the specific heat of the exhaust gases becomes lower

than the one for unburned gases. The curves for unburned and burned mixtures always tend to cross each other around 500 to 600 K. This might seem surprising because the abundance of triatomic molecules in the burned mixture indicates a higher specific heat. We checked this particularity and saw that different sources confirmed this phenomenon [28]. As can be seen in Figure 4.4, the dotted line (which is the line for a partially burned mixture) also crosses the curve of the unburned mixture around 500 to 600 K.

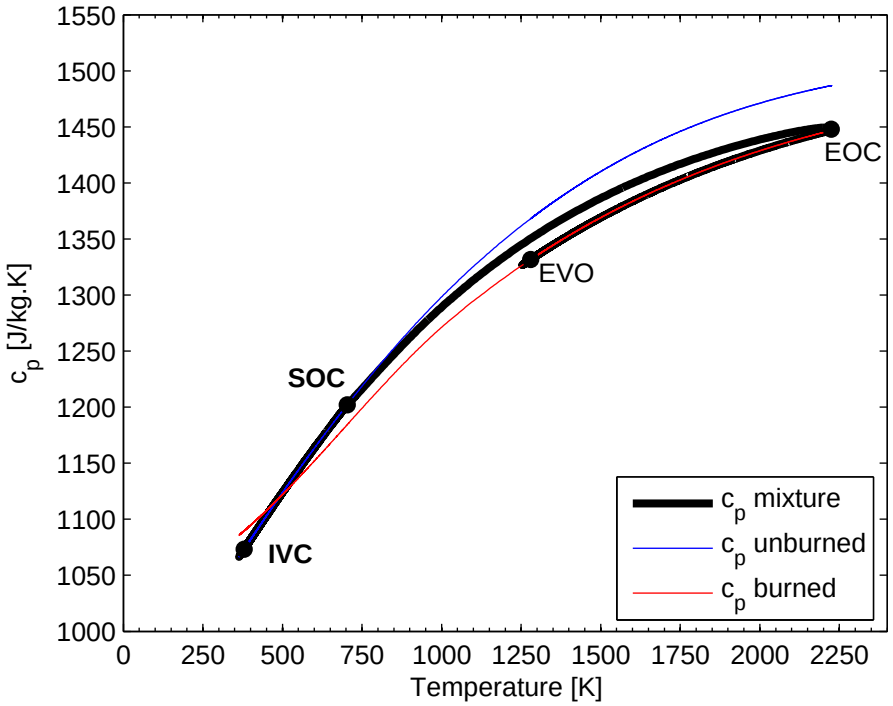

Figure 4.5: Specific heat during the closed part of the combustion cycle as a function of temperature for gasoline, $\lambda = 1$, IGN=13°$BTDC$

4.2.3 Variation of the specific heat ratio

In the course of time different models have been established to determine the specific heat ratio during compression, combustion and expansion. A summary of different specific heat ratio models has been created by *Klein and Eriksson* [29]. At first, a linear model was used by *Gatowski et al.* [30]. In this model, it is assumed that the specific heat ratio is a linear function of temperature. Later, a segmented model was used by *Heywood and Chun*. They segmented the closed part of the combustion cycle into three parts: compression, combustion and expansion. During the compression and expansion, the specific heat ratio varies linear with the temperature. During combustion, the γ is assumed to be constant. A third type of model is the polynomial model. Different polynomial models

have been constructed by *Brunt* [31], *Ceviz* [10], *Egnell* [32] and others. Some of these models also take gas composition into account. Besides these models, there also exist some computational programs like CHEPP and NASA which can be used to calculate the specific heat ratio. The decision to use the models or to use the programs depends on the time and effort one wants to put into the calculation. The programs are simulating the various conditions and therefore they are rather time consuming. The models on the other hand are easy to use and less time consuming, but a bigger approximation of the reality. *Brunt* [31], *Egnell* [32] and *Ebrahimi* [33] showed that the value of the specific heat ratio has a large impact on the heat release analysis. In order to perform a good heat release analysis, a proper γ is needed.

In this research, the γ is calculated directly using equation 4.3, where c_p and R are determined every time step during the closed part of the cycle. Figure 4.6 shows the result of other specific heat ratio models compared to our result. The experiment was carried out for SI combustion, gasoline as fuel and λ equal to 1.

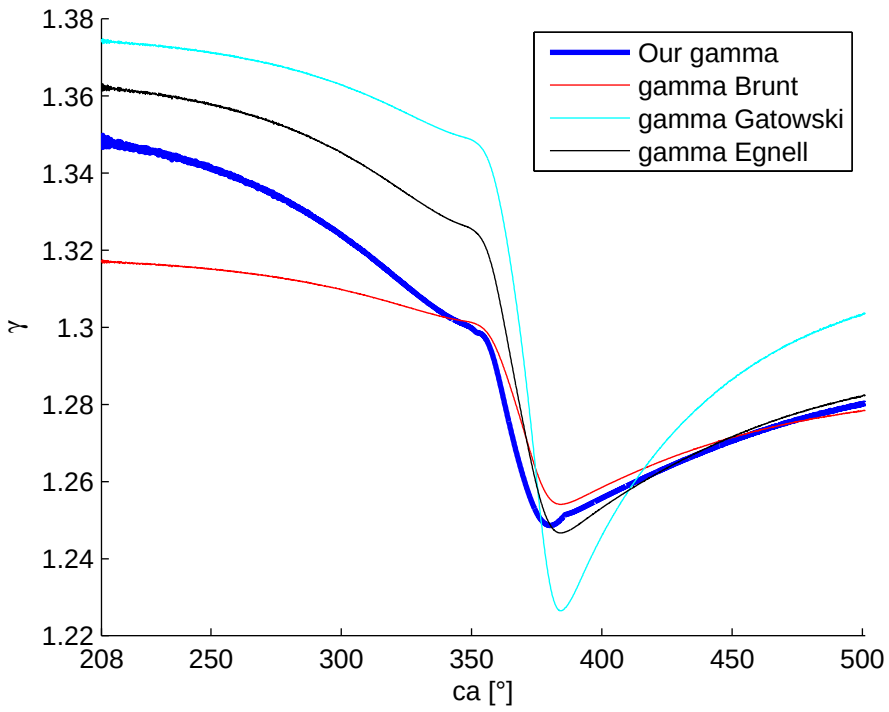

Figure 4.6: Specific heat ratio during the closed part of the combustion cycle for gasoline, $\lambda = 1$, IGN=15°$BTDC$

On this figure, it can be seen that *Gatowski* deviates the most from our result. It is

the most simplistic model assuming that γ is a linear function of temperature. The gas composition is not taken into account. *Brunt* uses a second order function based on measurements with C_8H_{16}. His function is the mean function for different air to fuel ratios, thus introducing errors. It is unclear for which temperature interval *Brunt* evaluated his function, but this also plays an important role in the correctness of his model. It can be seen that *Brunt* his model comes close to ours during combustion and expansion. *Egnell* also comes close to our model during and after combustion. His function is only valid for λ equal to 1 and most accurate for high temperatures above $800K$, since then the combustion takes place. *Assanis* also determined a variable specific heat ratio [20]. He made the calculations for HCCI using a chemical equilibrium program, similar to the NASA program. He constructed his function by fitting the results of the program to a 3^{rd} order polynomial. He also took the average of different measurements to take out the dependency of the specific heat ratio to the AFR, which can introduce an error. Since HCCI combustion deviates from SI combustion, these results could not be compared to ours.

Our variable γ is also compared to the findings of *Ceviz*. In figure 4.7 the specific heat ratio for the unburned and burned gases as a function of temperature can be found, next to our result for γ. Both results are shown for λ equal to 1. It can be seen that our specific heat ratio comes very close to the specific heat ratio of *Ceviz*. As can be seen from the figure, the red line follows the green line quite well up to 1000K. From then on it shifts towards the blue line which represents the γ for the burned mixture. The red line reaches a maximum temperature at the end of combustion and then turns back on the x-axis because temperature drops due to expansion and heat losses. As explained before, despite the abundance of tri-atomic molecules, the γ for the burned mixture is higher than for the unburned mixture because of a lower specific heat at this elevated temperatures together with a higher specific gas constant for burned gases.

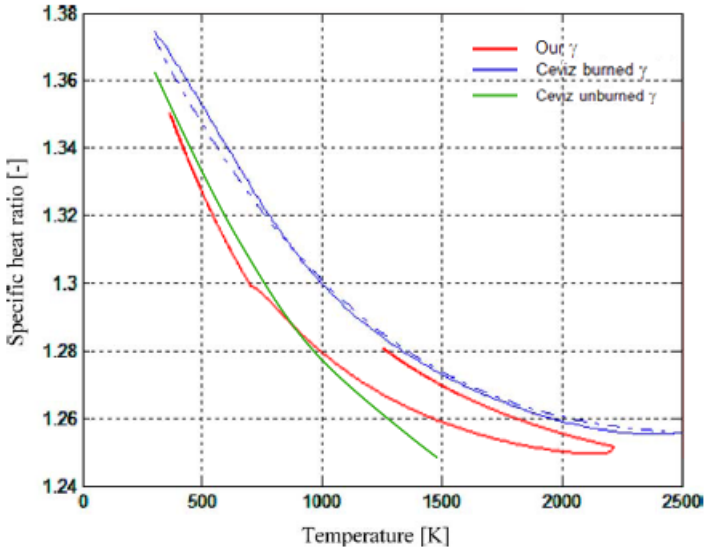

Figure 4.7: Specific heat ratio as a function of temperature for unburned mixture and burned mixture using *Ceviz* his function together with our specific heat ratio during the closed part of the combustion cycle

The calculated specific heat ratio from our model is also compared to *Heywood* his findings [27]. In figure 4.8, curves of the specific heat ratio that he found, are shown. It shows the γ as a function of temperature for different equivalence ratios and mass fraction burned. On the figure, our result is shown as well, for an experiment with SI combustion, gasoline as a fuel and λ equal to 1. It can be seen that the result comes very close to *Heywood* his result. Take note that in our curve the mass fraction burned is not constant, but changes during combustion. The combustion starts at around $700K$. From then on, γ increases as more burned gases are replacing the unburned gases.

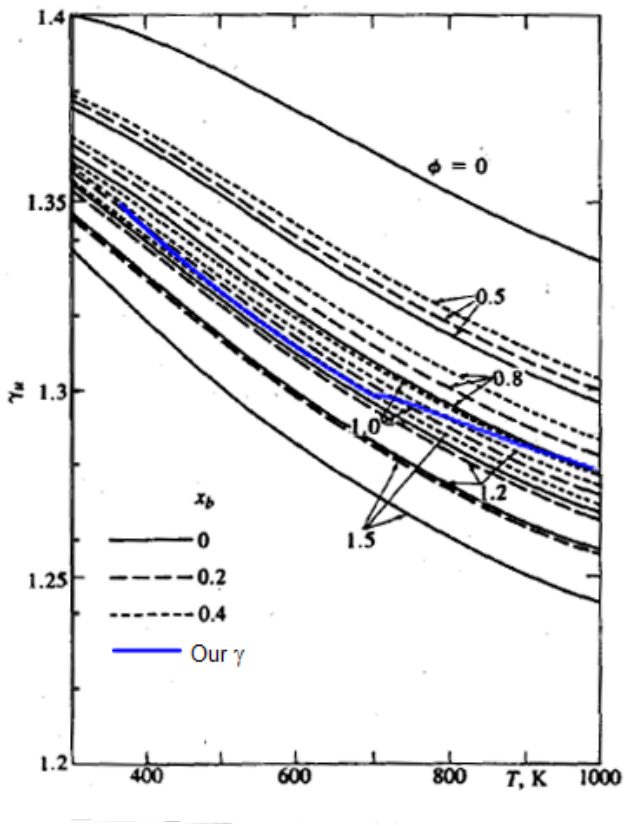

Figure 4.8: Specific heat ratio as a function of temperature, equivalence ratio and burned gas fraction $x_b = 0$ (unburned), $x_b = 0.2$, $x_b = 0.4$ (partially burned). Next to our result for the closed part of the combustion cycle till $1000K$ using SI with gasoline as fuel for $\lambda = 1$, IGN=$15°BTDC$ [27]

Having compared our model to other models, it can be concluded that our results come close to theirs. Differences between models can be explained by differences in simulating or obtaining results, the method that is being used to fit the results to a function and the predetermined conditions of the experiment or simulation (e.g. fuel, AFR). Take note that the mentioned models all are an approximation of measurements or simulations and they all are general polynomials as a function of temperature and sometimes also λ. These polynomials do not take, for instance, the type of fuel into account. Since our specific heat ratio is calculated using the in-cylinder pressure trace and the gas properties determined for every sample, one could assume our result will be more accurate.

4.2.4 Effect on Heat Release Rate

After defining the correct specific heat ratio during the closed part of the combustion cycle, γ can be filled out in equation 4.2. The effect of a variable γ instead of a constant γ can be seen in figure 4.9. In this figure the HRR is shown for a variable γ, $\gamma = 1.35$ and the mean value of the variable γ during the closed part of the combustion cycle: $\gamma = 1.2973$. The measurement is done in SI operation, using gasoline as fuel at λ equal to 1. It can be seen that when a constant value is assumed for the specific heat ratio, the HRR is significantly underestimated. This is the reason why a variable γ is needed. An underestimated HRR results in an incorrect lower cumulative heat release. These findings also corresponds to *Ebrahimi* his results [33].

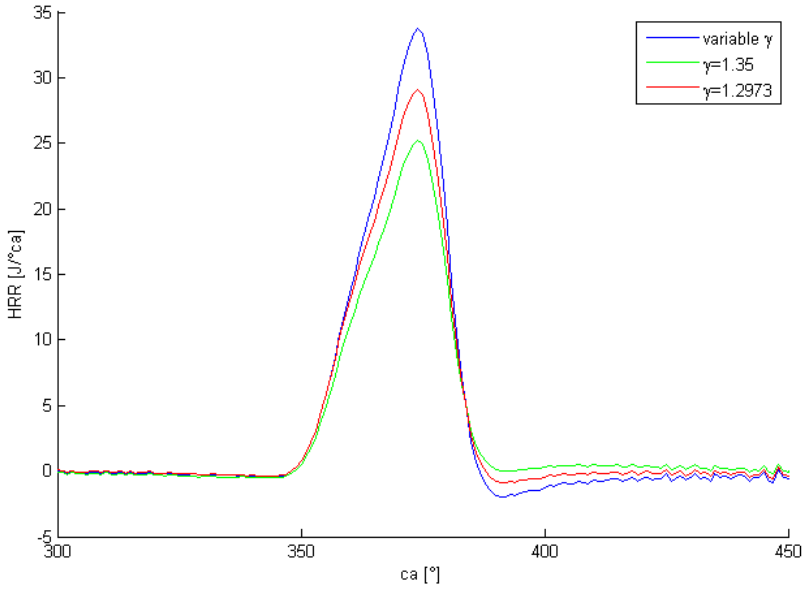

Figure 4.9: Heat Release Rate as a function of $°ca$ for different values of γ

4.3 Cumulative Heat Release

The reason why this heat release analysis is done, is to verify the results of the heat flux sensor. As already said in the introduction of this chapter, the heat flux can be measured and estimated in two ways. With a heat flux sensor one can measure it directly and with a heat release analysis one is able to estimate it from the pressure trace. The key to validating the heat flux sensor is to add the measured wall heat flux to the net heat release in order to satisfy the energy equation. By integrating equation 4.2 the net cumulative heat release

(CHR) is obtained. By integrating the measured wall heat flux, the cumulative heat loss is obtained. Adding both should equal the chemical energy contained in the burned fuel, assuming ideal combustion. Take note that the net CHR and wall heat loss are equal to $0J$ at SOC. Unfortunately, ideal combustion is never reached. This means that the amount of burned fuel is not equal to the amount of fuel introduced in the combustion chamber. Some of the mixture gets trapped into crevices between the cylinder wall, the piston and the piston rings, and some of the fuel is quenched against the cylinder wall. The most important source for unburned or partially burned fuel is the fact that with HCCI combustion the in-cylinder temperature remains low due to the diluted mixture. To account for these fuel losses, one can introduce a combustion efficiency η_{comb}:

$$Q_{ch,burned} = m_f \cdot LHV_f \cdot \eta_{comb} \tag{4.6}$$

The combustion efficiency could be determined by the measured exhaust gas composition. Unfortunately, for this thesis it was not possible to determine the combustion efficiency properly because of large uncertainties concerning the amount of injected fuel. As explained in chapter 3 the fuel mass flow rate could not be determined gravimetrically because of heating of the fuel by the fuel pump. The fuel mass flow in this thesis is determined with the measured air mass flow and the λ determined from the emission analyser with the equation of *Brettschneider* [23]. This introduces a substantial error on the fuel rate. This made a correct determination of the combustion efficiency impossible. Other papers mentioned combustion efficiencies between 0.9 and 0.98. These values are an indication, but may not be used since the combustion efficiency is dependent on the engine and the operating conditions. In order to perform a correct heat release analysis, the combustion efficiency has to be determined for the CFR engine using the right operating conditions.

Next, an example of a heat release analysis is shown. The measurement that is used, was performed in a study on heat losses on a CFR engine in SI operation running on hydrogen by *J. Demuynck* [34]. Since the measurement has proven to be correct, it can be of great use to test the heat release analysis. The operating conditions can be found in table 4.2. In figure 4.10 the results are shown. It can be seen that the sum of the wall heat losses and the net cumulative heat release tend to go to 95% of the energy that is brought into the cylinder by the fuel. This is expected to be a normal combustion efficiency. Unfortunately, the exhaust gasses were not analysed for this measurement. This makes it impossible to calculate the correct combustion efficiency, but seeing this graph it is expected that the heat release analysis will render correct results.

Table 4.2: Operating conditions

Fuel	H_2
Engine Speed [rpm]	600
CR	9
$T_{inlet}[°C]$	45.3
air flow [kg/h]	8.523
λ	1.79
IGN $[°BTDC]$	-5

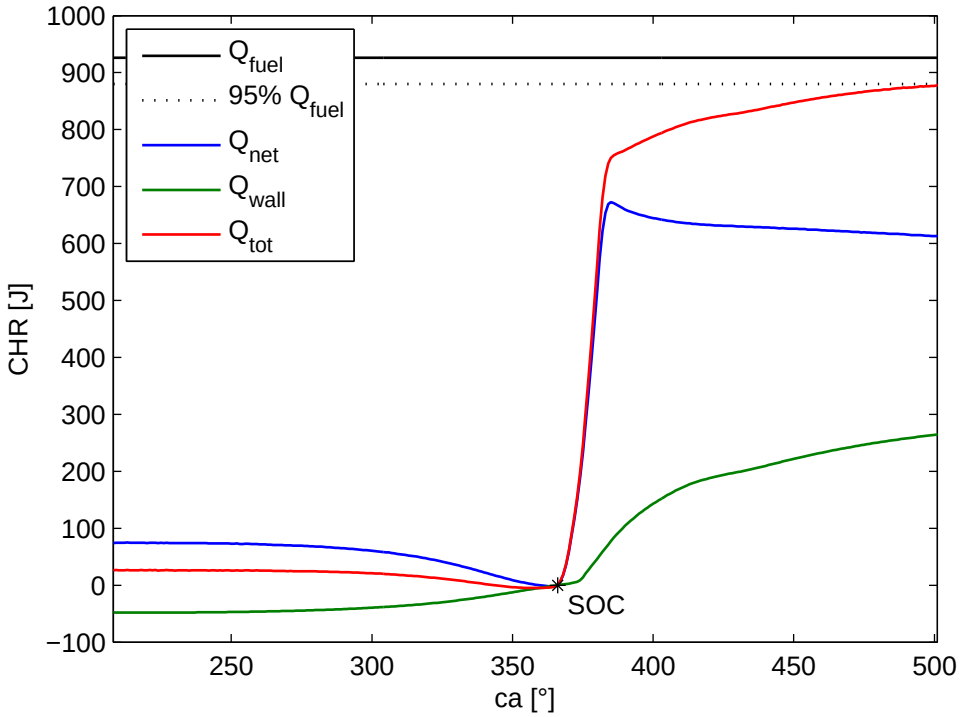

Figure 4.10: Heat release analysis of a CFR engine in SI operation with hydrogen as fuel

Chapter 5

Results

In this chapter, the various measurements that are performed on HCCI combustion will be discussed. All the experiments are carried out using gasoline (Euro 98). First, the engine settings are predicted in order to achieve HCCI combustion on the new engine setup. Next, the influence of the operating parameters is investigated. These are the excess air ratio, inlet temperature, EGR and CR. Finally, heat flux measurements are performed and compared with existing heat transfer models.

5.1 First HCCI measurement

Several experiments on HCCI are carried out in order to get some feeling with this new type of combustion. In order to achieve HCCI combustion for the first time, the inlet temperature of the mixture to obtain HCCI is estimated. *A. Charalambides* [19] found that the main combustion starts at temperatures of about $1050K$ or $777°C$ for iso-octane. To estimate the required inlet temperature, a polytropic process is assumed, see equation 5.1. Since the compression stroke of the combustion cycle can be assumed isentropic, the polytropic index is equal to the specific heat ratio γ. Using the in-cylinder volume at IVC, the in-cylinder volume at TDC and a combustion temperature around $1050K$ at TDC, the inlet temperature can be calculated. Figure 5.1 shows a graph of the needed inlet temperature for different compression ratios, using a γ of 1.35.

$$T \cdot V^{n-1} = C \tag{5.1}$$

For the first measurement on HCCI combustion, a CR of 13:1 is used. From our estimation, the inlet temperature should be around $160°C$. To be sure of HCCI combustion, we set the inlet temperature at $170°C$ and removed the spark plug from the setup. The operating conditions of the measurement can be found in table 5.1, the measured and calculated

data can be found in table 5.2. The excess air ratio is calculated as explained in appendix C.

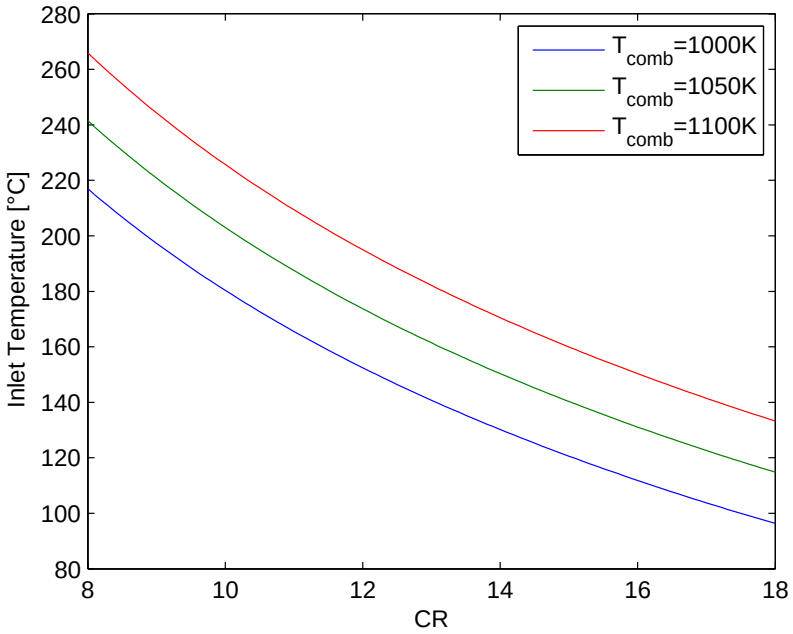

Figure 5.1: Inlet temperature as a function of different compression ratios for $\gamma = 1.35$

Table 5.1: Operating point

Fuel	Gasoline (Euro 98)
Engine Speed [rpm]	600
CR	13:1
$\%EGR$	0
$T_{inlet}[°C]$	170

From these measurements we can verify the most important characteristics of HCCI. First of all, the λ is very high, indicating lean combustion. Running on a λ of 4.62 would be impossible for a SI engine. The indicated efficiency η_i, see equation 5.2, does not turn out to be as high as could be achieved using HCCI. Take note that this efficiency is reached using a CR equal to 13:1. For HCCI operation, higher compression ratios are not uncommon. A higher CR will ensure a higher efficiency. From table 5.2 it can also be seen that the combustion occurs $7°ca$ before TDC and only $5°ca$ after TDC. A relative large amount of negative work is performed on the cylinder. An extra reason for this lower

Table 5.2: Measured and calculated values

λ	4.62
imep [bar]	1.5351
indicated Power (kW)	0.4754
sfc [g/kWh]	252.6
η_i[%]	32.12
CO_2 [vol%$_{dry}$]	3.01
CO [vol%$_{dry}$]	0.171
NO_x [ppm$_{dry}$]	0
SOC [$^\circ ca$]	353
Combustion duration [$^\circ ca$]	12

than expected efficiency could be high pumping work due to the rather old style two valve cylinder head. But as can be seen from Figure 5.3 the pumping work is very low. When this efficiency is compared with the literature, indicated efficiencies between 31 and 37 are acquired for compression ratios between 16:1 and 22.5:1 and 1000 rpm [12]. This is comparable to our result.

The emissions for HCCI operation are also important to investigate. Since a very lean mixture is applied, it is normal that low volume percentages of CO_2 are reached. No NO_X emissions were measured during the experiment, which is an important advantage of HCCI. The reason for this, are the low in-cylinder temperatures. The highest in-cylinder temperature, calculated from the ideal gas law, is $1223^\circ C$, which is below the NO_X-formation temperature. The challenge for HCCI is keeping the CO and HC emissions low. It can be seen that there is a relatively high amount of CO in the exhaust gases, which also can be explained by these low temperatures. Unfortunately, the HC emissions could not be measured. The SOC for this measurement is at $353^\circ ca$, or $7^\circ ca$ BTDC. The SOC is defined as the moment where the heat release rate becomes higher than 1.5 $J/^\circ ca$. As will be discussed in the next section, preheating and EGR can be used to change the SOC. This will affect imep, efficiencies and emissions. As expected, the duration for HCCI combustion is also shorter compared to SI combustion. This gives a higher degree of constant volume. As a result, the thermodynamic efficiency η_{th} increases because the cycle comes closer to the ideal Otto cycle, which is beneficial for the overall efficiency. The expression for thermodynamic efficiency can be found in equation 5.3

$$\eta_i = \frac{P_i}{\dot{m}_{fuel} \cdot LHV_{fuel}} \tag{5.2}$$

$$\eta_{th} = \frac{W_i}{W_{otto}} = \frac{\eta_i}{\eta_{otto}} \tag{5.3}$$

In figure 5.2 a graph for in-cylinder pressure and temperature can be found. The SOC is also shown on both graphs. Note the low in-cylinder temperature and the SOC at a temperature of $735°C$ or 1008K as estimated at the beginning of this chapter.

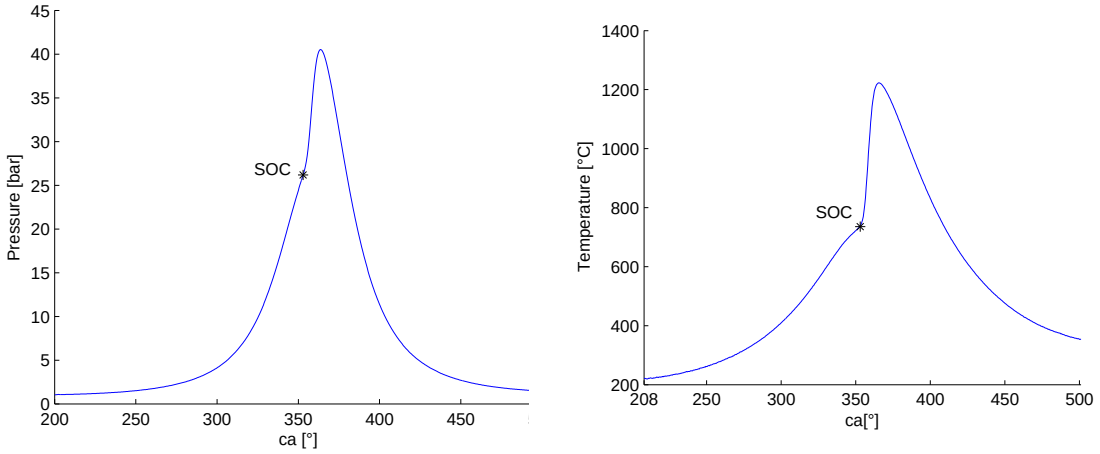

(a) Pressure

(b) Temperature

Figure 5.2: In-cylinder pressure and temperature as a function of crank angle for HCCI operation, $\lambda = 4.62$, $T_{in} = 170°C$, no EGR, CR 13:1

Figure 5.3 shows the pressure as a function of volume. It is clear that there are almost no throttle losses since the experiment was performed at WOT, resulting in a better efficiency. On this graph it can also be seen that after the point of SOC, an almost isochoric compression takes place due to the short and homogeneous combustion of HCCI. This results in a higher degree of constant volume and shifts the combustion cycle closer to the ideal Otto cycle.

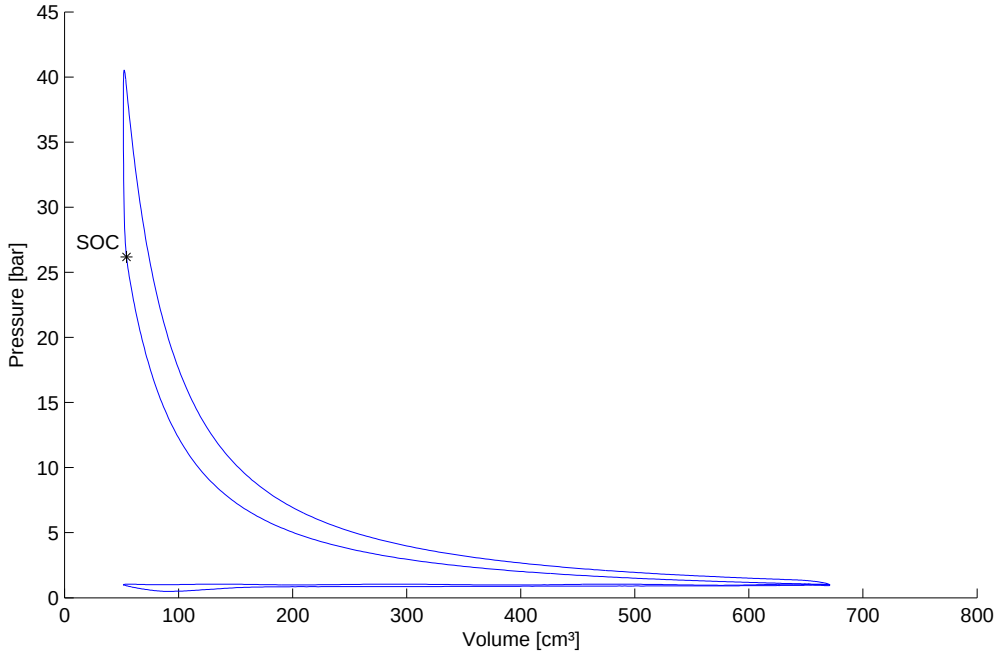

Figure 5.3: Pressure as a function of volume for HCCI operation, $\lambda = 4.62$, $T_{in} = 170°C$, no EGR, CR 13:1

5.2 Influence of engine parameters

In this section, the various parameters that affect HCCI combustion, like EGR, air preheating, excess air ratio and CR will be discussed, based on our measurements. The limitations concerning these parameters will also be discussed. This way we can check the potential and limitations of the new engine setup.

5.2.1 Effects of EGR

The effects of EGR on HCCI combustion will be briefly discussed, for a more thorough research on the effects of EGR, we refer to the literature. The effects of EGR are already mentioned in section 2.3, therefore this experiment serves merely as a validation. The experiment is conducted at a CR of 13:1, a constant fuel rate of about 0.112 kg/h and with an inlet temperature of $170°C$. Figure 5.4 shows the in-cylinder temperature during the closed part of the engine cycle for several EGR rates. The temperature during combustion, as well as the peak temperature decrease with rising EGR rates. The exhaust gas temperature increases slightly with increasing EGR rates. The lower peak temperature and slightly higher exhaust gas temperature can be explained by the slower combustion and later combustion phasing caused by the higher specific heat of EGR during compres-

sion, which can be seen in figure 5.5. This can also be deduced from the HRR in figure 5.6. Take note that changing the amount of EGR also changes the AFR, thus λ, since incoming air is replaced with exhaust gases. Increasing the EGR rate results in a decreasing λ, so a richer mixture is introduced into the cylinder.

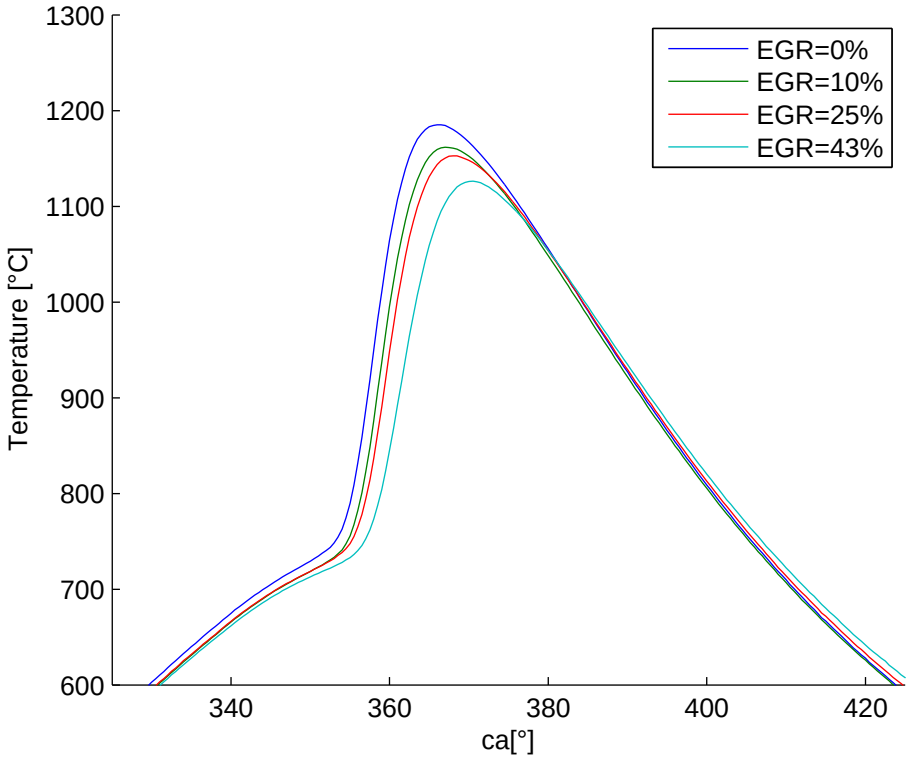

Figure 5.4: Temperature as a function of ca for different EGR rates for $T_{in} = 170°C$ and a constant fuel rate of 0.112 kg/h at CR13:1

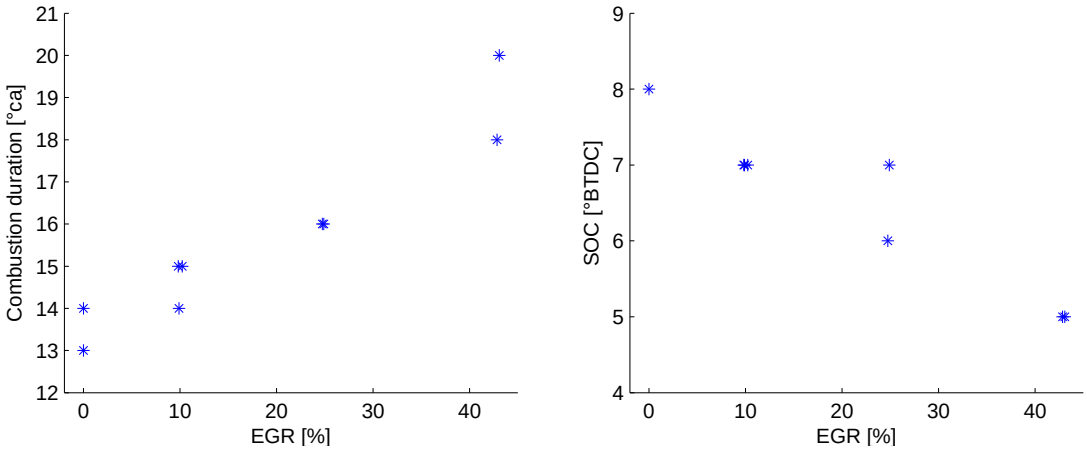

(a) Combustion duration (b) SOC

Figure 5.5: Combustion duration and SOC as a function of EGR rate for multiple measurements per operating point at $T_{in} = 170°C$, a constant fuel rate of 0.112 kg/h and CR 13:1

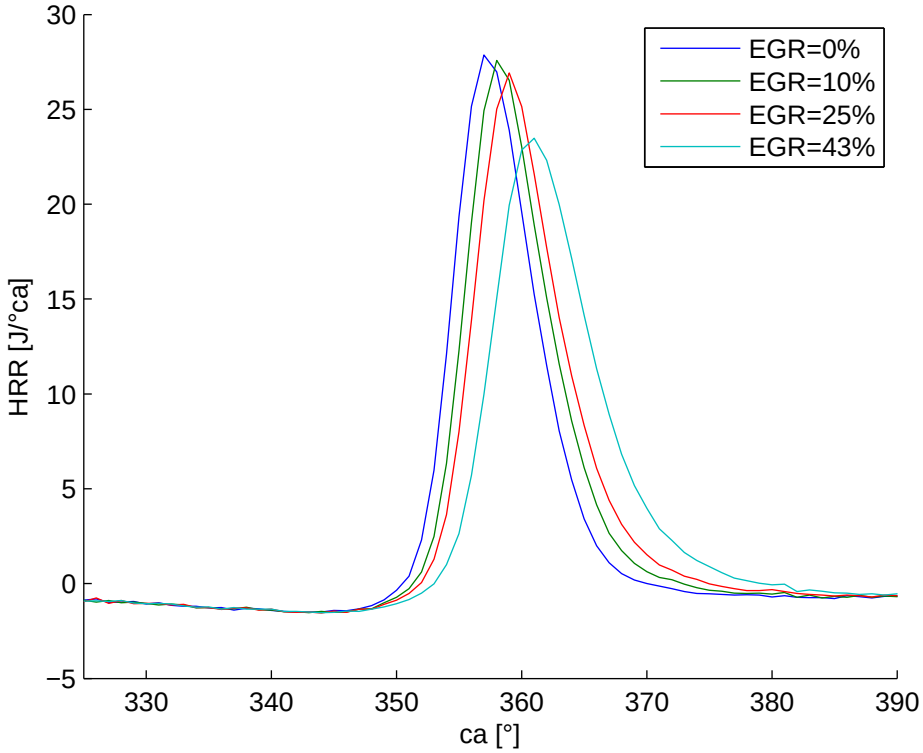

Figure 5.6: HRR as a function of ca for different EGR rates cycle for $T_{in} = 170°C$, a constant fuel rate of 0.112 kg/h and CR 13:1

5.2.2 Effects of preheating

The effects of preheating on HCCI combustion have also already been discussed in section 2.3. For this experiment, the CR is 14.75:1 and the fuel rate is kept constant at 0.100 kg/h. The inlet temperature is changed in steps of $10°C$. In figure 5.7 it can be seen, as expected, that increasing the inlet temperature causes a faster combustion that starts earlier. This happens because the combustion temperature is reached faster when compressing the hot mixture, resulting in earlier combustion. An earlier combustion brings along higher pressures and temperatures which result in a faster combustion. On figure 5.8 the earlier combustion for higher temperatures is also visible. A higher inlet temperature also results in a volumetric efficiency drop. Less mixture is drawn into the combustion chamber because of the lower density with higher temperatures. This would lead to lower pressures. It can be seen that the earlier and faster combustion is the dominant factor, resulting in an overall pressure rise. Take note that a rise in pressure does not necessarily imply a rise in imep. For this measurement the imep rises with higher temperatures, but this is not always the case. Because of the higher temperatures the SOC is earlier and the combustion duration is shorter. This causes the combustion to be phased more before TDC, resulting in more negative work on the piston. From figure 5.7 it can be seen that for a temperature of $130°C$ and $140°C$ the combustion is even phased completely before TDC. This results in a high amount of negative work on the piston. However, due to the early combustion also the pressure rises resulting in a higher amount of positive work on the piston. So there are two counteracting effects that influence the imep.

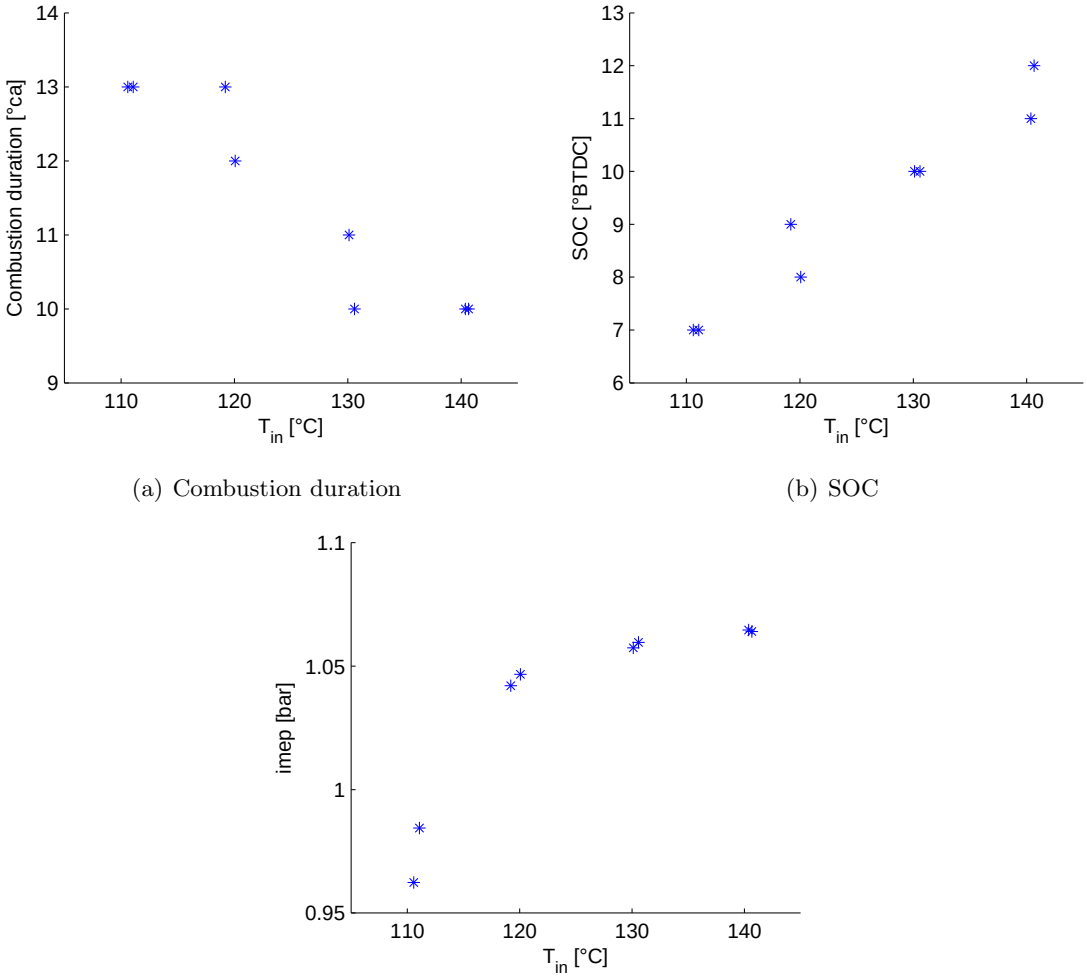

(a) Combustion duration

(b) SOC

(c) imep

Figure 5.7: Combustion duration, SOC and imep as a function of inlet temperature for multiple measurements per operating point for a constant fuel rate of 0.100 kg/h, no EGR and CR 14.75:1

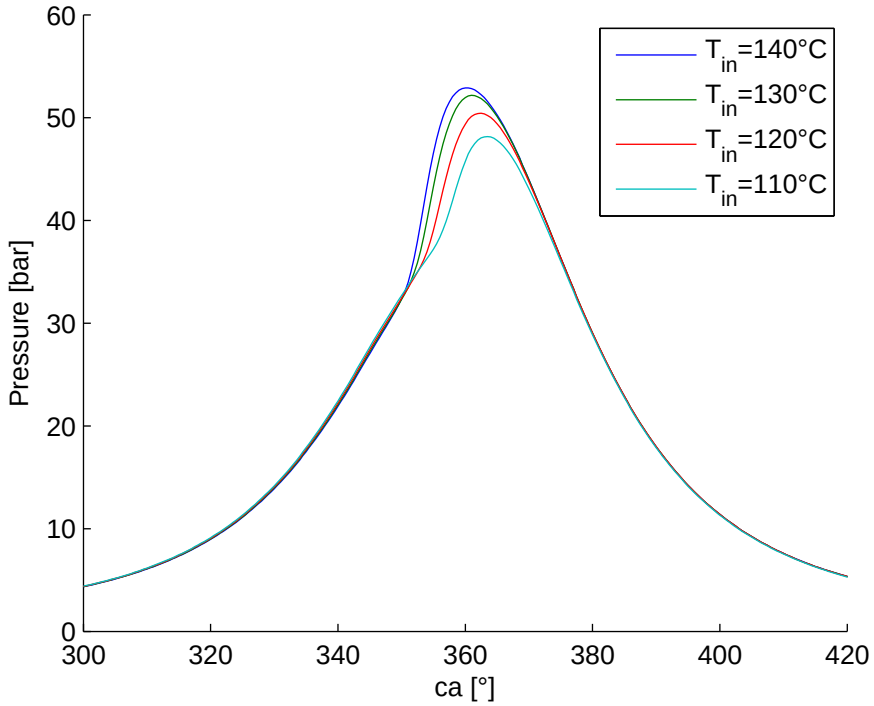

Figure 5.8: Pressure as a function of ca for different inlet temperatures and a constant fuel rate of 0.100 kg/h, no EGR and CR 14.75:1

5.2.3 Effect of CR

To investigate the effect of CR on the combustion, the following experiment is carried out. Using a constant fuel rate of 0.105 kg/h and constant inlet temperature of 180°C, the CR is changed. This gives the results from figure 5.9. The result shows that using higher compression ratios advances the combustion. This is normal, since the auto-ignition temperature and pressure are reached earlier in the cycle. The duration of the combustion also decreases with higher CR. Although better efficiencies and a higher imep can be reached using a higher CR, for this experiment this is not the case because temperature and fuel rate are kept constant. The engine settings are not optimized for each CR. A high CR combined with a relatively high inlet temperature results in a shorter combustion and an earlier SOC. These two factors together result in negative work during the compression, since the biggest part of combustion takes place during the compression. For the CR of 14:1 the combustion is even phased completely before TDC. This results in significant losses, which imply a low imep and a low efficiency.

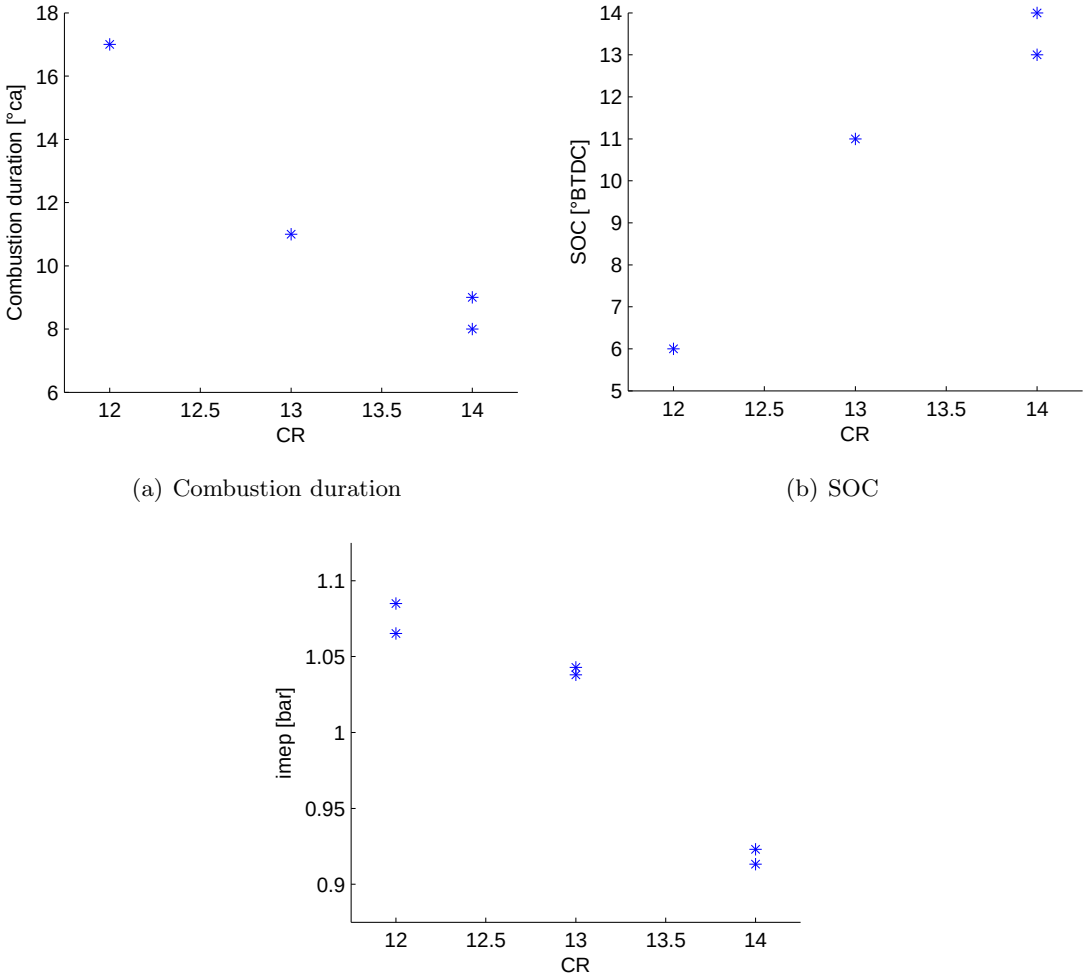

(a) Combustion duration

(b) SOC

(c) imep

Figure 5.9: Combustion duration, SOC and imep for various compression ratios for multiple measurements per operating point with constant inlet temperature of 180°C and a fuel rate of 0.105 kg/h

5.2.4 Effect of excess air ratio λ

As in most engines, the engine load is determined by changing the amount of injected fuel. A richer mixture means that more chemical energy is introduced in the cylinder. This leads to a higher HRR, higher pressures and thus a higher torque level. If the mixture is too lean and the flammability limit is reached, misfires occur. If the mixture is too rich, pressure rise rates are so high that knock related problems occur. The effect on the SOC is negligible. In-cylinder thermal conditions are the dominant factor concerning the SOC. Because we regulate the inlet temperature with the air preheater the cooling effect of the fuel vaporization is avoided. The different amounts of injected fuel only slightly change the gas properties of the entire mixture during compression. The temperature and pressure

build-up during the compression stroke will be almost the same for different excess air ratios, leading to the same SOC. For lean mixtures, the combustion is slower. This can be linked to the chemical reactions taking place. A lean mixture means less available energy to be released. This results in a lower pressure and lower temperature, which results in a slower chemical reaction, thus slower combustion. The main reason of the decreasing imep with higher λ is the fact that less energy is introduced in the cylinder. All these findings can be found in figure 5.10.

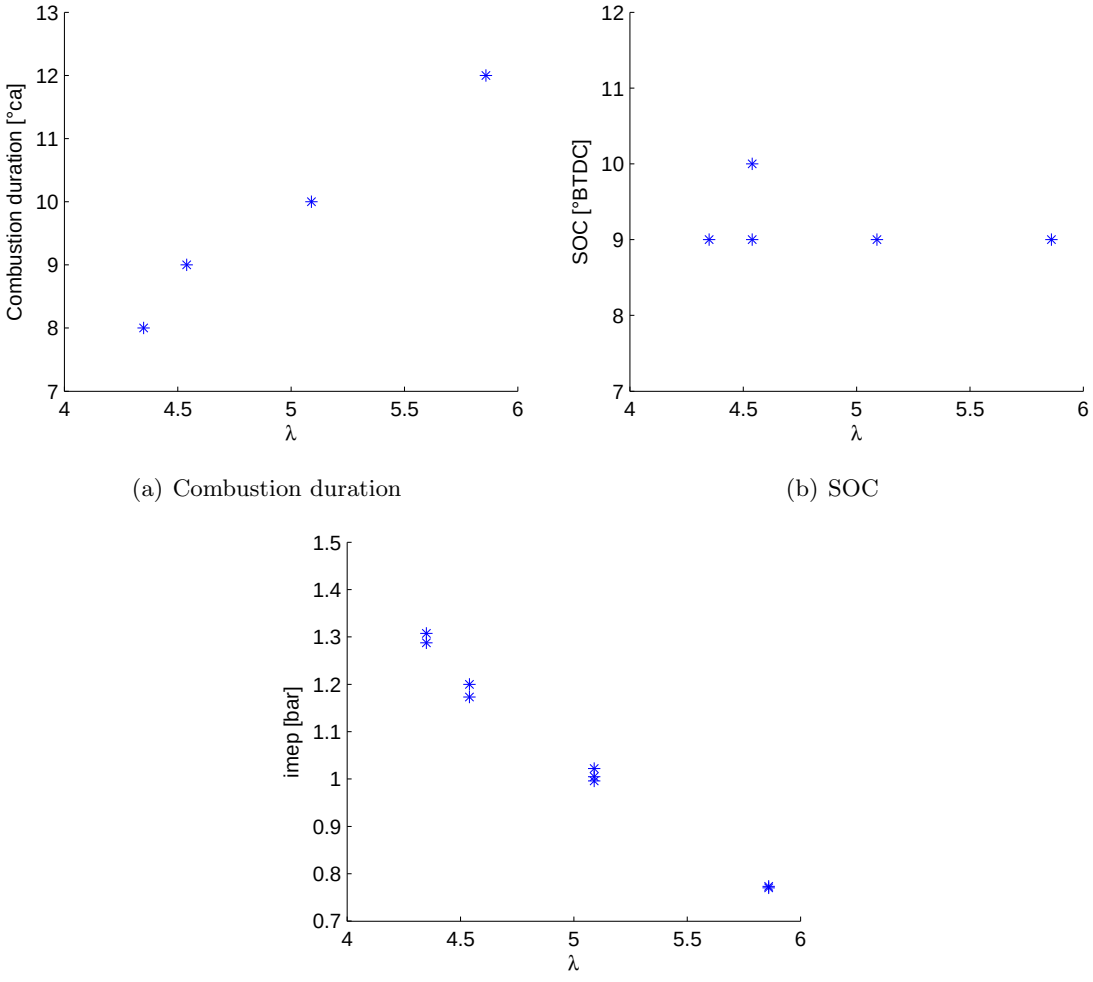

(a) Combustion duration

(b) SOC

(c) imep

Figure 5.10: Combustion duration, SOC and imep as a function of λ for multiple measurements per operating point with CR 13:1 and an inlet temperature of $180°C$

5.2.5 Limits of HCCI for CR 13

Now the influence of EGR, preheating, CR and excess air ratio are known, the limits of HCCI combustion concerning load (determined by the AFR) and temperature are examined for one CR as shown in figure 5.11. To have a full image of the possible operating conditions of the CFR engine setup, the procedure that is done for CR 13:1, should be repeated for more compression ratios. During the measurements it became clear that compression ratios ranging from 11:1 up to 14.75:1 are possible. For the CR of 13:1 the inlet temperature was varied from 140°C to 200°C. For each fixed inlet temperature the AFR was varied until the upper (rich) and lower (lean) load limit was reached. To extend the upper load limit, a fixed amount of EGR was applied for each inlet temperature. So the upper load limits with EGR are not a limit as such. They could be extended if more EGR is applied. As already mentioned in section 2.2, the upper load limit of HCCI is defined by knock-like phenomena and the lower load limit is defined by a COV_{imep} of 10%. In our setup, knock is clearly audible when pressure rise rates of 5 $bar/°ca$ are reached, so this was defined as the upper load limit for the CFR engine setup. Using a CR of 13:1 and no EGR the limits of various output parameters for several intake temperatures can be found in figure 5.11. The lowest inlet temperature that is needed to have a stable combustion is at 140°C. When a higher CR is used, stable combustion could be achieved at lower temperatures. The upper limit of our inlet temperature is around 200°C, since then the auto-ignition temperature of gasoline is almost reached at the inlet.

From these results, it can be seen that a higher inlet temperature makes it possible to have a leaner mixture or higher λ. It also results in a larger operating range. The effect on the SOC, combustion duration and imep are the combined effects of varying AFR and inlet temperature as discussed in the previous section.

As can be seen from figure 5.11 the combustion duration becomes shorter for higher inlet temperatures. Take note that a higher inlet temperature comes along with a slightly leaner mixture for the lower as well as for the upper limits. In the previous sections it was explained that higher inlet temperatures lead to a shorter combustion duration and that leaner mixtures lead to a longer combustion duration. From the results it can be concluded that the inlet temperature is the dominant factor since combustion duration is shorter when going from the left to the right on the x-axis of figure 5.11. From the combustion duration for the same temperature it can clearly be seen that it is longer for leaner mixtures. Take note that for lowest inlet temperatures the combustion duration is extremely long. This could be the consequence of non-uniform combustion, where a flame

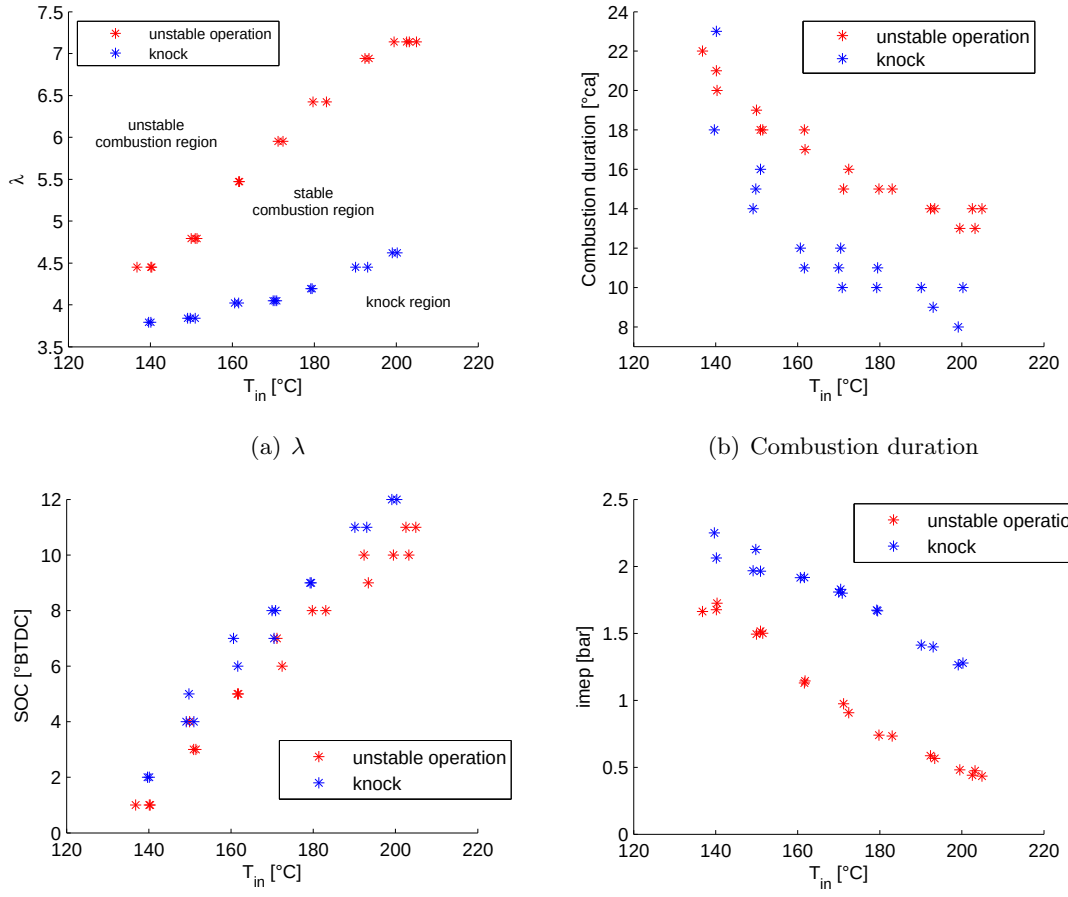

(a) λ

(b) Combustion duration

(c) SOC

(d) imep

Figure 5.11: The limits of λ, combustion duration, SOC and imep for multiple measurements per operating point for different inlet temperatures with CR 13:1

front may be present. This should not be the case for HCCI. For higher inlet temperatures combustion durations of approximately $10°ca$ can be reached when running on a relatively rich mixture, which is more convenient for HCCI combustion. Take note that a combustion duration of $23°ca$ is measured for the upper limit for an inlet temperature of 140°. This is an anomaly which can be dedicated to the low inlet temperature which results in unstable operation at CR 13:1.

As expected, the SOC becomes earlier when increasing the inlet temperature. Again, it can be seen that the influence of the mixture composition on the SOC is very small. Differences of 1 to $2°ca$ are measured. Nevertheless, it can be seen that for richer mixtures (at the same temperature) the SOC is a bit earlier. The SOC is defined as the first crank angle where the heat release rate is higher than 1.5 $J/°ca$. Very short before this moment, the combustion already started to develop. For a richer mixture the fuel molecules are

located closer to each other. So it is possible that this early combustion development occurs faster for a richer mixture. But as already explained, for HCCI the combustion occurs at different locations at the same time, without the presence of a flame front. Still there will be some inhomogeneity resulting in very little flame fronts expanding from the spots where combustion was initiated. It is believed that these little early-flame developments occur faster for richer mixtures and therefore the SOC (as it is defined in this thesis) is a little earlier for a richer mixture.

The imep decreases with rising inlet temperature, since the volumetric efficiency decreases with increasing inlet temperature. A hotter mixture is less dense, resulting in less mass that is drawn into the cylinder. The fuel rate for the hotter mixtures are also lower, resulting in less energy that is introduced into the cylinder by fuel. Another reason is that the combustion duration becomes shorter with increasing inlet temperature, and the SOC is earlier. This results in more negative work on the piston for high temperatures, which means a lower imep will be obtained. For a constant inlet temperature, the imep is higher for the rich mixture, since more chemical energy is introduced into the cylinder.

Using EGR, the upper load limit of HCCI can be extended and the combustion also becomes more stable. Figure 5.12 shows the change in limits when EGR is applied. For each measurement an arbitrarily chosen EGR rate of 35% is used. This way, much richer mixtures are obtained. These richer limits are not limits as such. The EGR rate can be chosen higher than 35%, depending on the inlet temperature. It can be seen that the operating range of HCCI can be extended by over 100% when EGR is used. Details about the measurements can be found in appendix D. The method for calculating EGR can be found in appendix C.

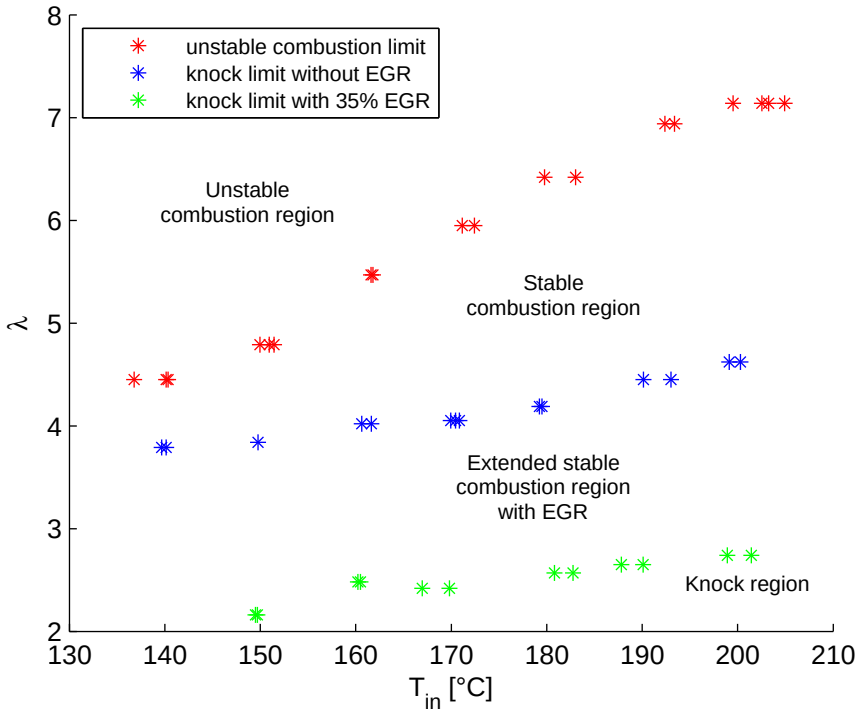

Figure 5.12: Limits of HCCI for different inlet temperatures with and without EGR (35%) for the rich mixtures and CR 13:1

5.3 Heat flux measurements on HCCI

Using a single-layer TFG heat flux sensor located at the position where the spark plug used to be (position P1 on figure 3.2), heat flux measurements are performed while in HCCI operation. No other positions were tested, but it is expected that for HCCI less spatial variations occur than in SI or CI operation, leading to an acceptable measurement for the global heat flux. This will be explained further in this section. First the methods to calculate the heat fluxes are examined. Next, a discussion of the general course of the wall heat fluxes follows, together with the results of the heat release analysis. Finally, the convective heat transfer coefficient is calculated and compared to several known correlations.

The results are based on two measurement sets using an inlet temperature of $180°C$ and $150°C$, both for a CR of 13:1. The fuel rate is changed within the operating range of HCCI for the inlet temperature of $180°C$ and $150°C$ respectively. Table 5.3 shows the conditions at which the experiments are done.

Table 5.3: Operating conditions

Fuel	Gasoline (RON 98)	Gasoline (RON 98)
Engine Speed [rpm]	600	600
CR	13	13
$\%EGR$	0	0
$T_{inlet}[°C]$	180	150
Excess air ratio (λ)	4.35, 4.53, 5.09 and 5.86	4.24 and 4.54
Coolant temperature [$°C$]	100	100
Throttle position	WOT	WOT

5.3.1 Wall heat flux calculation methods

Two possibilities for calculating the heat flux are proposed, the Fourier method and the FIR-method. Each can be calculated using different approaches. In total, there are four different methods that are examined, these are: the FIR_{gas}, the FIR_m, the $FOUR_{1T}$ and the $FOUR_{2T}$ method. The basic ideas of each method can be found in appendix C and in the master's thesis of *S. Broekaert and T. De Cuyper* [6].

They concluded that there are no significant differences between these methods. The FIR_m and $FOUR_{2T}$ methods give very similar results, as well as the FIR_{gas} and $FOUR_{1T}$ methods. This is due the way the steady state component of the heat flux is calculated. The FIR_m and $FOUR_{2T}$ methods use the in-depth temperature (provided by the in-depth thermocouple) and the FIR_{gas} and $FOUR_{1T}$ make use of the gas temperature. Because in this research HCCI operation is performed, the results of the four methods should be closer to each other, since the gas temperature is more accurately determined due to the absence of a flame front. This assumption is tested for HCCI operation. An example of the heat fluxes to the wall for the different methods can be found in figure 5.13 during the closed part of the cycle. In this figure, it is clear that the methods do not deviate that much from each other. It can also be seen that the error bars for the different methods overlap, so it is allowed to assume that the four different methods give the same result. Only during compression and expansion the methods differ the most, but still not significantly. As expected, the differences between the four methods are smaller than in SI operation. This is the result of the uniform combustion of HCCI. During further wall heat flux measurements, the FIR_{gas} method will be used. The choice to use this method can be found in the simplicity of the calculation which results in less calculating time.

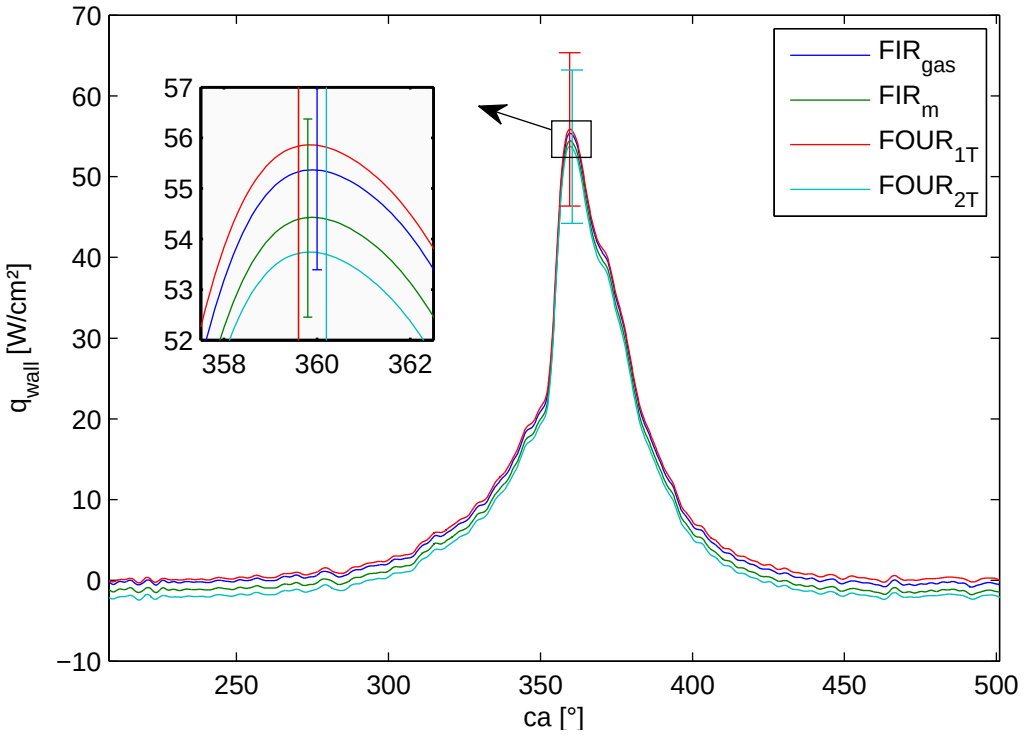

Figure 5.13: The wall heat flux as a function of crank angle, calculated using the four possible methods

5.3.2 Wall heat fluxes in HCCI operation

In figure 5.14 the pressure and the wall heat flux can be found as a function of crank angle for various excess air ratios during the closed part of the cycle. As expected, a richer mixture (lower λ) results in higher peak pressures, and higher heat fluxes. During the earlier part of the compression stroke (until about 300°ca) and during the latter part of the expansion stroke (from about 430°ca) the wall heat flux is almost non-existent. This is normal, since the temperature of the mixture is in the range of the wall temperature. The temperature of the wall (the temperature of the TFG) and the temperature of the mixture (calculated from the ideal gas law) can be seen in table 5.4 for various crank angle positions. It can be seen that there has to be a relatively high temperature difference between the gas mixture and the wall in order for the heat flux to be important. This is based on the heat flux that becomes higher than 1 W/cm^2 at 300°ca and again lower than 1 W/cm^2 at 430°ca. Take note that besides the temperature difference, the convection coefficient also plays an important role in the wall heat flux. During combustion, the convection coefficient rises, which also results in an increasing wall heat flux. A discussion of the heat flux coefficient follows later in this section. From the curves in figure 5.14 it can be seen

that the changes in slope of the pressure and wall heat flux follow the same trend. For a rich mixture, the pressure and wall heat flux rise faster, whereas for a lean mixture, they both rise slower. This could lead to the assumption that the pressure rise rate can be linked to the rise rate of the wall heat flux. This, in turn, could lead to an alternative way in measuring the upper limit of HCCI which is determined by a maximum pressure rise rate. The peak pressure and peak wall heat flux occur simultaneously. This is normal, since the peak pressure implicates peak temperature, and at peak temperature the wall heat flux will peak.

Table 5.4: Wall and mixture temperature

ca [°]	IVC (208°)	300°	SOC (349°)	$T_{mix,max}$ (360°)	$T_{TFG,max}$ (375°)	430°	EVO (501°)
T_{wall} [°C]	227.4	227.8	234.8	244.3	248.9	238.9	234.1
T_{mix} [°C]	227.4	424.3	760.7	1300	1130.9	542.0	327.6
$\triangle T$ [°C]	0	196.5	525.9	1055.5	882.0	303.1	93.4

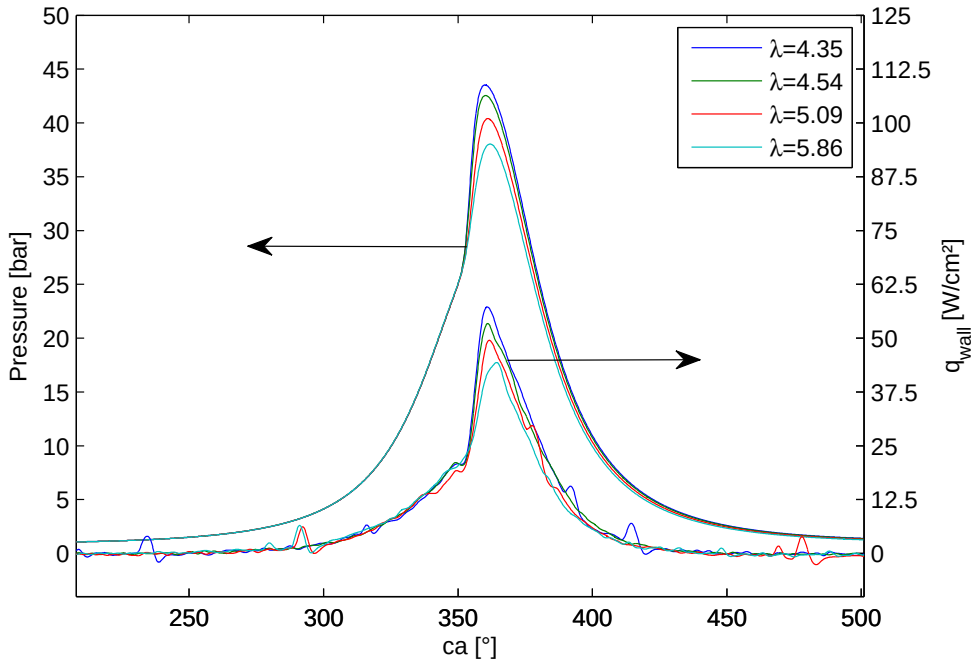

Figure 5.14: The pressure and wall heat flux as a function of crank angle for different excess air ratios for an inlet temperature of 180°

5.3.3 Heat Release Analysis for HCCI combustion

As mentioned in section 4.3 a heat release analysis can be used to verify the results of the heat flux sensor and the assumption that one heat flux sensor at the cylinder head will suffice to represent the global heat flux. From figure 4.2 in section 4.1 it could be seen that for HCCI combustion heat flux traces at different locations in the cylinder are very similar. Research [20] has shown that a spatially averaged heat flux of multiple heat flux traces is a good representative of the global heat flux. In this thesis, we have only one heat flux sensor at our disposal. To see if one heat flux sensor at one certain spot in the combustion chamber will suffice, the net CHR and the cumulative heat loss should add to a constant that is equal to the energy of the burned fuel as explained in sections 4.1 and 4.3. As already mentioned, neither the fuel rate or the AFR could be determined properly. The fact that the fuel rate could not be determined properly, means that we were not able to determine the amount of chemical energy released by the burned fuel. The uncertainty about the AFR leads to uncertainties about the gas properties like the specific heat ratio γ. As explained in section 4.1 γ is used to determine the net heat release. This leads to uncertainties about the cumulative net heat release. This means that the heat release analysis can only give indicative results.

On figure 5.15 it can be seen that the net CHR reaches a maximum and then lowers during the expansion stroke. This behavior can be explained as follows. At the SOC the net CHR is $0J$. During combustion, heat is released, resulting in work on the piston and a rise of the internal energy of the mixture. This can be seen as the rise of the net CHR. When combustion is completed, the net CHR reaches a maximum. After this point, the mixture starts to lose energy because of the wall heat fluxes, which can be seen as the decrease in net CHR.

The total CHR reaches a maximum and should be constant after this maximum, equal to the energy of the burned fuel. Since we are not able to determine the energy of the burned fuel, we will only check if the total CHR converges to a constant value. This is not completely the case for these measurements. It can be seen from the figure that the total heat release starts to decrease after its maximum. Physically, this is impossible since the total heat release should be equal to the energy of the burned fuel. When this sum decreases, this would mean that some energy is disappearing, which is impossible according to the first law of thermodynamics. A possible reason is that the global heat flux is underestimated because only the heat flux at the cylinder head is measured. It is possible that the heat flux through the piston surface or cylinder liner is slightly bigger

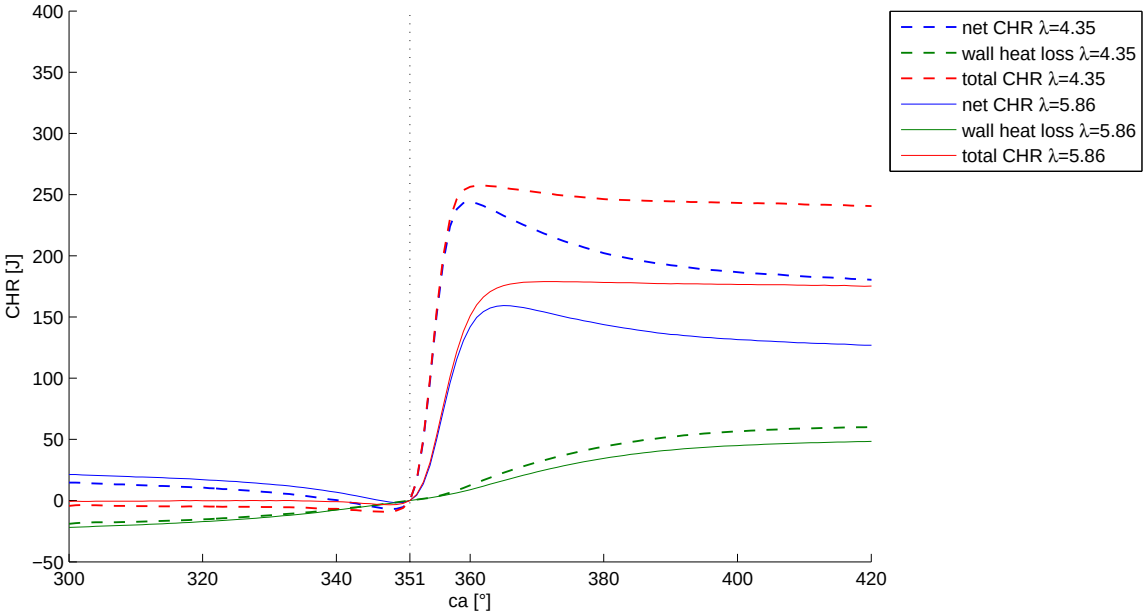

Figure 5.15: The net CHR, wall heat loss and total CHR for a rich and a lean mixture

and thus the measured heat flux at the cylinder head is not a good representative of the global heat flux. The cylinder liners are more cooled than the cylinder head and the piston surface. This can be seen from figure 3.1. Therefore it is possible that the heat flux through the liner is bigger and therefore the measured heat flux at the cylinder head underestimates the global heat flux. To verify this hypothesis the data is examined a little deeper.

In order to quantitatively show this drop in total CHR, calculated values for an inlet temperature of 150°C and 180°C are shown in table 5.5. In this table, the excess air ratio, the SOC, the combustion duration and the difference between the maximum value of the total CHR and the value of the total CHR at 420°ca can be found. This last value can be used to study the decrease in the total CHR. Ideally, this decrease should be zero, the higher the value, the more incorrect the total CHR. The following trend can be seen. The earlier the combustion begins and the shorter the combustion duration, the bigger the drop after the peak of the total cumulative heat release. This could indicate that combustion phasing has an influence on the distribution of the heat losses through the different surfaces of the cylinder. Therefore the in-cylinder geometry was examined during combustion. In table 5.5 you can see in the last column the average cylinder volume during combustion divided by the maximum cylinder volume. There seems to be a trend that a

large drop in total CHR occurs for larger in-cylinder volumes. The smaller the in-cylinder volume, the smaller the better-cooled liner surface becomes. The cylinder head surface and piston surface stay the same. So the smaller the volume, the smaller the importance of the heat flux through the liners. If indeed the heat flux through the liners are bigger than anywhere else in the cylinder, this could be a reason why the heat flux is underestimated for all measurements and especially for those measurements whose combustion occurs for larger in-cylinders volumes (when the importance of the liner is bigger).

To verify this, more measurements should be done. Unfortunately we were not able to perform more heat flux measurements due to problems with the TFG amplifier. For future research it should be further verified with more measurements if one heat flux sensor is a good representative of the global heat flux or if the global heat flux is underestimated because the heat flux through the cylinder liners is bigger than the heat flux at the cylinder head. Besides, an incorrect determined mixture composition leads to errors in the net CHR, which also could be an explanation for the decreasing total CHR, since our fuel rate could not be determined accurately. An error analysis for the wall heat loss shows an error of about 14 J at 425°ca. This error should be combined with the error from the net CHR, but since our net CHR is determined incorrectly due to the roughly estimated fuel rate, a full error analysis cannot be carried out. Unfortunately no strict conclusions can be made from this data, so for now we assume that the measured heat flux is a good representative for the global heat flux, this could be further examined in the future.

Table 5.5: Heat flux measurements for $CR = 13$

T_{in} [°C]	λ	SOC [°$BTDC$]	Comb. Dur. [°ca]	$Q_{tot,max} - Q_{420°ca}$ [J]	$V_{cyl,av,comb}$[%]
180	4.35	11	9	18	8.11
180	4.54	11	9	18	8.11
180	5.09	10	10	12.5	7.98
180	5.86	10	12	8.5	7.95
150	4.24	6	13	8	7.83
150	4.54	6	13	7	7.83

5.3.4 HCCI heat flux correlations

As mentioned in section 2.5, several heat flux correlations for HCCI are being proposed. The most important are the *Woschni* [21], *Assanis* [20], *Annand* [35] and *Hohenberg* [22]

correlation. In this subsection, these correlations will be evaluated for HCCI combustion in a CFR engine using the TFG heat flux sensor. With this sensor, the heat flux is calculated from temperature measurements. The convection coefficient can then be calculated with the following equation:

$$q = Q/A = h_c \cdot (T_{gas} - T_{wall}) \tag{5.4}$$

In this equation, Q is the total heat transfer, h_c is the convection coefficient, T_{gas} the gas temperature and T_{wall} is the wall temperature. h_c can be calculated since T_{gas} can be calculated from the ideal gas law, T_{wall} is measured by the TFG sensor. The convection coefficient can also be defined using the Nusselt number:

$$Nu = \frac{h_c \cdot L}{k} \tag{5.5}$$

With Nu the Nusselt number, h_c the convection coefficient, L the characteristic length and k the thermal conductivity. For forced convection, the Nusselt number can be written as a function of the Reynolds number (5.6) and Prandtl number (5.7). The Reynolds number is defined as:

$$Re = \frac{v \cdot L}{\nu} \tag{5.6}$$

with v the fluid velocity, L the characteristic length, and ν the kinematic viscosity. The Prandtl number is defined as:

$$Pr = \frac{\nu}{\alpha} \tag{5.7}$$

with α the thermal diffusivity.

The Nusselt number can be written as:

$$Nu = aRe^b Pr^c \tag{5.8}$$

where a, b and c are determined empirically based on the flow conditions. The mentioned heat flux correlations are based on equation 5.8. The Prandtl number is almost constant and around 0.7 for most gasses, so most of the correlations include this number into parameter a [34]. All the mentioned correlations are based on the Reynolds analogy of equations 5.5 to 5.8. The most straightforward correlation is the *Annand* correlation, which is a direct expression of equation 5.8 with the Prandtl number equal to 0.7:

$$h_c = a \cdot \frac{k}{L} \cdot Re^b = a \cdot \frac{k}{L} \cdot (\frac{v \cdot L}{\nu})^b \tag{5.9}$$

where a depends on the type of engine and should have a value between 0.35 and 0.8 [35]. Parameter b should be equal to 0.7. The characteristic length is defined as the cylinder bore and the characteristic velocity as the mean piston speed. The thermal conductivity k and kinematic viscosity ν are gas properties and are calculated for each time step. In the original correlation these gas properties were taken constant during the cycle because it simplified the calculation. *Annand* suggested to evaluate the gas properties at the average charge temperature derived from the cylinder pressure, charge mass and cylinder volume [35]. So the *Annand* correlation that is used, is actually an improved version where the gas properties are determined almost instantaneous.

For the correlations of *Woschni*, *Assanis* and *Hohenberg*, assumptions are made concerning the gas properties in order to calculate the convection coefficient as a function of only the cylinder bore, the characteristic velocity, the cylinder pressure and temperature:

$$\rho \sim \frac{p}{T} \tag{5.10}$$

$$k \sim T^n \tag{5.11}$$

$$\mu \sim T^m \tag{5.12}$$

The exponents n and m differ from correlation to correlation. This leads to the following general equation:

$$h_c(t) = \alpha_s L(t)^{-j} P(t)^k T(t)^{-l} v(t)^m \tag{5.13}$$

In this equation, h_c is the (convectional) heat transfer coefficient of the gas boundary layer at the cylinder walls, α_s is a scaling factor which is changed with the engine geometry, L is the characteristic length, P and T are the instantaneous in-cylinder pressure and temperature respectively and v is the instantaneous characteristic velocity. The correlations only differ in exponents (j, k, l and m), the characteristic length L and the characteristic velocity v. In table 5.6 a summary of the exponents is given.

Table 5.6: Exponents for different heat flux correlations

	j	k	l	m
Original *Woschni*	0.2	0.8	0.53	0.8
Assanis	0.2	0.8	0.73	0.8
Hohenberg	0.06	0.8	0.4	0.8

For the characteristic velocity, all correlations make use of the mean piston speed. *Woschni* suggested to add an extra term to the characteristic velocity to account for the effect of the combustion on the heat transfer. Therefore he added the pressure difference between the fired and motored condition. The resulting characteristic velocity is given in equation 5.14.

$$v(t)_{Woschni} = c_1 \cdot \overline{s}_p + c_2 \cdot \frac{V_s \cdot T_r}{P_r \cdot V_r} \cdot (P - P_{mot}) \tag{5.14}$$

In this equation c_1 and c_2 are constants. c_1 is 6.18 during the scavenging period and 2.28 during compression, combustion and expansion. c_2 is 0 during scavenging and compression and 0.00324 during combustion and expansion. V_s is the swept volume and T_r, P_r and V_r are the temperature, pressure and volume at IVC. The characteristic velocity in the *Assanis* correlation is almost the same as that of *Woschni*. The only difference is that the constant c_2 is reduced to 1/6 of its original value. *Hohenberg* defined the characteristic velocity as the mean piston speed added with a constant equal to 1.4.

For the characteristic length *Annand* and *Woschni* used the cylinder bore. *Assanis* suggested to use the instantaneous chamber height instead. *Hohenberg* proposed to use the diameter of a sphere with the same volume of the in-cylinder volume. The characteristic length according to *Hohenberg* is given in equation 5.15. The scaling factor α_s can be adapted depending on the engine geometry. *Woschni*, *Assanis* and *Hohenberg* all suggested a value of 130 for the scaling factor when the pressure is expressed in bar, or a scaling factor of 0.0130 when the pressure is expressed in Pa.

$$L(t)_{Hohenberg} = \sqrt[3]{\frac{6 \cdot V(t)_{cyl}}{\pi}} \tag{5.15}$$

In figure 5.16, the wall heat fluxes for the correlation and the measured heat flux is shown for λ equal to 4.54 and an inlet temperature of $180°C$. The heat fluxes for the correlations are calculated using T_{gas} and T_{wall}. In figure 5.17 the convection coefficients of the different correlations and the one calculated from the measured heat flux are shown for the same λ and inlet temperature. For the *Annand* correlation, the scaling factor a is set to the lowest value of 0.35. From these figures, it can be seen that *Woschni* and *Assanis* differ the most from our measurement. *Woschni* underestimates the heat flux during compression and overestimates it during combustion and expansion. *Assanis* underestimates the heat flux during the whole cycle. The *Hohenberg* and *Annand* correlation come closest to the measurement. The *Hohenberg* correlation comes close, but still deviates from the

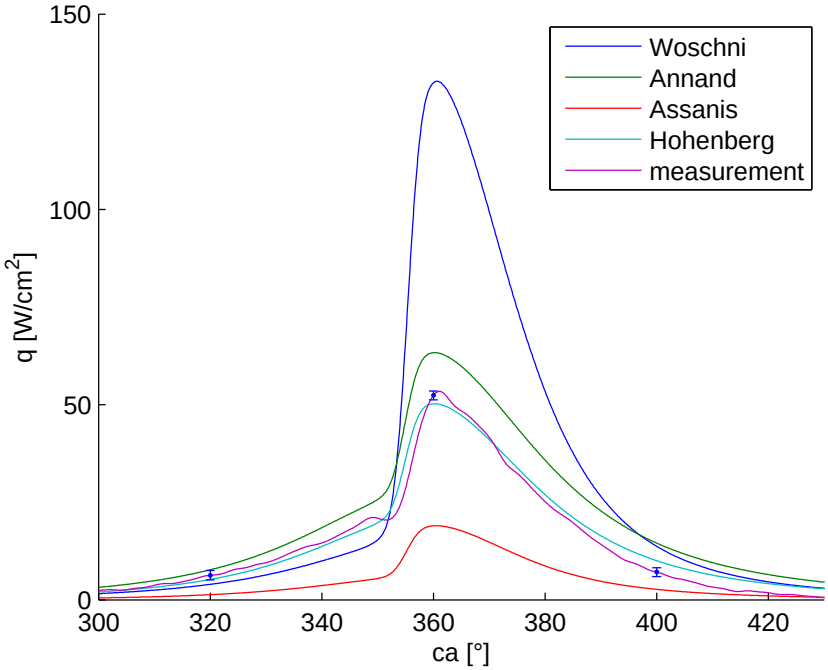

Figure 5.16: The wall heat flux from the heat flux measurements compared to the correlations, for $\lambda = 4.54$, $T_{in} = 180°C$ and CR 13:1

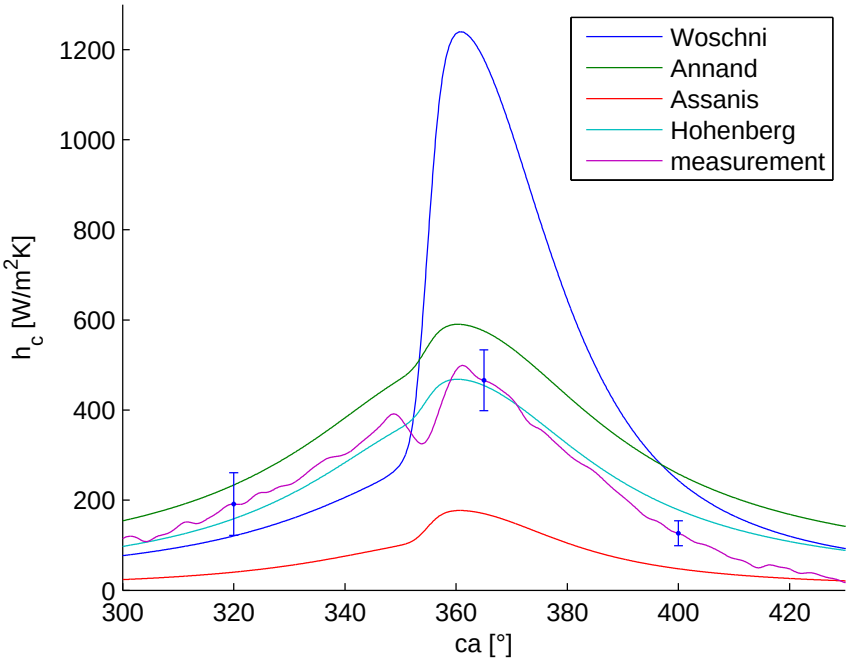

Figure 5.17: The convection coefficient for the various heat flux correlations compared to the convection coefficient calculated from the heat flux measurements, for $\lambda = 4.54$, $T_{in} = 180°C$ and CR 13:1

measured heat flux, especially during the expansion stroke. The *Annand* correlation overestimates the heat flux during the whole cycle. Seeing these results, it can be concluded that none of the heat flux correlations are able to estimate the measured wall heat flux accurately. This could be due to wrongly determined exponents, a wrong scaling factor, a wrong characteristic length, a wrong characteristic velocity or a combination of these errors. It is believed that structural changes need to be made to the correlations since *Woschni* and *Hohenberg* developed their correlations for SI and CI engines and *Assanis* changed some constants in the *Woschni* correlation in order to fit his HCCI heat flux measurements. *Annand* did not make any assumption. Nevertheless, we will now try to fit these correlations to our results by changing the scaling factor since this is dependent on engine geometry.

In order to eliminate the effect of the scaling factor in each correlation, an optimal scaling factor was determined for the measurement above, at a λ of 4.54 and an inlet temperature of $180°C$. This is done by minimizing the mean square error between the measured heat flux and the calculated heat flux using the correlations for different scaling factors. The results for the best scaling factors can be found in table 5.7. It can be seen by optimizing the scaling factors, *Hohenberg* and *Assanis* give the best result. *Woschni* gives the worst result. This was also concluded by *Soyhan*, as explained in section 2.5. Take note that the scaling factor of *Annand* is optimal for a value out of the range of 0.35 and 0.8. The heat flux and convection coefficient with optimized scaling factors can be found in figure 5.18 and 5.19 respectively.

Table 5.7: Best scaling factor for the different correlations

Correlation	Best scaling factor	Mean square error of heat flux [W/cm^2]
Woschni	0.0054	1.94
Assanis	0.0363	1.12
Hohenberg	125	1.14
Annand	0.2580	1.35

Although the mean square error is minimized for the correlations, the estimated heat flux from the correlations can still deviate a lot from the measured heat fluxes in some parts of the cycle. This can be seen from the *Hohenberg* correlation. The optimized *Hohenberg* correlation looks worse than the original one. This is because only the interval between 300 and $430°ca$ is shown. The *Hohenberg* correlation lies above the measured

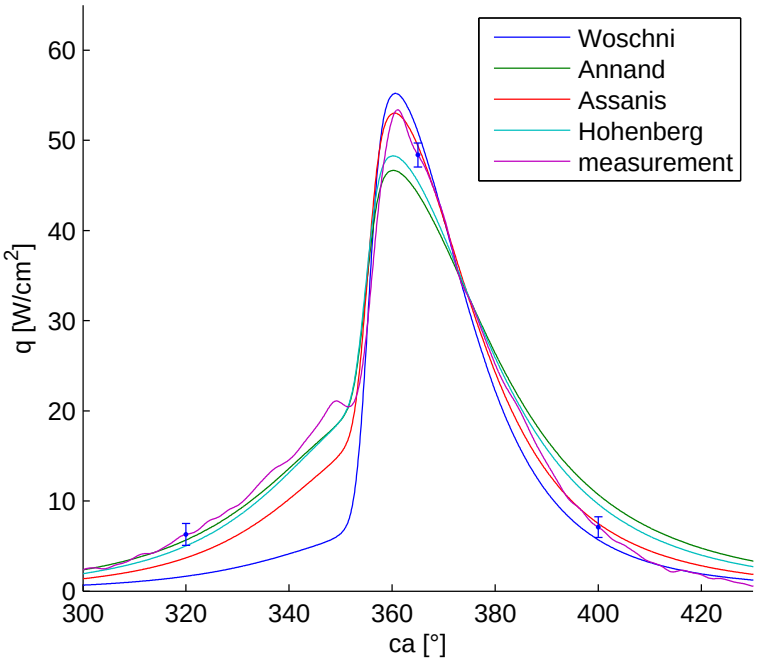

Figure 5.18: The wall heat flux from the heat flux measurements compared to the correlations, for $\lambda = 4.54$, CR 13:1, $T_{in} = 180°C$ and optimized scaling factors

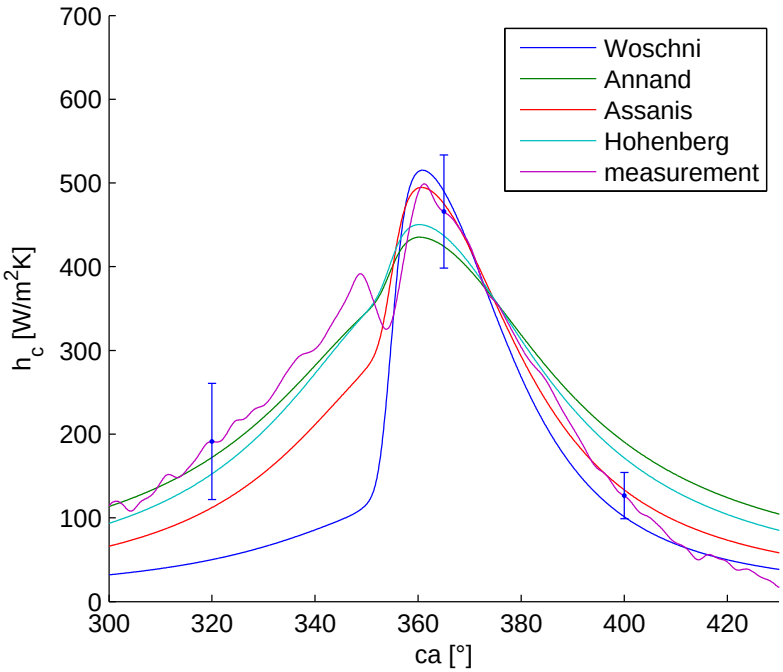

Figure 5.19: The convection coefficient for the various heat flux correlations compared to the convection coefficient calculated from the heat flux measurements, for $\lambda = 4.54$, CR 13:1, $T_{in} = 180°C$ and optimized scaling factors

heat flux during expansion. For the optimized scaling constant, the correlation is lowered. Although the error is small, the heat flux resulting from this correlation fails to estimate the peak heat flux and overestimates the heat flux during expansion. The same goes for the *Annand* correlation. When looking at the graphs, one could say that *Assanis* follows the measured heat flux the best, since it is able to predict the heat flux well during combustion and expansion. Because the heat flux is not estimated well during compression, the mean square error of the *Assanis* correlation is higher. Actually the most critical part of the cycle for HCCI combustion is the compression stroke. The main motivation of this research is to develop a heat transfer correlation that contributes to a global HCCI model that is able to simulate HCCI combustion and above all is able to predict the SOC. The SOC is very dependent on what happens during the compression stroke. When the heat transfer is overestimated, the gas temperature will be underestimated which ultimately results in a SOC that is predicted later in the cycle than should be. The opposite holds for an underestimation of the heat transfer during compression. If only the compression stroke is considered, the *Annand* and *Hohenberg* correlation give the best results. A good correlation should be able to predict the wall heat flux correctly during the whole cycle and not only during some parts of it. This is not the case for any discussed correlation. They all follow the same trend, but none of them is completely correct.

The optimal scaling factors are now kept fixed and are tested for various operating conditions to see how the correlations are able to change along with the measured heat flux. The wall heat flux is shown in figures 5.20 and 5.21 for λ equal to 4.35 and 5.86 respectively. Using an inlet temperature of $150°C$ and varying λ, the optimized scaling factors result in the graphs on figures 5.22 and 5.23. For these operating conditions, the same conclusions can be made as for the measurement with λ equal to 4.53. *Woschni* his result is not reliable, his correlation only comes close to the measurement during the expansion. *Annand* comes close during compression, underestimates the peak flux and overestimates the heat flux during expansion. The same goes for *Hohenberg*, although his result is slightly better compared to *Annand*. *Assanis* estimates the wall heat flux best during combustion and expansion, but deviates a lot during compression. Take note that for an inlet temperature of $150°C$, the peak wall heat flux is better estimated by *Annand* and *Hohenberg* compared to the measurements at $180°C$. Nevertheless, they still underestimate the peak.

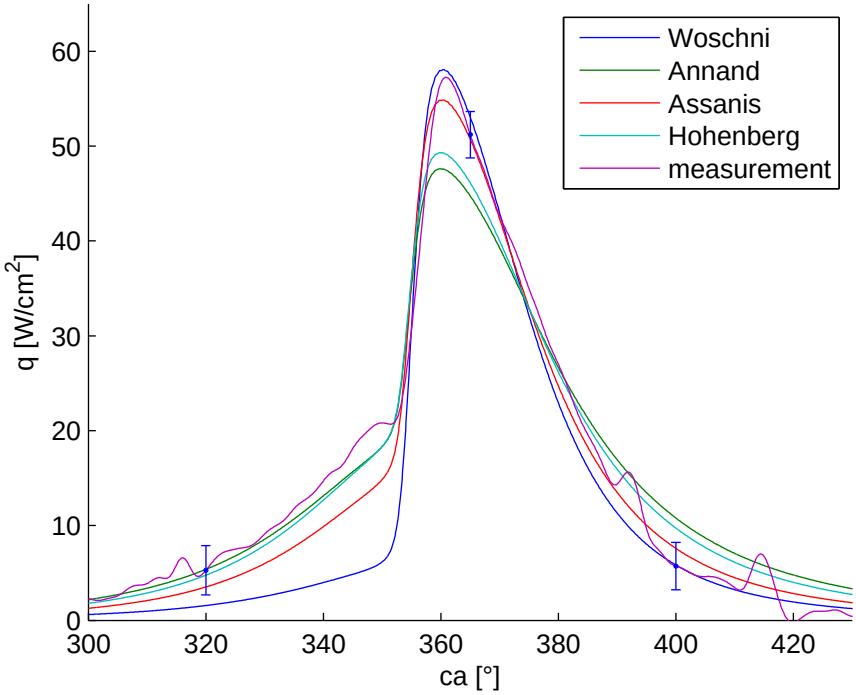

Figure 5.20: The wall heat flux for $\lambda = 4.35$ with $T_{in} = 180°C$, optimized scaling factors and CR 13:1

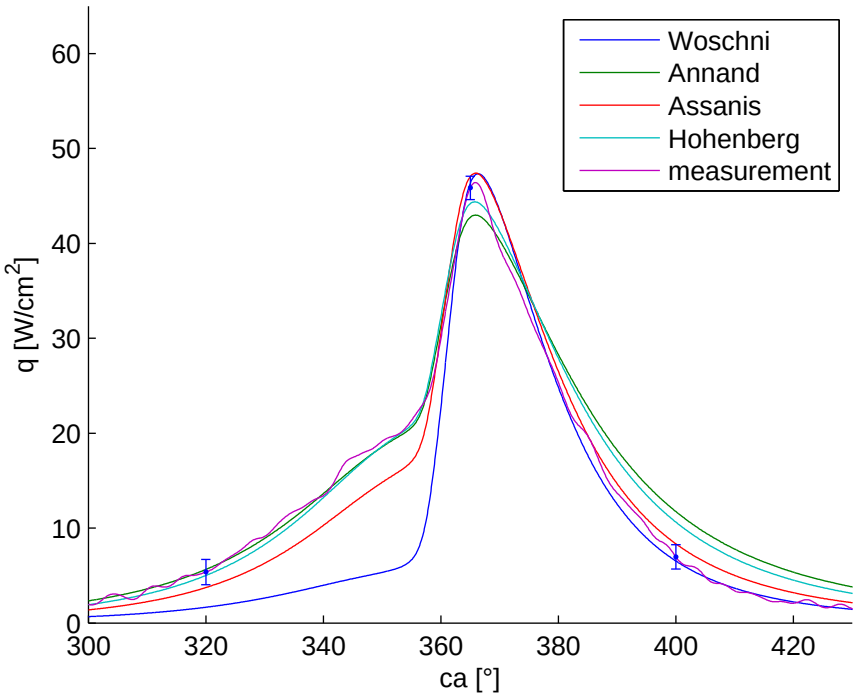

Figure 5.22: The wall heat flux for $\lambda = 4.54$ with $T_{in} = 150°C$, optimized scaling factors and CR 13:1

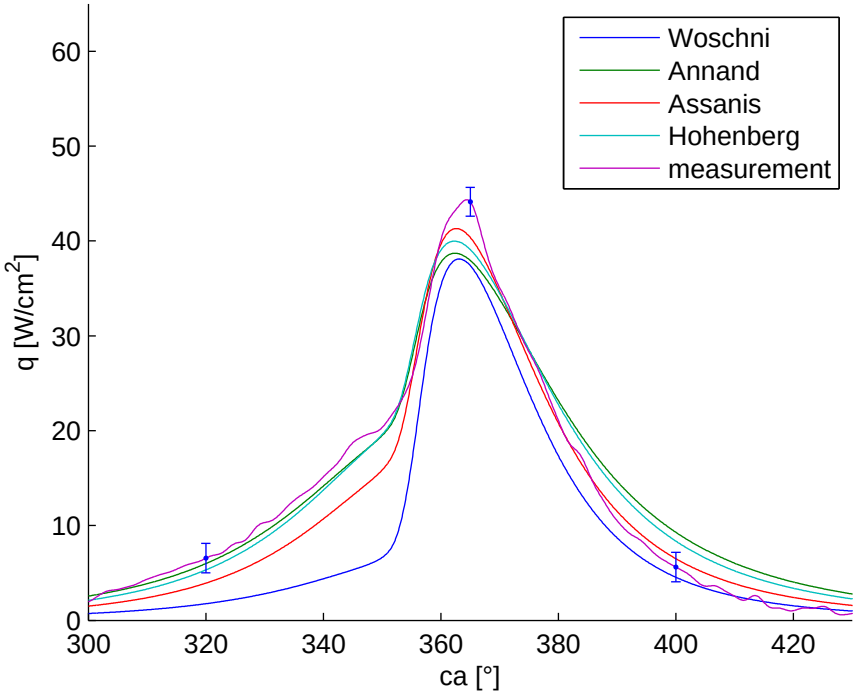

Figure 5.21: The wall heat flux for $\lambda = 5.86$, with $T_{in} = 180°C$, optimized scaling factors and CR 13:1

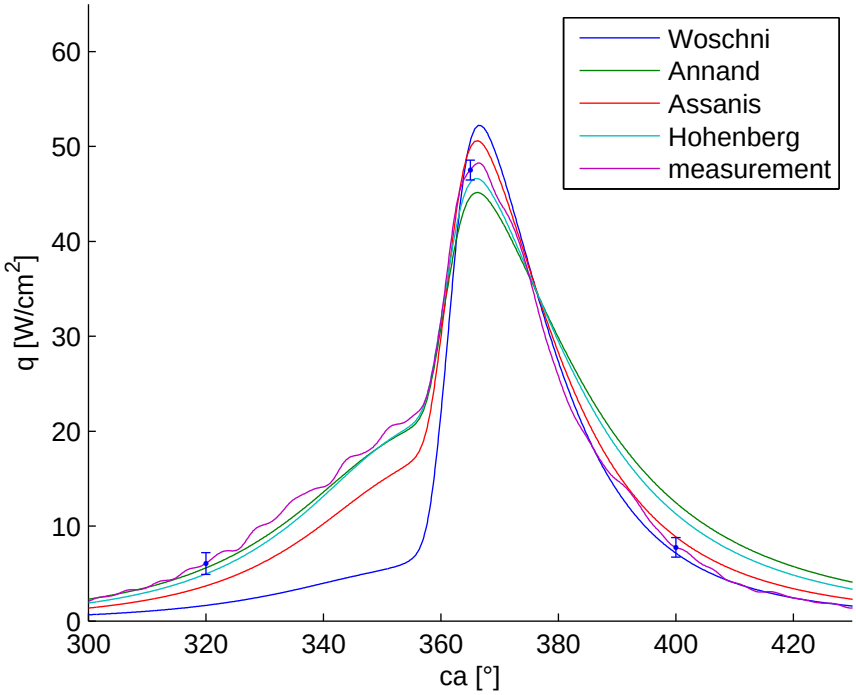

Figure 5.23: The wall heat flux for $\lambda = 4.24$ with $T_{in} = 150°C$, optimized scaling factors and CR 13:1

From all these correlations, *Annand* is the most basic one with the least assumptions. The other correlations use assumptions for the gas properties. This leads to the thought that *Annand* has the most potential to give the best result. Therefore, the *Annand* correlation is changed in order to get a better result. Since the gas properties, the in-cylinder pressure and the gas temperature are determined instantaneous, one could also try to determine an instantaneous characteristic length. Instead of using the bore as characteristic length, the characteristic lengths of *Assanis* and *Hohenberg* are tested. The results can be found in table 5.8. It can be seen that by using the characteristic length of *Assanis*, which is the instantaneous in-cylinder height, the error is reduced significantly. Using the characteristic length of *Hohenberg*, also results in an improvement, but not as big as with the characteristic length of *Assanis*. Take note that the scaling factor is even lower than before. The error when the characteristic length of *Assanis* is used, is even lower than the one of *Assanis*, which means that this adapted *Annand* correlation comes closest to the measured heat flux during the whole cycle. This result can also be found in figure 5.24, which depicts the heat flux of the original *Annand* and the adapted *Annand* correlations. For the adapted *Annand* correlations, the peak of the heat flux is higher and the heat flux during expansion is lower, compared to the original *Annand*. This brings this correlation closer to the measured heat flux. Although the adapted correlations come closer to the measured heat flux over the whole cycle, the heat flux during compression is a little worse estimated than with the original correlation. Therefore, the improvement to the original correlation is not as good as the lower mean square error suggests. The result for other λ values can be found in figure 5.25 and 5.26.

Table 5.8: Best scaling factor for the different correlations and adapted *Annand* correlations

Correlation	Best scaling factor	Mean square error of heat flux [W/cm^2]
Woschni	0.0054	1.94
Assanis	0.0363	1.12
Hohenberg	125	1.14
Annand ($L_{Assanis}$)	**0.1460**	**0.95**
Annand ($L_{Hohenberg}$)	**0.222**	**1.17**

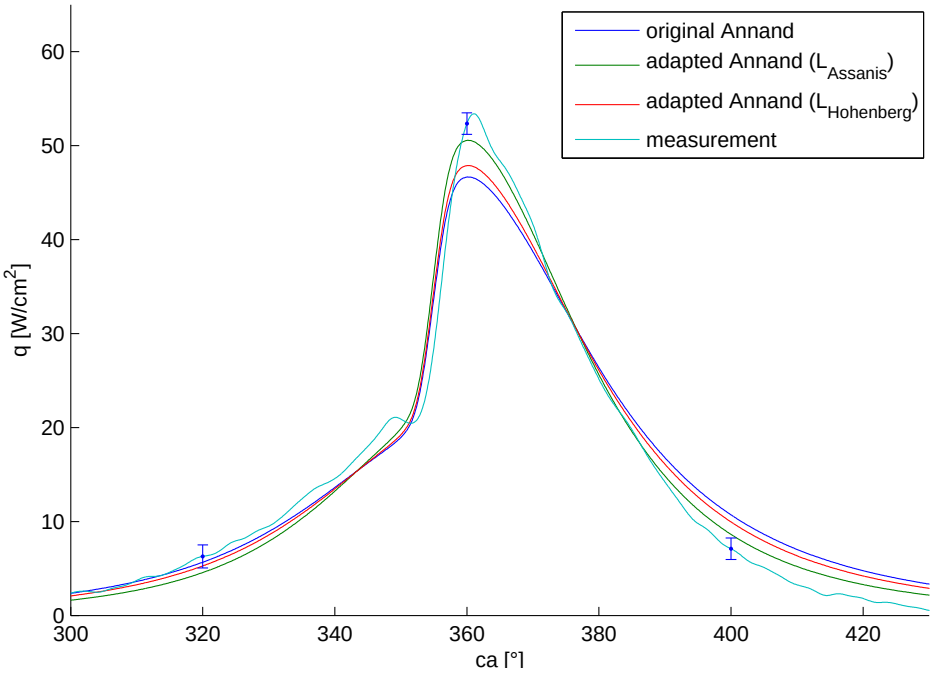

Figure 5.24: The original *Annand* correlation compared to the adapted *Annand* correlation for $\lambda = 4.54$, CR 13:1, $T_{in} = 180°C$ and optimized scaling factors

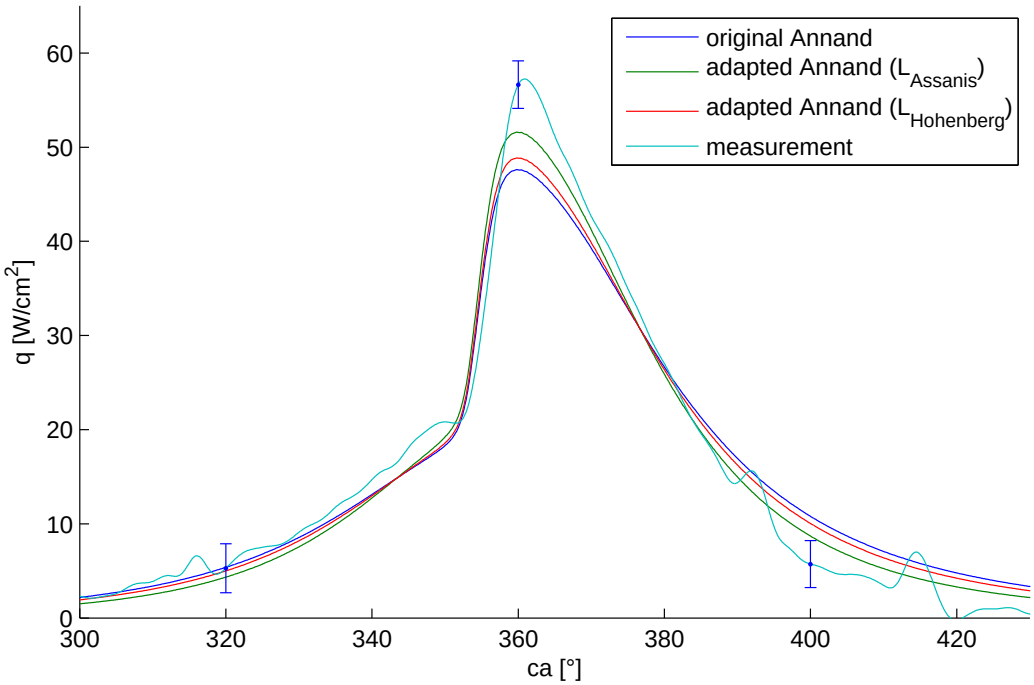

Figure 5.25: The original *Annand* correlation compared to the adapted *Annand* correlations for $\lambda = 4.35$, CR 13:1, $T_{in} = 180°C$ and optimized scaling factors

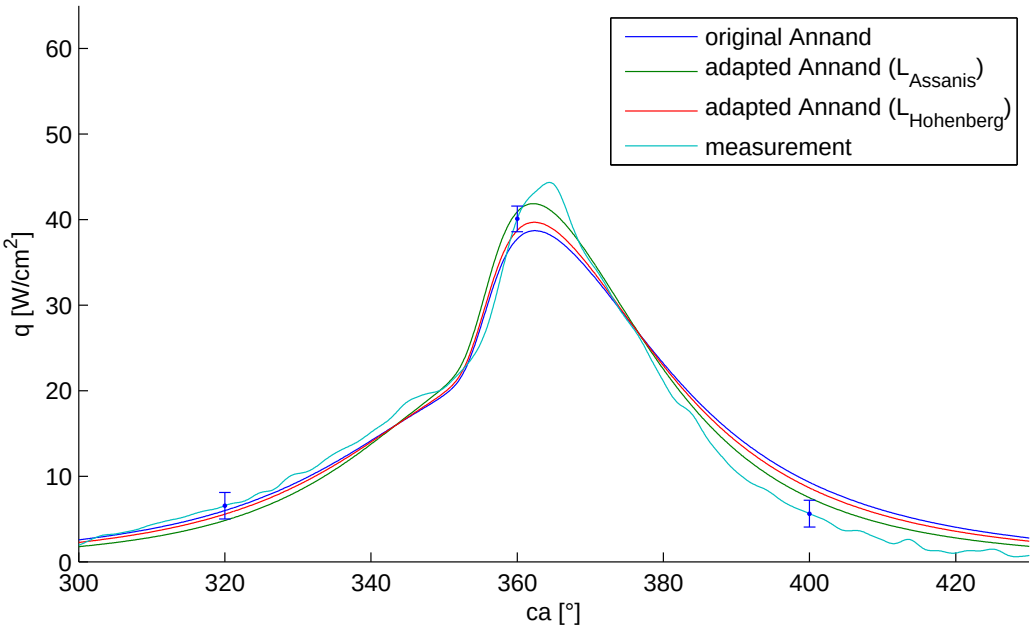

Figure 5.26: The original *Annand* correlation compared to the adapted *Annand* correlations for $\lambda = 5.86$, CR 13:1, $T_{in} = 180°C$ and optimized scaling factors

It can be concluded that the existing heat flux correlations come closer to the measured heat flux when changing the scaling factor. Their results are better, but they still cannot fully represent the measured heat flux. It is however unsatisfactory to adjust coefficients substantially for each different HCCI engine. Apart from this, the optimized scaling factors have only been tested in a limited operating range. This is for inlet temperatures of $150°C$, and $180°C$ and for various air to fuel ratios. Although the main conclusions stayed the same in this operating range, drastic changes in operating conditions should be investigated as well. This could go from big changes in the CR to using different fuels. This way, the robustness of an optimized heat flux correlation can be checked. Since wall heat fluxes are important for HCCI combustion, a good heat flux correlation needs to be used. The discussed heat flux correlations come close, but there is still a lot of room for improvement. Most of these correlations are also developed to match SI or CI engine data. A heat flux correlation based on the principles of HCCI combustion could render better results.

Chapter 6

Conclusions

In this last chapter, the most important conclusions that are made in this thesis will be discussed. This is followed by some recommendations and ideas for future research.

6.1 Conclusions

A study on HCCI combustion has been made. This includes a discussion on the principles of HCCI, the benefits and drawbacks, the various parameters that influence HCCI combustion and some recent developments concerning HCCI. It is explained that HCCI is a combustion proces that depends primarily on chemical kinetics, which is determined by the mixture composition and in-cylinder thermal conditions. The in-cylinder thermal conditions are influenced by the wall heat fluxes. Therefore an investigation into these wall heat fluxes is of great importance in order to fully understand HCCI combustion.

The setup of an existing CFR engine was changed and extended in order to run in HCCI operation. This was done by introducing an EGR and air preheating system. HCCI operation was successfully reached and the most important parameters influencing the combustion were examined. These include EGR, excess air ratio, CR and air preheating. The load limits, which are determined by the excess air ratio and inlet temperature, were also examined for a CR of 13:1.

Some flaws in the setup were revealed. Solutions to these shortcomings were proposed. A first important flaw was the determination of the fuel flow. Since gravimetrical measurements were not an option the fuel flow had to be determined using the exhaust gas composition. This introduced an important error on the excess air ratio and the fuel mass flow. Second, the determination of the EGR rate was done with the volume balance method, which is not the most accurate method. Preferably the molar balance method on

a CO_2 basis should be used. Finally, the HC emissions could not be measured. Since the temperatures during HCCI combustion are rather low, HC emissions cannot be neglected.

Heat flux measurement were carried out on the engine using a single layer TFG heat flux sensor. First, the different methods to calculate the wall heat flux were checked. The conclusion was that there was no significant difference between the methods. After this, the general course of the heat flux during HCCI combustion was discussed. A heat release analysis was performed as well. In this analysis, a variable specific heat ratio was introduced. The heat release analysis was compared with other sources, and validated with a measurement with hydrogen as a fuel in SI operation. Unfortunately, the acquired data from the heat release analysis for HCCI did not allow to make strict conclusions. This analysis should be carried out again, but with a correct measured mass fuel flow. Then the energy introduced into the cylinder can be calculated, as well as the combustion efficiency. The goal of such a heat release analysis is to validate if one heat flux sensor is sufficient to characterize the wall heat flux in the whole cylinder. After performing the heat release analysis, the various heat flux correlations that are proposed for HCCI combustion are investigated. These are *Annand*, *Woschni*, *Assanis* and *Hohenberg*. It could be concluded that for the unmodified correlations, *Hohenberg* gave the best result. *Annand* came close, but overestimated the heat flux during the whole cycle. *Woschni* and *Assanis* differed a lot from the measurements. Although *Hohenberg* comes close to the measured heat flux, it still deviates in some parts of the cycle, which means none of the correlations were able to estimate the wall heat flux accurately. The scaling factors of the various correlations were changed in order to get better results. We succeeded in improving the various correlations. However, it is rather unsatisfactory to adjust the coefficients of the correlations substantially for every HCCI engine. Therefore, a new correlation needs to be constructed, based on the principles of HCCI. Because we thought that the *Annand* correlation had some potential, we adapted the *Annand* correlation with a time-varying characteristic length since this was fixed in the original equation and the length scale in an engine can hardly be called constant. This gave better results, but still there were some deviations from the measured heat flux.

6.2 Future research

Improvements on the setup

Having done many measurements, some flaws in the setup revealed themselves. Some possible solutions to these shortcomings are proposed.

- It was noticed that the fuel rate could not be determined gravimetrically. This is caused by the heating of the fuel, which causes the evaporation of the fuel. In order to limit this evaporation, the fuel needs to be cooled. This would result an accurate determination of the mass fuel flow.
- The gas composition at the inlet of the engine is not accurately determined. It is believed that this is caused by a too small mixing length of the exhaust gas stream and the fresh incoming air. Therefore, we suggest to place the branch point more downstream at the inlet, which allows a better mixing of the two streams.
- Since HC emissions are not negligible for HCCI combustion, we suggest to introduce an emission analyser capable of measuring HC emissions into the system.
- During the combustion, the gas properties are changed linear. It might be better to determine the mass fraction burned using a *Wiebe* function.

Possible research

Since HCCI is a large research topic, we were unable to investigate all the various facets which come along with HCCI combustion. Further possible research on HCCI could be:

- Expanding the measurements for HCCI. This means: other compression ratios, other inlet temperatures, other EGR rates, other fuels and even other engine speeds if possible.
- Does it suffice to represent the wall heat flux in the whole cylinder, using only one heat flux sensor? This could be examined by measuring the heat flux at multiple points or by carrying out a heat release analysis.
- In this thesis, the focus was more on understanding the combustion process of HCCI. These days, emissions and efficiencies are important factors. It would be interesting to focus on possible ways to lower the CO and HC emissions and increase the efficiency.

Appendix A

Building test setup

The methodology when rebuilding the setup of the CFR engine is already explained in section 3. In this chapter, the several workpiece drawings as well as several assembly drawings of the newly build setup can be found.

A.1 Workpiece Drawings

In table A.1 a list of the several workpiece drawings can be found.

Table A.1: Workpiece drawings

Figure	
A.1	Inlet
A.2	Outlet
A.3	Part before buffer vessel
A.4	Part after buffer vessel
A.5	Mixing section of air and EGR
A.6	Y-piece of mixing section
A.7	Buffer vessel

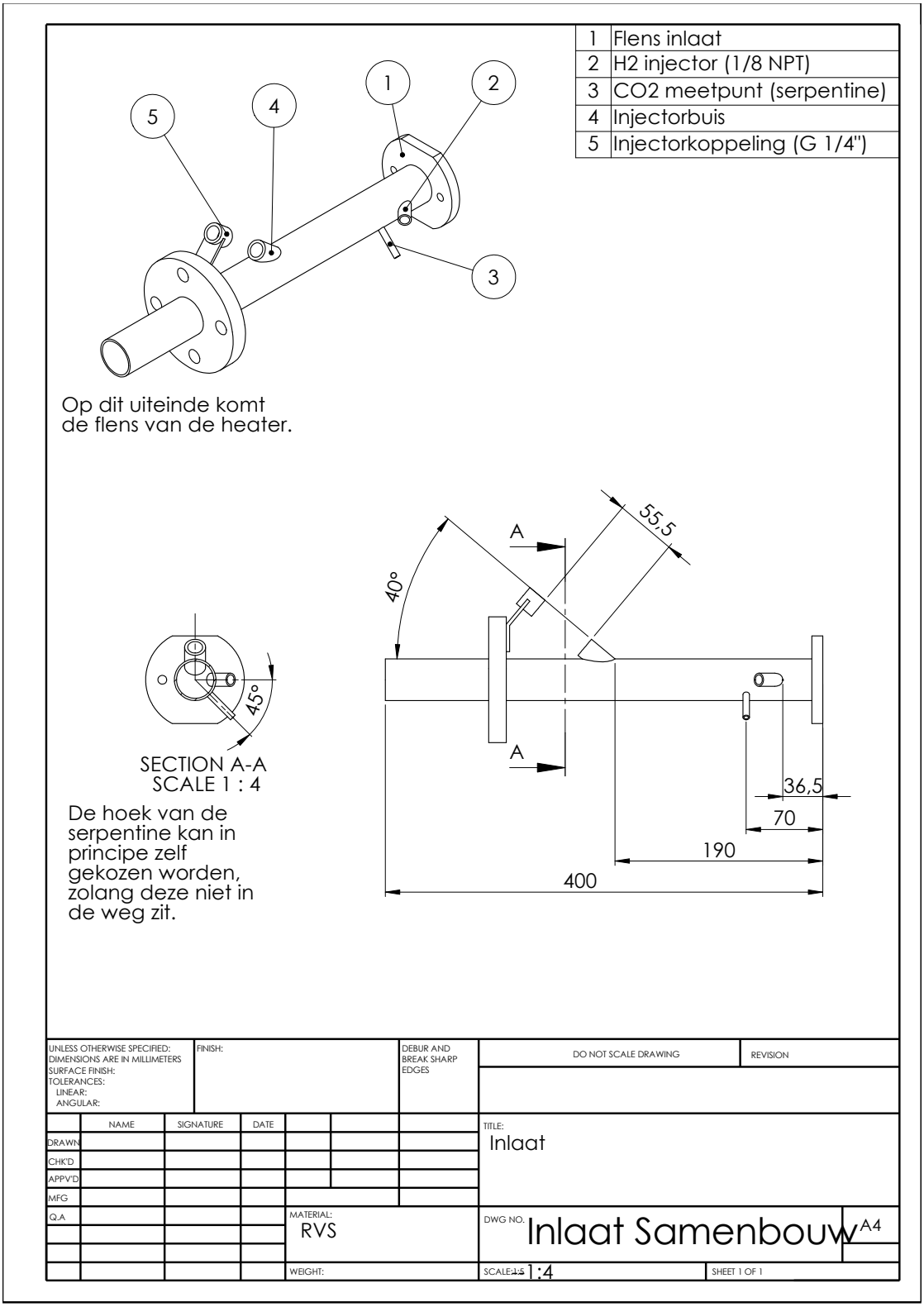

Figure A.1: Workpiece drawing of inlet

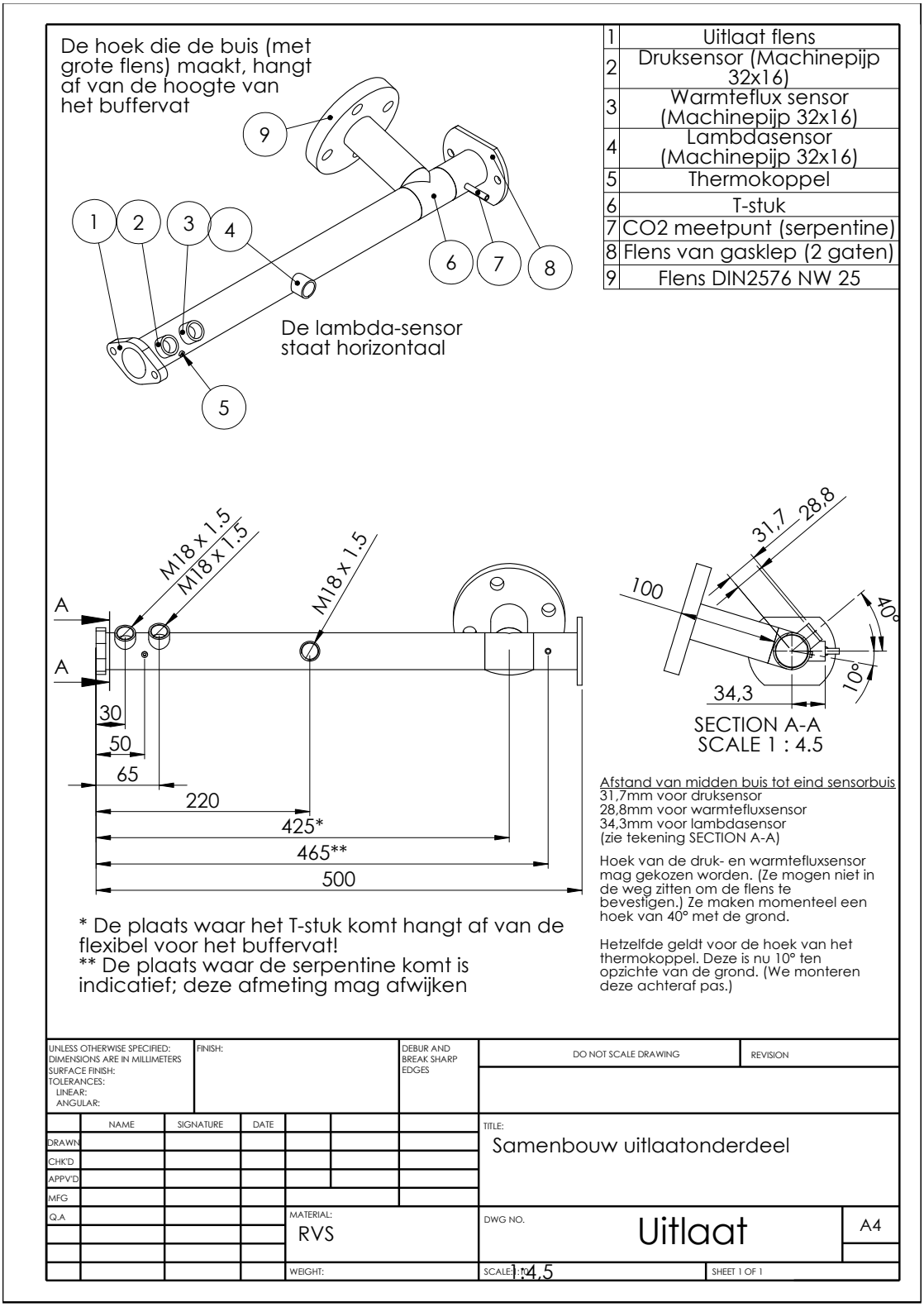

Figure A.2: Workpiece drawing of outlet

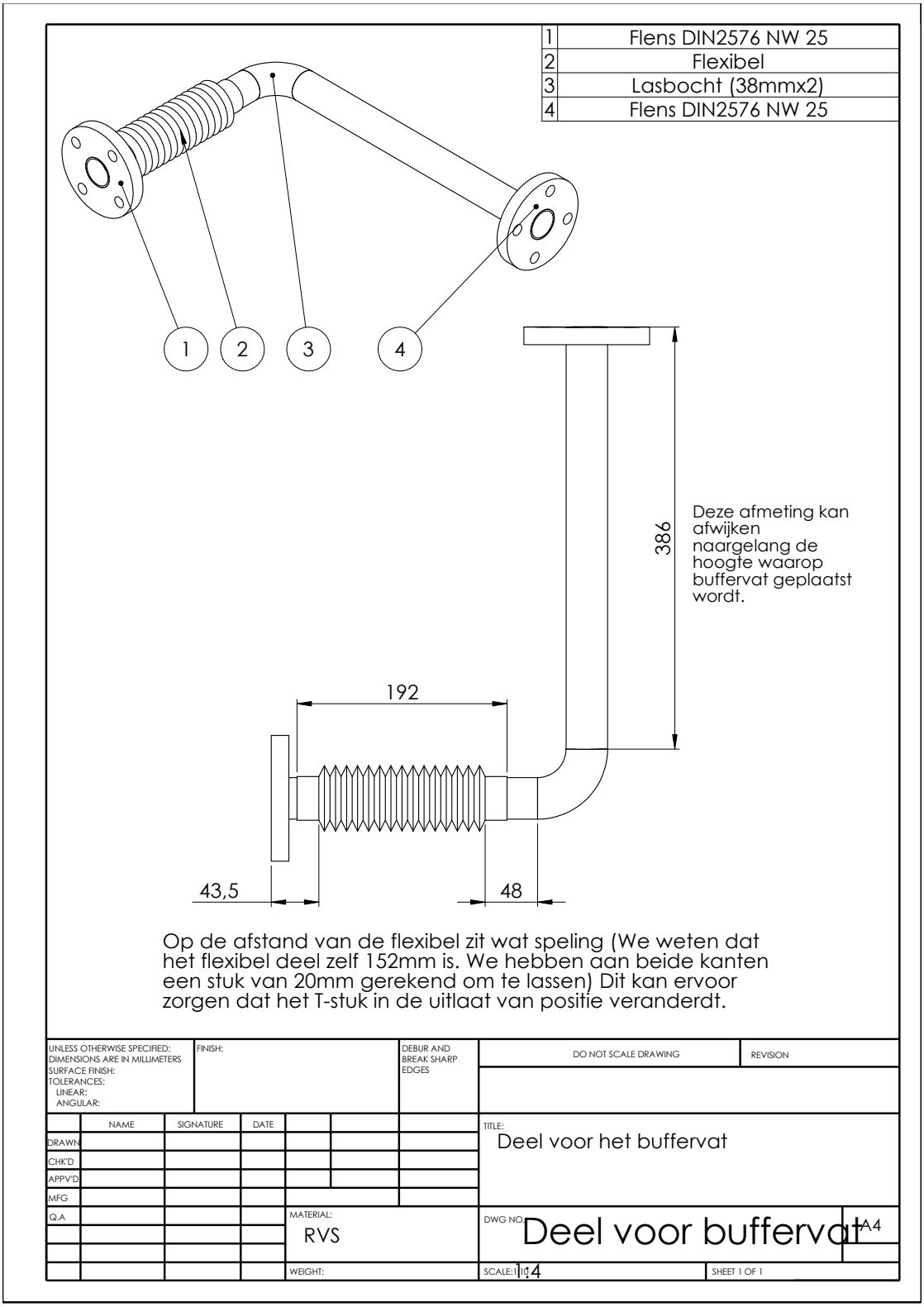

Figure A.3: Workpiece drawing of part before buffer vessel

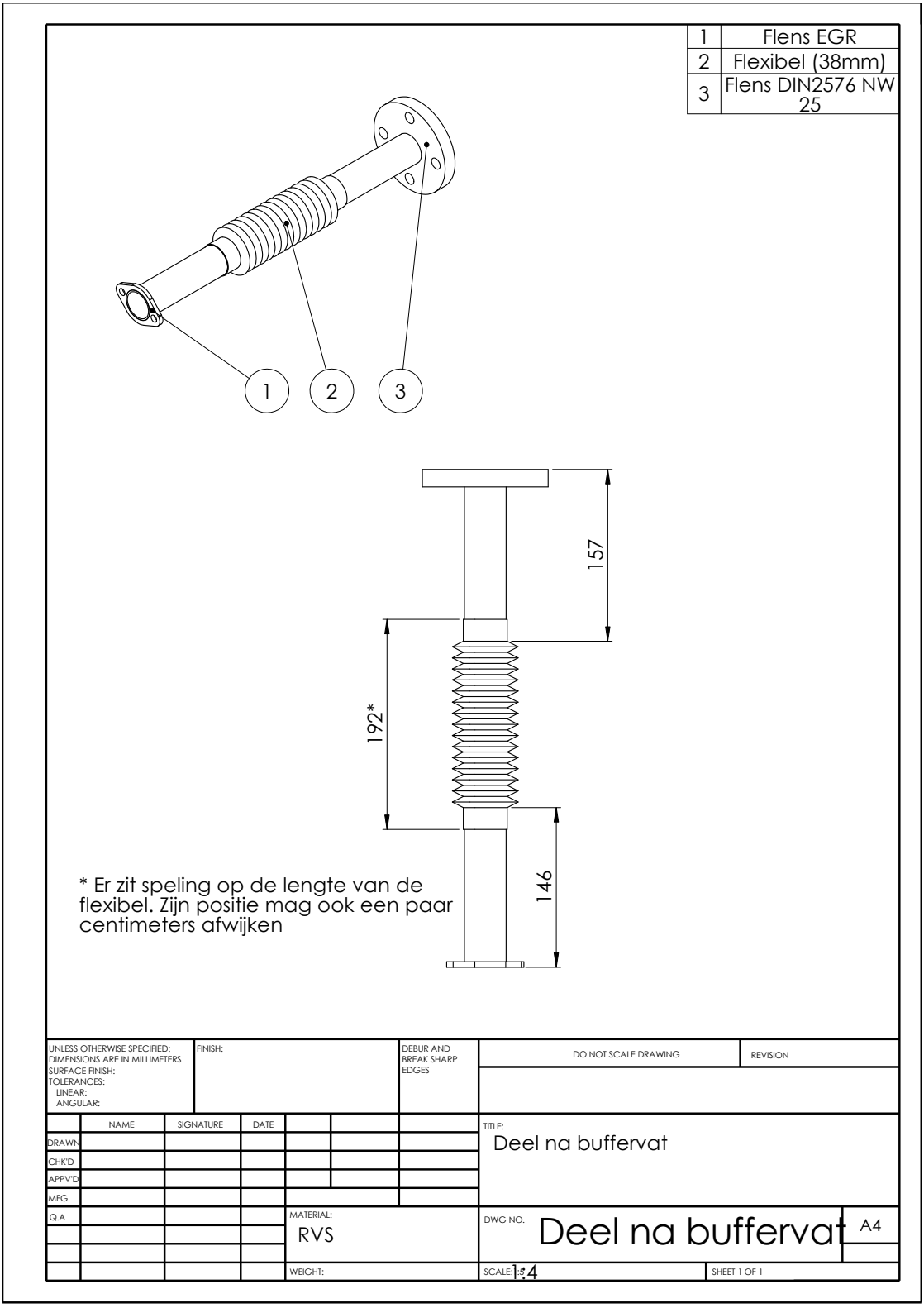

Figure A.4: Workpiece drawing of part after buffer vessel

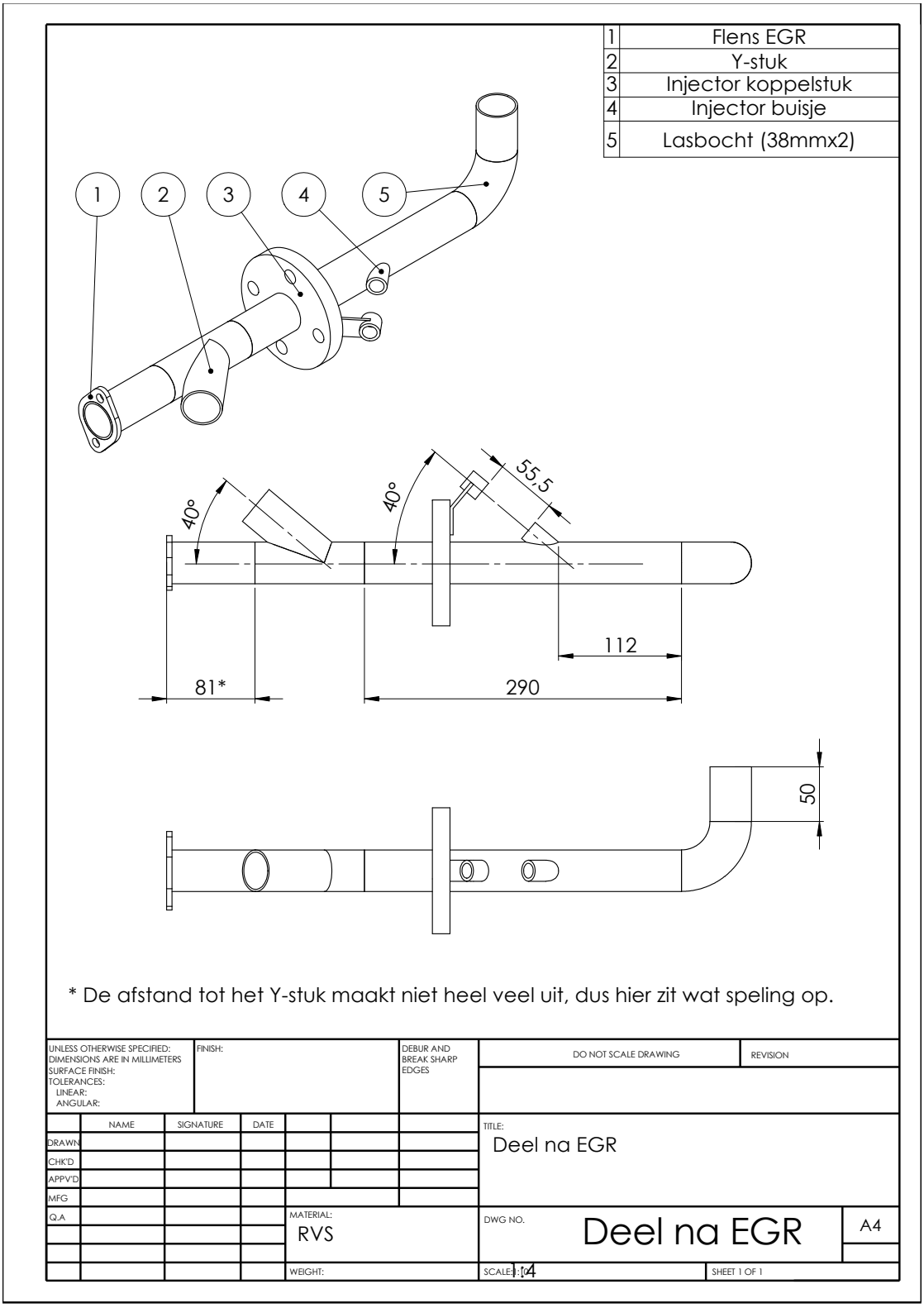

Figure A.5: Workpiece drawing of mixing section of air and EGR

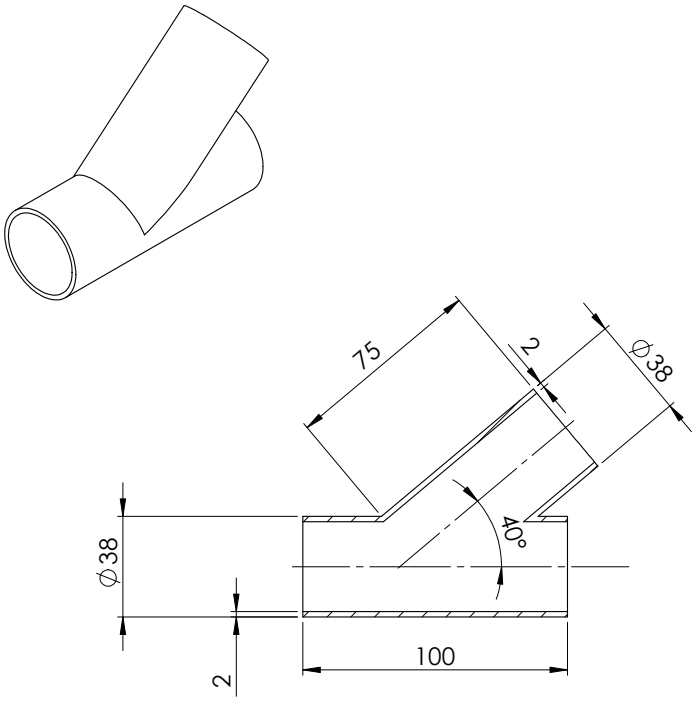

De lengtes zijn indicatief, en mogen in zekere mate afwijken.

UNLESS OTHERWISE SPECIFIED: DIMENSIONS ARE IN MILLIMETERS SURFACE FINISH: TOLERANCES: LINEAR: ANGULAR:	FINISH:				DEBUR AND BREAK SHARP EDGES	DO NOT SCALE DRAWING / REVISION
	NAME	SIGNATURE	DATE			TITLE: Y-stuk aan inlaat
DRAWN						
CHK'D						
APPV'D						
MFG						
Q.A				MATERIAL: RVS		DWG NO. Y-stuk / A4
				WEIGHT:		SCALE:1:2 / SHEET 1 OF 1

Figure A.6: Workpiece drawing of Y-piece in mixing section

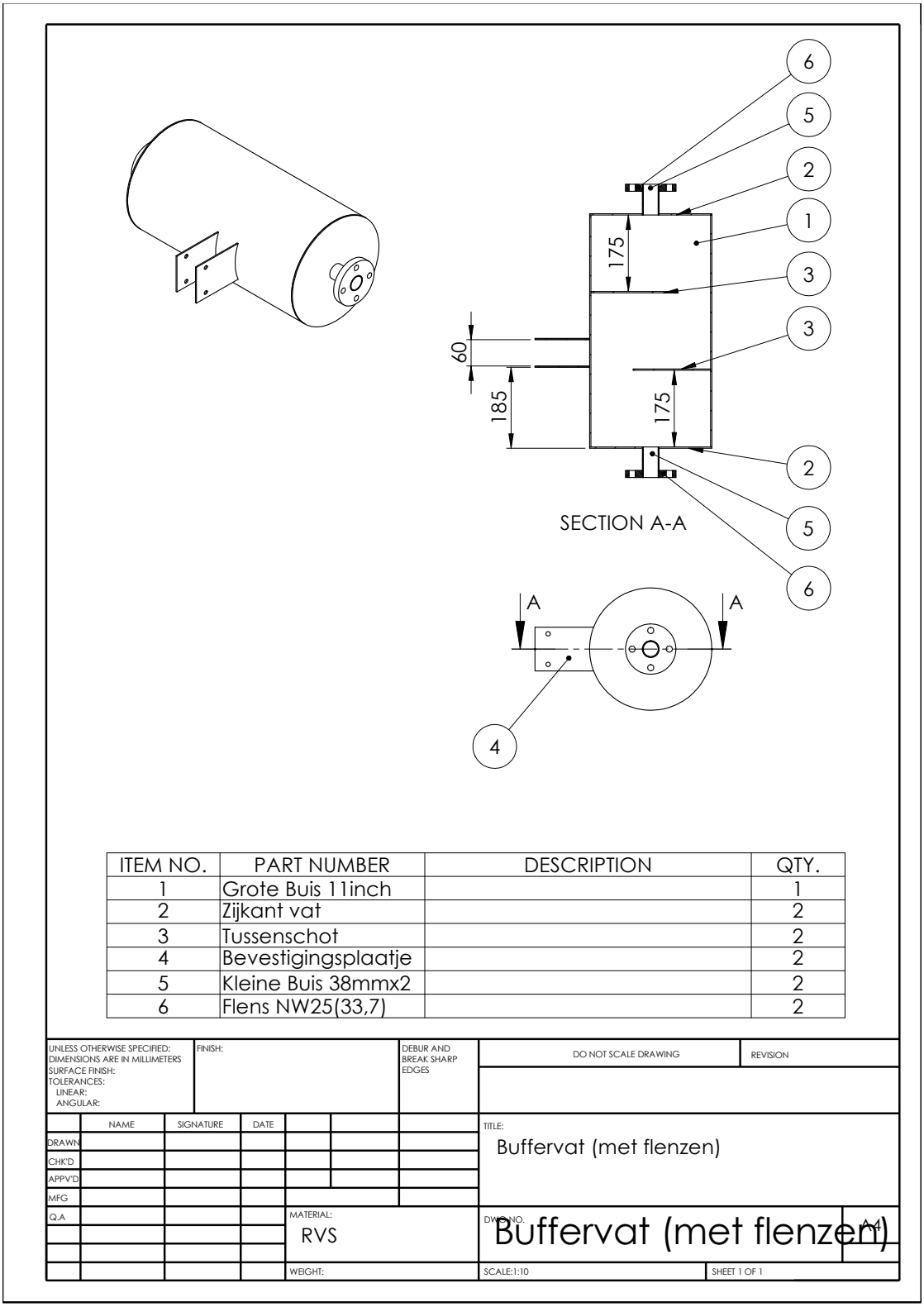

ITEM NO.	PART NUMBER	DESCRIPTION	QTY.
1	Grote Buis 11inch		1
2	Zijkant vat		2
3	Tussenschot		2
4	Bevestigingsplaatje		2
5	Kleine Buis 38mmx2		2
6	Flens NW25(33,7)		2

UNLESS OTHERWISE SPECIFIED:
DIMENSIONS ARE IN MILLIMETERS
SURFACE FINISH:
TOLERANCES:
LINEAR:
ANGULAR:

FINISH:

DEBUR AND BREAK SHARP EDGES

DO NOT SCALE DRAWING | REVISION

	NAME	SIGNATURE	DATE
DRAWN			
CHK'D			
APPV'D			
MFG			
Q.A			

MATERIAL: RVS

WEIGHT:

TITLE: Buffervat (met flenzen)

DWG NO. Buffervat (met flenzen) A4

SCALE:1:10 | SHEET 1 OF 1

Figure A.7: Workpiece drawing of the buffer vessel

A.2 Assembly Drawings

In table A.2 a list of the several assembly drawings can be found.

Table A.2: Assembly drawings

Figure	
A.8	Top view of setup
A.9	Front view of setup
A.10	Side view of setup
A.11	Perspective view of setup
A.12	Perspective view of setup

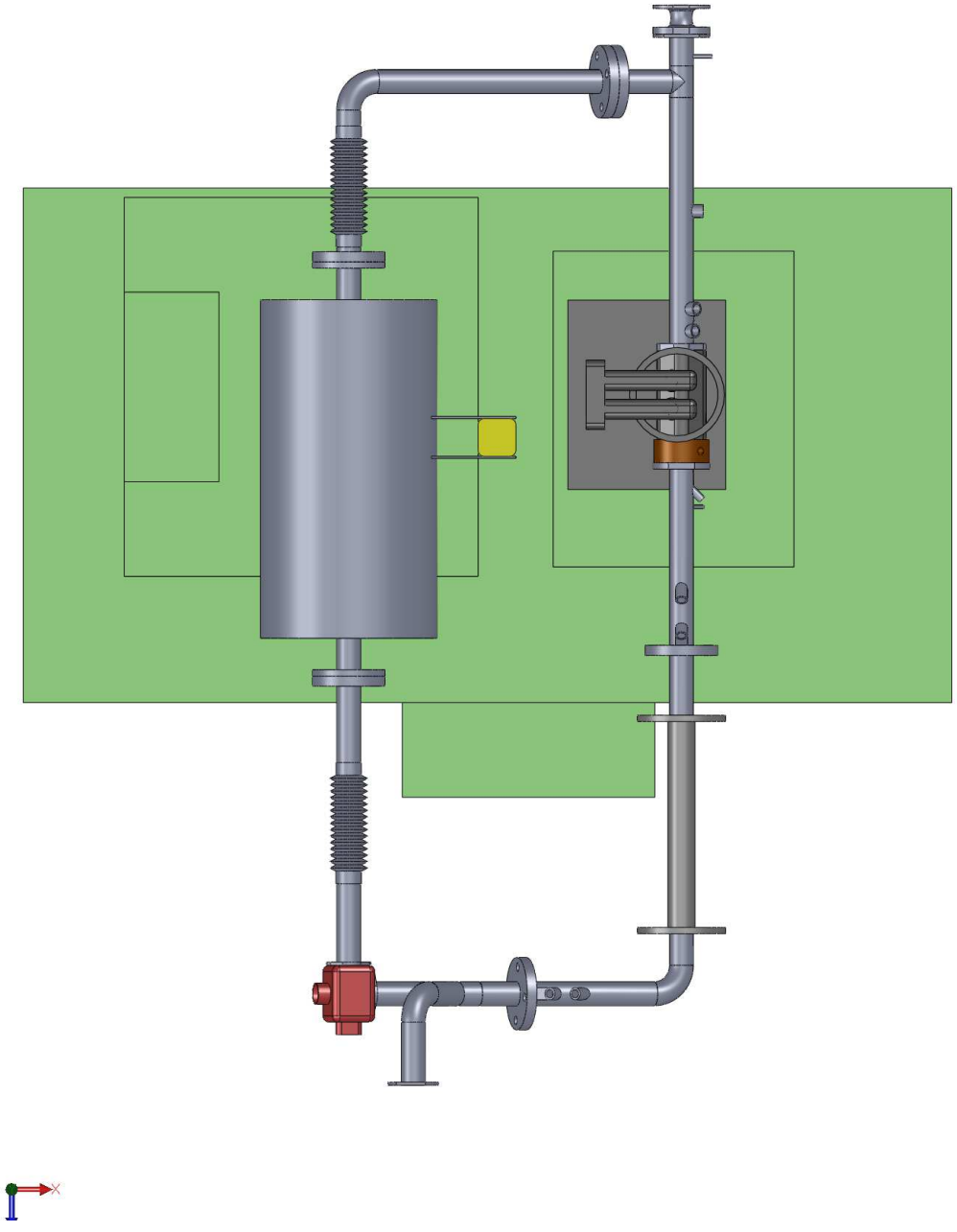

Figure A.8: Assembly drawing of setup: top view

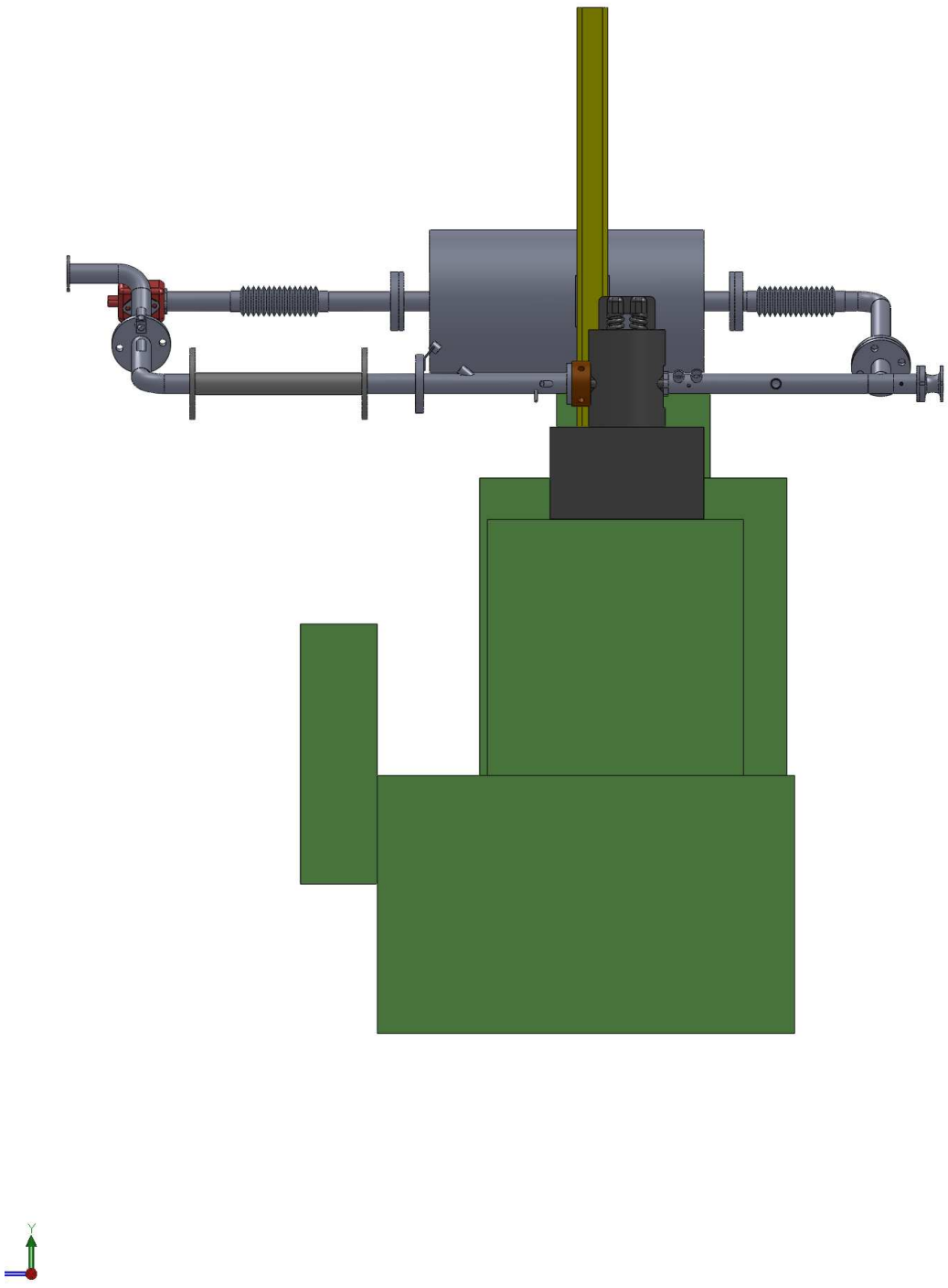

Figure A.9: Assembly drawing of setup: front view

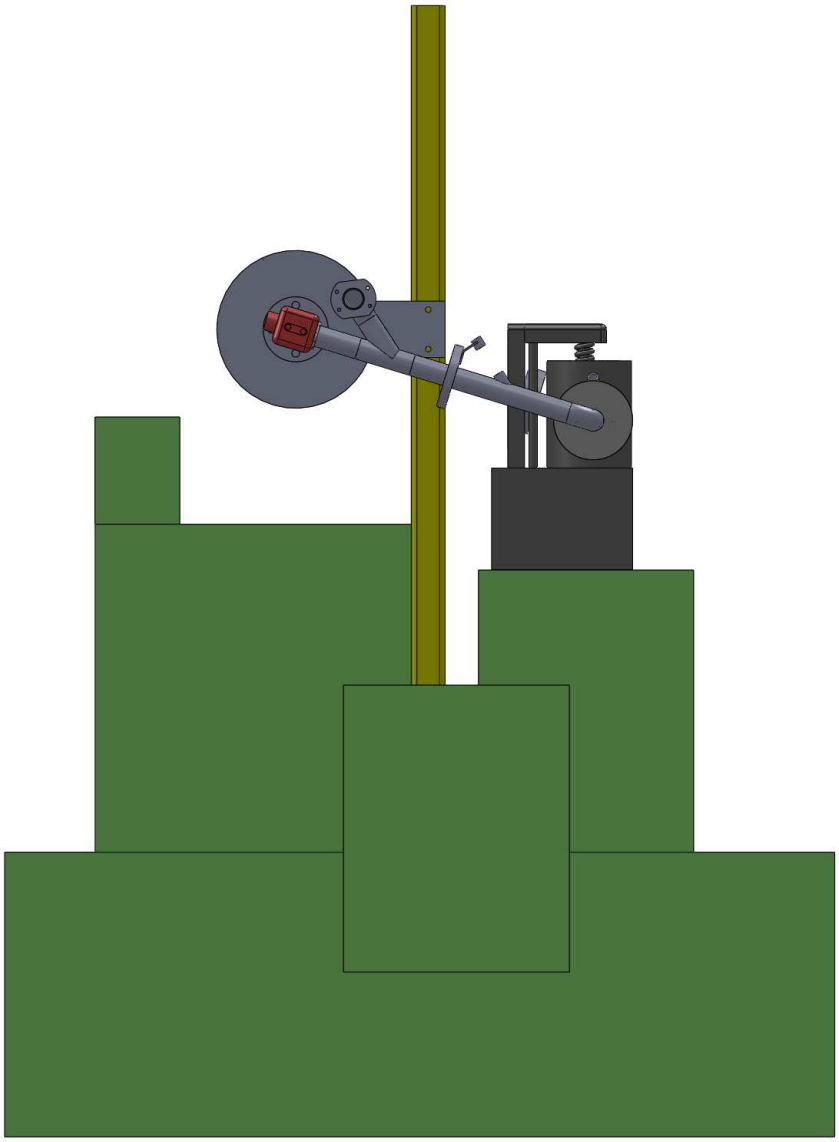

Figure A.10: Assembly drawing of setup: side view

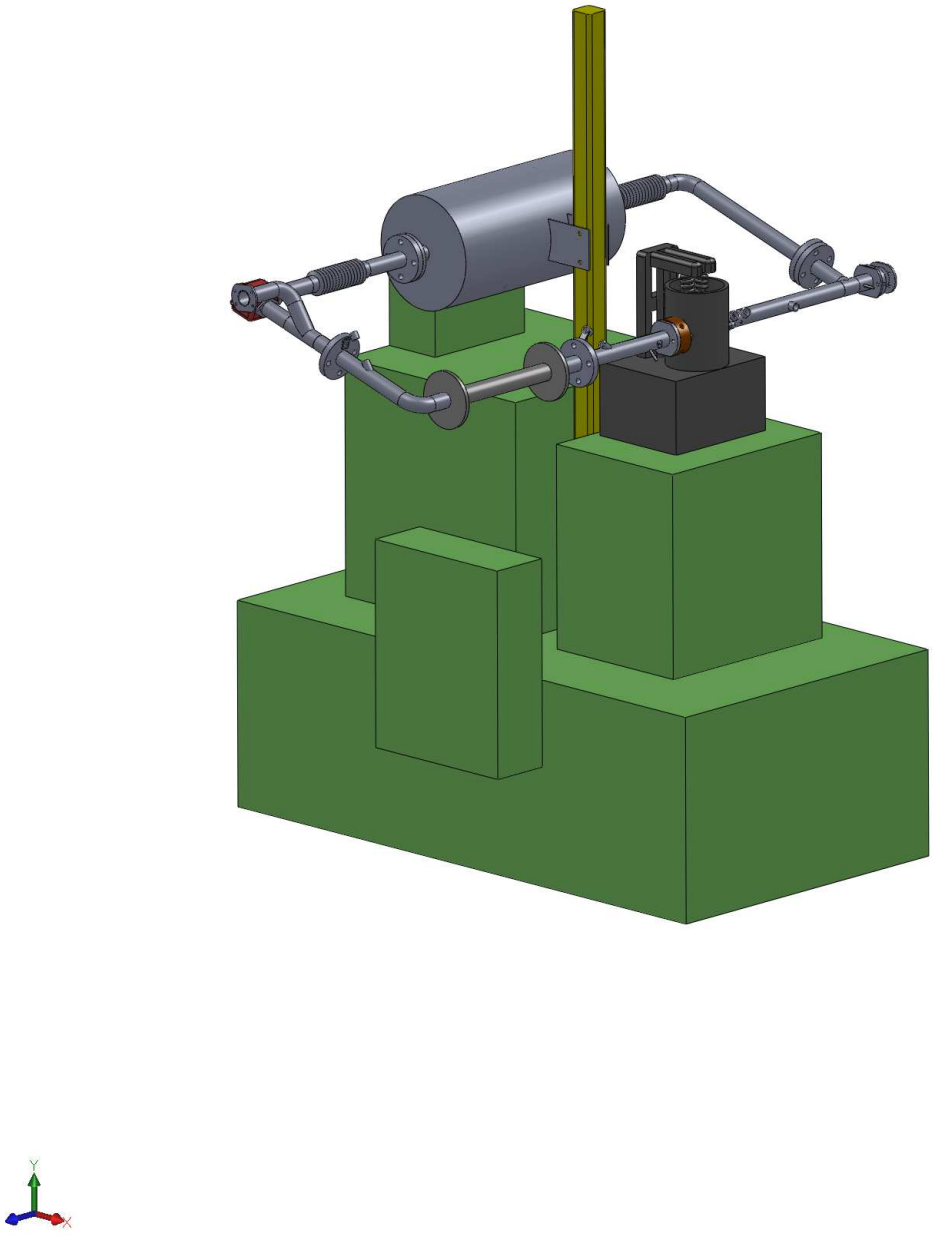

Figure A.11: Assembly drawing of setup

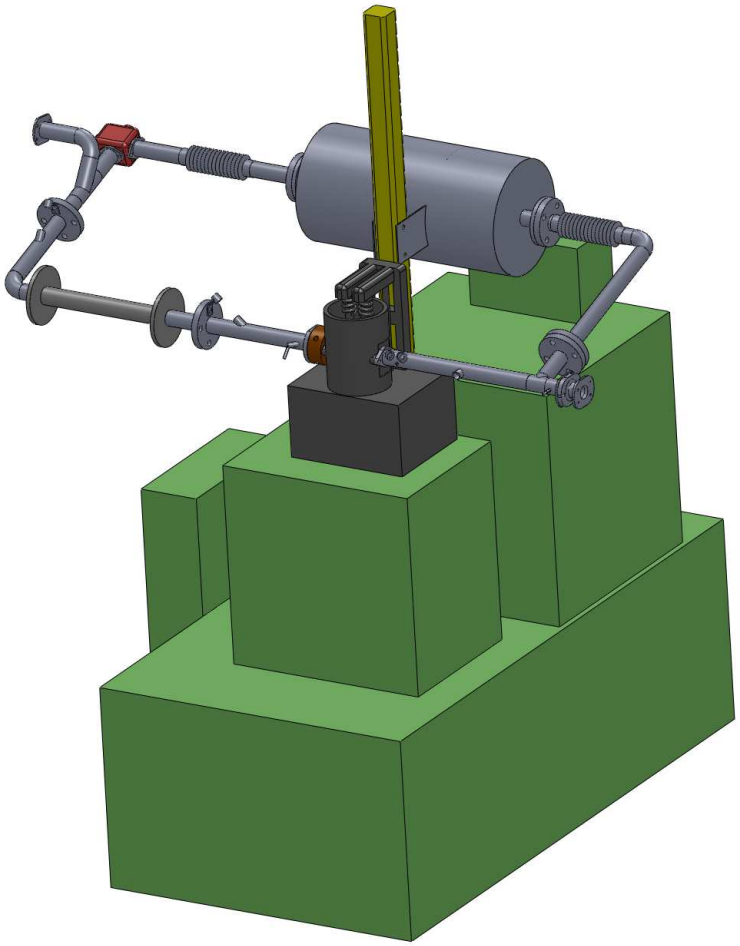

Figure A.12: Assembly drawing of setup

Appendix B

Setup Validation

In order to validate the setup and check if the newly installed EGR loop and air preheater work, some experiments on EGR and preheating are done. The experiments are done using SI. The effects of EGR and preheating are straightforward and can be compared to experiments conducted on other setups.

B.1 Effects of EGR

We tested the effects of EGR using methane as a fuel. The AFR is kept constant during the experiments. When more EGR is applied, the fuel flow is lowered in order to maintain stoichiometric combustion. Figure B.1 shows the pressure plot of the experiment, figure B.2 shows a temperature plot of the experiment. As can be seen on the figures, the maximum pressure and temperature are lowered when a higher percentage of EGR is applied. Because more exhaust gases are introduced into the cylinder, less air and fuel can react, resulting in less power. The lower maximum temperature can be explained by the higher specific heat capacity of exhaust gases due to more triatomic molecules like H_2O and CO_2. This results in less NO_X emissions. More EGR results in a longer combustion duration and a lower heat release rate. The slower combustion and the slightly increased inlet temperature, due to the hot exhaust gases, result in a higher exhaust gas temperature. It can be concluded that the EGR system works properly. Since a broad discussion on EGR is beyond the scope of this thesis, we refer to the literature for a more detailed study on EGR effects.

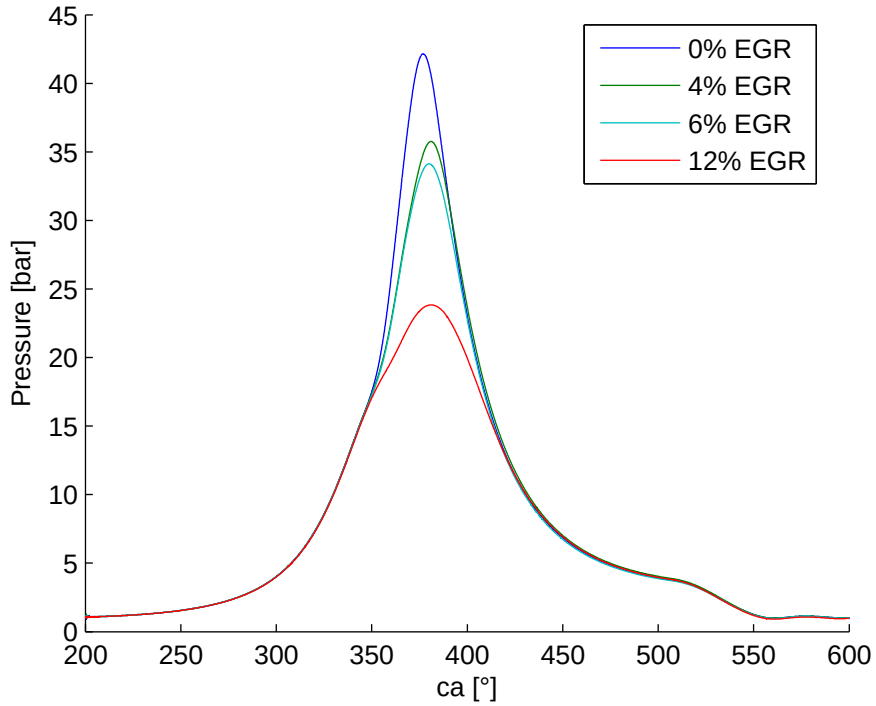

Figure B.1: Pressure for different percentages of EGR; $\lambda = 1$; CR=9:1; IGN=17°$BTDC$

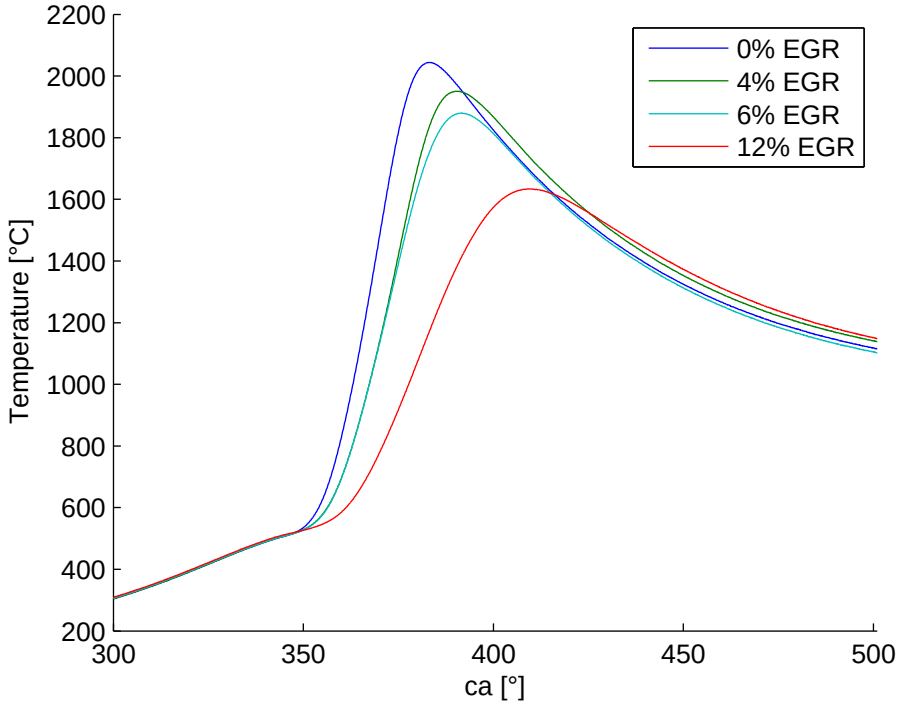

Figure B.2: Temperature for different percentages of EGR; $\lambda = 1$; CR=9:1; IGN=17°$BTDC$

B.2 Effects of preheating

With the air preheater, we are able to heat up the mixture to temperatures up to 400°C. The heating skills of the preheater are tested in motored conditions, when the engine is used as a compressor. The temperature at the inlet is controlled with the PID-controller. By adapting the voltage over the heater with the potentiometer the inlet temperature can be kept within a range of 3°C around the set point.

The heater was also tested in fired condition using methanol as a fuel. A graph of the in-cylinder gas temperature can be found in figure B.3. Only the closed part of the cycle is shown on the graph (from IVC to EVO). As expected, the temperature during compression is higher for the preheated mixture, so is the temperature during combustion. The combustion duration is also shorter for the heated mixture.

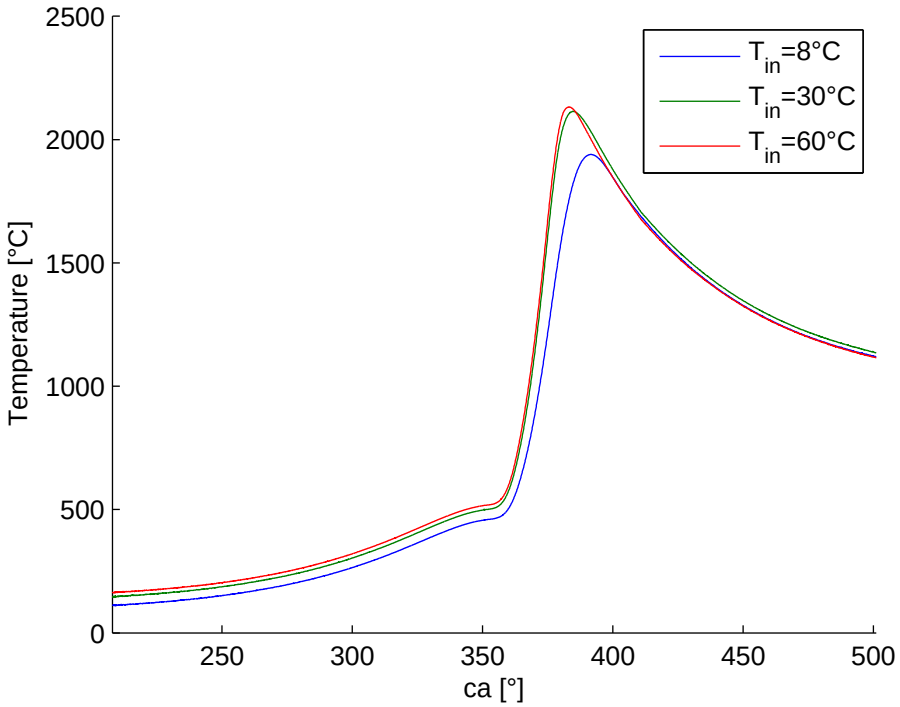

Figure B.3: In-cylinder gas temperature for a preheated and non-preheated mixture of methanol and air at WOT, $\lambda = 1$, CR=9:1, IGN=9°$BTDC$

When heating up the mixture, knocking manifests more easily. During our tests, knocking occurs for a λ of 1 and an ignition timing of 9°$BTDC$ at inlet temperatures of about 60°C. Increasing the inlet temperature from 30°C to 60°C does not give much changes. This can be explained by two counteracting effects. Because the temperature of the incoming

mixture is higher, the overall temperature should increase, as is the case when heating from $8°C$ to $30°C$. Although the incoming mixture is hotter, the load that is brought into the cylinder is lower. Heating up the air, results in a lower density. Therefore, less air is available for combustion. In order to maintain stoichiometric combustion, the fuel flow should be lowered as well. This effect would result in a lower temperature. These two effects, result in no significant changes between the combustion for $30°C$ and $60°C$.

Appendix C

Calculations and Error analysis

In this appendix, all calculations that were needed in this thesis will be written out. An error analysis will be carried out as well.

C.1 Calculations

C.1.1 Indicated values

First, the equations that are used to calculate the indicated values in this thesis, will be given. Most of these equations can be found and are explained in *Introduction to Internal Combustion Engines* by *R. Stone* [36] or *Internal Combustion Engine Fundamentals* by *J. Heywood* [27].

Indicated work per cycle

$$W_i = \oint pdV \tag{C.1}$$

The indicated work per cycle W_i in Joule can be found by calculating the enclosed area of the p-V diagram.

Indicated power output

$$P_i = \frac{W_i \cdot N \cdot 60}{n_g} \tag{C.2}$$

with N the crankshaft rotational speed in rpm and n_g the number of crank revolutions for each power stroke per cylinder. Since the CFR engine has a rotational speed of 600 rpm and uses a four-stroke cycle, N equals 600 rpm and n_g equals 2.

Indicated mean effective pressure

$$imep = \frac{W_i}{V_s} \tag{C.3}$$

with W_i in Joules and V_s the swept volume in m^3, the imep is expressed in Pa.

Specific fuel consumption

$$sfc = \frac{\dot{m}_f}{P_i} \tag{C.4}$$

with $\dot{m}_f$ the fuel mass flow and P_i the indicated power output.

Indicated efficiency

$$\eta_i = \frac{P_i}{\dot{m}_f \cdot H_u} \tag{C.5}$$

With H_u the lower heating value of the fuel. For gasoline this is $H_u = 44.4\ MJ/kg$.

C.1.2 Load limits of HCCI

To define the load limits of HCCI, the coefficient of variation of the imep and the pressure rise rate are used as a criterium. These can be calculated as follows:

Coefficient of variation of the imep

$$COV_{imep} = \frac{\sigma_{imep}}{\bar{imep}} \cdot 100 = \frac{\sum (imep - \mu_{imep})^2}{\mu_{imep}} \cdot 100 \tag{C.6}$$

with σ_{imep} the standard deviation of the imep and μ_{imep} the mean imep. Take note that the COV is calculated over a number of cycles. In our case, it is calculated over 100 cycles. The COV_{imep} defines the cyclic variability in indicated work per cycle. The criterion for stable combustion is a COV_{imep} under 10%.

Pressure rise rate

$$\frac{dp}{d\theta} = p(n + 1°ca) - p(n) \tag{C.7}$$

with p(n) the pressure at crank angle n. The pressure rise rate indicates how fast the pressure rises during a time duration of $1°ca$. For HCCI, the upper load limit is defined by a maximum pressure rise rate of 5 $bar/°ca$ for the CFR engine. Sometimes a value of 10 $bar/°ca$ is found in the literature.

C.1.3 Excess air ratio λ and fuel flow rate from exhaust gas composition

The excess air ratio λ is calculated from the exhaust gas composition with the equation of Brettschneider [23]:

$$\lambda = \frac{\left[CO_2\right] + \left[CO/2\right] + \left[O_2\right] + \left[NO/2\right] + \left(\frac{H_{cv}}{4} \cdot \frac{3.5}{3.5 + \frac{\left[CO\right]}{\left[CO_2\right]}} - \frac{O_{cv}}{2}\right) \cdot \left(\left[CO_2\right] + \left[CO\right]\right)}{(1 + \frac{H_{cv}}{4} - \frac{O_{cv}}{2}) \cdot \left(\left[CO_2\right] + \left[CO\right] + \left[HC\right]\right)} \tag{C.8}$$

Where $\left[\mathrm{X}\right]$ is the gas volume concentration of gas X, H_{cv} is the atomic ratio of hydrogen to carbon in the fuel and O_{cv} is the atomic ratio of oxygen to carbon in the fuel. Since we always used gasoline as a fuel, O_{cv} is zero in this equation. The atomic ratio of hydrogen to carbon is 1.87 [27]. It was not possible to determine the amount of hydrocarbons. Therefore $\left[\mathrm{HC}\right]$ is set to zero for this equation. This introduces a substantial error for the excess air ratio. It should be seen as an indication of the real excess air ratio.

The fuel flow rate could not be determined gravimetrically as explained in chapter 3. Therefore it was decided to determine the fuel flow from the excess air ratio as calculated above and the air flow measured with a Bronkhorst F-106BZ mass flow sensor:

$$\dot{m}_{fuel} = \frac{\dot{m}_{air}}{AFR} = \frac{\dot{m}_{air}}{\lambda \cdot AFR_{stoich}} = \frac{\dot{m}_{air}}{\lambda \cdot 14.7} \tag{C.9}$$

The stoichiometric air-to-fuel ratio is always 14.7 in our case because we only performed measurements with gasoline (RON98).

C.1.4 %EGR

To control and monitor the exhaust gas recirculation we define %EGR as follows.

$$\%EGR = \frac{\dot{m}_{EGR}}{\dot{m}_{EGR} + \dot{m}_{air} + \dot{m}_{fuel}} \tag{C.10}$$

There are three mass flows that need to be determined. The air mass flow is measured with a Bronkhorst F-106BZ mass flow sensor. The fuel flow is calculated as in appendix C.1.3. The EGR mass flow was first calculated with the fractions of CO_2 at the inlet and outlet. As explained in chapter 3 an incorrect fraction of CO_2 at the inlet was measured. Therefore we used a volume balance method to determine the EGR mass flow rate. Both methods are described below.

Molar balance method on a CO_2 basis The principle and derivation of this formula can be found in the thesis of *J. Dierickx and Y. Huyghebaert* [37]. This method makes no use of any assumption and is therefore quite accurate. It is a widespread method and used by most of the researchers when the EGR mass flow needs to be determined.

$$\dot{m}_{EGR} = \dot{m}_{air} \cdot \frac{MM_{EGR}}{MM_{air}} \cdot \frac{y_{CO_2,air} - y_{CO_2,mix}}{y_{CO_2,mix} - y_{CO_2,EGR}} \tag{C.11}$$

In this equation MM_{EGR} and MM_{air} are the molar mass of exhaust gas and air respectively. These values are determined with a Matlab script. The air mass flow is measured with a Bronkhorst F-106BZ mass flow sensor. The molar fraction of CO_2 in the air is 0.0397% and the molar fractions of CO_2 in the exhaust gas (outlet) and mixture (inlet) are measured with the emission analyser. Take note that the emission analyser measures dry volume fractions. The gas mixtures are treated as ideal gases and therefore molar fraction is equal to volume fraction. A dry/wet correction is used to convert the dry fractions to wet fractions. This is described below.

Volume balance method After the first EGR measurements it was clear that %EGR was not determined correctly. Therefore we switched to another, less accurate method. As explained in chapter 3 this method is acceptable in our case because we could control inlet temperature and thus the error that normally follows from mixing with hotter exhaust gases is avoided.

The volume balance method assumes that the total mass introduced in the cylinder is independent of inlet temperature and gas properties. This way, two situations can be compared: one with and one without EGR. This method thus assumes an equal volumetric efficiency for both situations, as shown in figure C.1. In our case this is a very acceptable assumption. Normally an engine setup does not dispose of an air preheater. Without an air preheater the total mass introduced in the cylinder drops when applying EGR because the temperature of the exhaust gases is higher and the density is lower than that of fresh air. Since an internal combustion engine is a volumetric machine, the total mass of the intake mixture drops because the density drops due to the higher intake temperature. A volume balance then introduces a big error. Since the new setup disposes of an air preheater, the temperature of the intake mixture can be kept constant with and without EGR. The only error introduced in our case is the difference in density between fresh air and exhaust gas at the same temperature. At $150°C$ the density of fresh air is $0.835kg/m^3$ while the density of exhaust gas is $0.831kg/m^3$ for an excess ratio λ of 3 which is typical for HCCI

combustion. This is a minor difference, the volume balance method is quite accurate in our case but still the calculation of the %EGR with this method is an indication of the real %EGR.

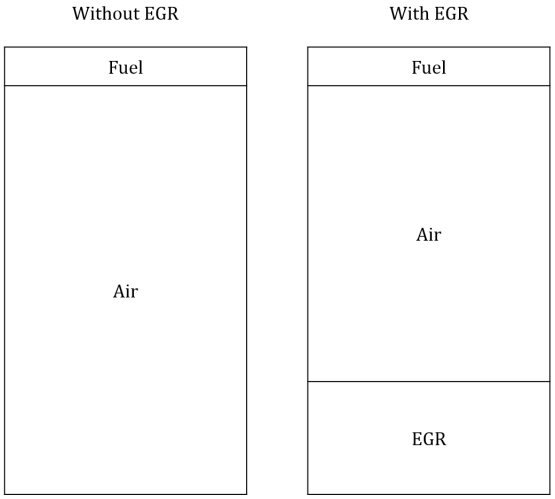

Figure C.1: Schematic representation of the cylinder content with and without EGR

As can be seen from figure C.1 the difference of air volume flow rate between these two situations then is the EGR volume flow rate.

$$\begin{aligned} \dot{m}_{EGR} = \rho_{EGR} \cdot (Q_{air,withoutEGR} - Q_{air,withEGR}) = \rho_{EGR} \cdot \frac{\Delta \dot{m}_{air}}{\rho_{air}} \\ = \frac{\frac{p_{EGR}}{R_{EGR} \cdot T_{EGR}}}{\frac{p_{air}}{R_{air} \cdot T_{air}}} \cdot \Delta \dot{m}_{air} = \frac{R_{air}}{R_{EGR}} \cdot \Delta \dot{m}_{air} \end{aligned} \tag{C.12}$$

In this equation ρ_{EGR} is the density of the recirculated exhaust gas. This is calculated with the ideal gas law as in the equation above. The pressure and temperature is the same for the EGR and for the intake air, so these factors are eliminated in the equation. The composition of the exhaust gas is calculated with a Matlab script. With this composition the specific gas constant for the exhaust gas is calculated.

Dry/wet correction for CO_2 and CO The emission analyser measures the dry volume fractions. The water vapour is condensed and captured in a condense cup in order to prevent the water vapour to enter the emission analyser. Dry and wet fractions or concentrations are related to each other through the following equation:

$$frac_{wet} = k_w \cdot frac_{dry} \tag{C.13}$$

With

$$k_w = \frac{1}{1 + \alpha \cdot 0.005 \cdot (vol\%_{CO_{dry}} + vol\%_{CO_{2,dry}}) + k_{w2}} \tag{C.14}$$

And

$$k_{w2} = \frac{1.608 \cdot y_{H_2O}}{1000 + (1.608 \cdot y_{H_2O})} \tag{C.15}$$

And

$$y_{H_2O} = 0.622 \cdot \frac{\phi \cdot p_s}{p_{air} - \phi \cdot p_s} \tag{C.16}$$

And

$$p_s = exp(A \cdot T^{-2} - B \cdot T^{-1} + C - D \cdot T + E \cdot T^2 - F \cdot T^3 + G \cdot T^4 + H \cdot ln(T)) \tag{C.17}$$

With

A = -2.9912729 $\cdot 10^3, B = 6.0170128 \cdot 10^3, C = 1.887643845 \cdot 10^1, D = -2.8354721 \cdot 10^{-2}, E = 1.7838301 \cdot 10^{-5}, F = 8.415041 \cdot 10^{-10}, G = 4.4412543 \cdot 10^{-13}, H = 2.858487 \cdot 10^0$.

The last equation is proposed by A. Wexler and estimates the saturation pressure with an accuracy of ±2 Pa as explained in the thesis of *J. Dierickx and Y. Huyghebaert* [37].

In these equations:

- α = the ratio of hydrogen to carbon (1.87 for gasoline [27])
- y_{H_2O} = the absolute humidity of the intake air [g water / kg air]
- ϕ = the relative humidity of the intake air
- p_s = the saturation pressure of the intake air [kPa]

This dry/wet correction is only valid for CO_2, CO and HC. Since we always measured zero NO_X emissions, no dry/wet correction for NO_X was necessary.

C.1.5 In-cylinder gas temperature

The in-cylinder gas temperature is calculated with the ideal gas law. Since for HCCI combustion the mixture is nearly homogeneous at every moment of the cycle, this is a good assumption.

$$T = \frac{p_{cyl} \cdot V_{cyl}}{m_{mix} \cdot R_{mix}} \tag{C.18}$$

In this equation the mass of the mixture m_{mix} is constant through the entire cycle. The cylinder pressure is measured for every sample and the volume is calculated for every sample. The specific gas constant of the mixture is dependent of the mixture composition. This composition is calculated with the Matlab script.

C.1.6 Net heat release rate

The net HRR can be expressed as:

$$\delta Q_{net} = \delta U_s + \delta W \tag{C.19}$$

δU_s can be written as:

$$\delta U_s = m c_v dT \tag{C.20}$$

Differentiating the ideal gas law ($pV = mRT$), gives:

$$mdT = \frac{1}{R}(pdV + Vdp) \tag{C.21}$$

This expression can be substituted in equation C.20:

$$\delta U_s = \frac{c_v}{R}(pdV + Vdp) \tag{C.22}$$

Using $\delta W = pdV$ equation C.22 can be written as:

$$\frac{dQ_{net}}{d\theta} = \frac{c_v}{R}(p\frac{dV}{d\theta} + V\frac{dp}{d\theta}) + p\frac{dV}{d\theta} \tag{C.23}$$

With $\gamma = c_p/c_v$ and $R = c_p - c_v$, the final expression for the net HRR is obtained:

$$\frac{dQ_{net}}{d\theta} = \frac{\gamma}{\gamma - 1}p\frac{dV}{d\theta} + \frac{1}{\gamma - 1}V\frac{dp}{d\theta} \tag{C.24}$$

C.1.7 Calculating the wall heat flux

Several methods are described in the master thesis of *S. Broekaert and T. De Cuyper* [6] for calculating the wall heat flux. These methods can be described as follows:

2T Fourier method The $FOUR_{2T}$ method is based on the one-dimensional conduction equation in a material C.25, with $\alpha = \frac{k}{\rho c_p}$ the thermal diffusivity. The wall temperature is divided into Fourier components as in equation C.26. In this equation, A_n and B_n are the Fourier coefficients, w is half of the angular velocity of the engine and B_1 resembles the average wall temperature.

$$\frac{\partial T}{\partial x} = \alpha \frac{\partial^2 T}{\partial x^2} \tag{C.25}$$

$$T_w(t) = B_1 + \sum_{n=1}^{N} (A_n cos(nwt) + B_n sin(nwt)) \tag{C.26}$$

Assuming the temperature in the wall at position $x = l$ is constant, which can be measured with an in-depth thermocouple which is integrated in the TFG sensor, and using equation C.25 the temperature can be found as a function of time and position. Substituting this temperature function in equation C.27 for $x = 0$ the instantaneous wall heat flux can be found.

$$q = q_{ss} + q_{trans} = \frac{Q}{A} = -k \frac{\mathrm{d}T}{\mathrm{d}x} \tag{C.27}$$

1T Fourier method The $FOUR_{1T}$ method only makes use of one measured temperature, the wall temperature. This means that only the transient heat flux can be found. In order to determine the steady state heat flux q_{ss} the gas temperature is used. This temperature can be calculated using the ideal gas law. Once again, this assumption is more acceptable for HCCI combustion than for SI combustion because of the uniform combustion. The instantaneous wall heat flux can be found assuming the wall heat flux is 0 when the temperature of the wall and the temperature of the gas are the same.

FIR methods The Finite Impulse Response (FIR) methods assume the sensor is a Linear Time-invariant (LTI) system. It is characterized by an impulse response h. Figure C.2 shows a scheme of the LTI-system. The heat flux can be calculated using a discrete convolution of the wall temperature and characteristic impulse response of the sensor, as in equation C.28.

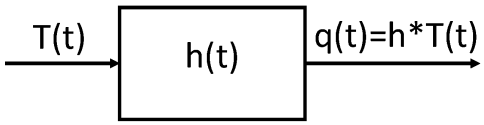

Figure C.2: Scheme of the LTI-system

$$q[n] = \sum_{k=0}^{N-1} h[k] \cdot T[n-k] \tag{C.28}$$

Take note that this also only result in the transient heat flux. There are some ways to calculate the steady state component, and this is where a distinction can be made between some FIR methods:

- FIR_{gas}
  This method can be compared to the $FOUR_{1T}$ method. The steady state heat flux is calculated assuming the heat flux is 0 when the wall temperature and the gas temperature are the same.

- FIR_{DC}
  This method makes use of Fourier's law, equation C.29. The wall temperature is assumed to be the B_1 value or DC component of the Fourier decomposition. Using the temperature of the in-depth thermocouple and the thermal property ak_1 of the sensor, the steady state heat flux follows. ak_1 is the ratio of the depth of the thermocouple and the thermal conductivity k.

- FIR_m
  This method is analogous to the FIR_{DC} method. Instead of making use of the DC component of the wall temperature, the mean wall temperature is now being used.

$$q_{ss} = \frac{Q}{A} = k\frac{T_{wall} - T_{depth}}{l_{depth}} = \frac{T_{surface} - T_{depth}}{ak_1} \tag{C.29}$$

C.2 Error analysis

In this section, the errors are calculated for the quantities that are used in the calculations. The absolute error of variable X is indicated as AE_X and the relative error as RE_X.

C.2.1 Measured quantities

Atmospheric conditions

The atmospheric conditions are measured using a sensor of manufacturer ATAL. The absolute error on the atmospheric temperature, pressure and relative humidity are given in table C.1.

Table C.1: Absolute errors on the atmospheric conditions of the ATAL sensor

Variable X	AE_X	Unity
T_{atm}	$0,4$	$°C$
p_{atm}	130	Pa
RH	2,5	%

Engine speed

The engine speed is measured using a crank angle interpolator type 2614 of manufacturer COM GmbH. In table C.2 the absolute error on the engine speed is given.

Table C.2: Absolute error on the measured engine speed

Variable X	AE_X	Unity
N	6	rpm

Pressures

The in- and outlet pressure is measured with a Kistler 4075A10 pressure sensor. The signal of this sensor is amplified using a Kistler 4665 amplifier. The in-cylinder pressure is measured with a Kistler 701A pressure sensor. The signal of this sensor is amplified using a Kistler 5064 amplifier. The amplified pressure signals are read by a PXI-6143 module of National Instruments. The errors of the sensors and measurements devices are shown in table C.3.
The error analysis shows that the error induced by the amplifiers and the PXI/6143 module are negligible compared to the error of the pressure sensor. The errors on the measured pressures are shown in table C.4.

Table C.3: Absolute and relative errors of the pressure measurement devices

Variable X	AE_X	RE_X [%]	Unity
Kistler 4075A10	$0,03$	-	bar
Kistler 701A	-	1	bar
Kistler 4665	-	$0,1$	$-$
Kistler 5064	-	$0,1$	$-$
PXI-6143	$2,5$	-	mV

Table C.4: Absolute and relative errors on measured pressures

Variable X	AE_X	RE_X [%]	Unity
p_{inlet}	$0,03$	-	bar
p_{outlet}	$0,03$	-	bar
$p_{cylinder}$	-	1	bar

Temperatures

All temperatures are measured using a K type thermocouple. These are read by a PXI-6224 module of National Instruments. The error on these temperatures are shown in table C.5.

Table C.5: Absolute error on measured temperatures

Variable X	AE_X	Unity
$T_{type\ K}$	5	$°C$

Flows

For liquid fuels the fuel flow can be determined gravimetrically by measuring the fuel consumption during a certain time interval. The air flow is measured using a Bronkhorst F-106BZ flow sensor. In table the C.6 error is shown for the air flow.
The mass flow of liquid fuels can be calculated with:

$$\dot{m}_{liquid} = \frac{\Delta m}{\Delta t} \tag{C.30}$$

The absolute error on the mass flow becomes:

Table C.6: Absolute error on the air flow

Variabele X	AE_X	Unity
Q_{air}	$0,2$	Nm^3/h

$$AE_{\dot{m}_{liquid}} = \sqrt{\left(\frac{AE_{\Delta m}}{\Delta m}\right)^2 + \left(\frac{AE_{\Delta t}}{\Delta t}\right)^2}\frac{\Delta m}{\Delta t} \tag{C.31}$$

The errors on the measured time interval Δt and the measured mass fuel Δm are shown in table C.7.

Table C.7: Absolute error on mass flow for liquid fuels

Variable X	AE_X	$RE_X[\%]$	Unity
Δm	1	-	g
Δt	1	-	s

Take note that in this thesis, the fuel flow could not be determined gravimetrically, since the fuel heated up too much, which caused it to evaporate rapidly. This resulted in a wrong determination of the fuel flow. The fuel flow is determined using the exhaust gas composition, as explained in previous section. Since this method only gives an indication of the real λ and mass fuel flow, an error analysis applied to this method would have no significant meaning. Therefore, the following calculations are applied to gravimetrically determined mass fuel flows, which should render more accurate results.

C.2.2 Calculated quantities

To estimate the error on a calculated quantity, an error analysis has to be carried out. This analysis is based on the work of Taylor. For a function f, dependent of variables a, b and c, the absolute error can be calculated as:

$$AE_f = \sqrt{\left(\frac{\partial f}{\partial a}AE_a\right)^2 + \left(\frac{\partial f}{\partial b}AE_b\right)^2 + \left(\frac{\partial f}{\partial c}AE_c\right)^2} \tag{C.32}$$

The relative error is calculated as the ratio of the absolute error on the function value:

$$RE_f = \frac{AE_f}{f} \tag{C.33}$$

In-cylinder mass

The total in-cylinder mass is calculated by taking the sum of the charge that is introduced into the cylinder and the rest gases, still present in the cylinder after closure of the exhaust valve.

$$m_{mixture} = m_{air} + m_{fuel} + m_{rest} \tag{C.34}$$

With

$$m_{air} = \frac{2\dot{m}_{air}}{60\ N} \tag{C.35}$$

$$m_{fuel} = \frac{2\dot{m}_{fuel}}{60\ N} \tag{C.36}$$

$$m_{rest} = \frac{p_{cyl}V_{cyl}}{R_{rest}T_{exhaust}} \tag{C.37}$$

with m_{rest} evaluated at the closure of the exhaust valve and N the rotational speed in rpm. The relative errors of the separate components are

$$RE_{m_{air}} = \sqrt{RE_N^2 + RE_{\dot{m}_{air}}^2} \tag{C.38}$$

$$RE_{m_{fuel}} = \sqrt{RE_N^2 + RE_{\dot{m}_{fuel}}^2} \tag{C.39}$$

$$RE_{m_{rest}} = \sqrt{RE_{p_{cyl}}^2 + RE_{T_{exhaust}}^2 + RE_{R_{rest}}^2} \tag{C.40}$$

The relative error on the total in-cylinder mass is

$$RE_{m_{mixture}} = \sqrt{RE_{m_{air}}^2 + RE_{m_{fuel}}^2 + RE_{m_{rest}}^2} \tag{C.41}$$

Excess air ratio and AFR

The AFR is calculated with

$$\text{AFR} = \frac{m_{air}}{m_{fuel}} \tag{C.42}$$

The relative error can be determined with

$$RE_{\text{AFR}} = \sqrt{RE_{m_{air}}^2 + RE_{m_{fuel}}^2} \tag{C.43}$$

The excess air ratio λ can be calculated with

$$\lambda = \frac{\text{AFR}}{\text{AFR}_{\text{stoichiometric}}} \tag{C.44}$$

The error on this ratio can be calculated as:

$$RE_\lambda = \sqrt{RE^2_{\text{AFR}} + RE^2_{\text{AFR}_{\text{stoichiometric}}}} \tag{C.45}$$

Because $\text{AFR}_{\text{stoichiometric}}$ is a constant for a specific fuel, the relative error on λ is equal to the relative error on AFR:

$$RE_\lambda = RE_{\text{AFR}} \tag{C.46}$$

Specific gas constant

In fired conditions, the specific gas constant R_{inlet} of the mixture at the inlet can be calculated as:

$$R_{inlet} = \frac{\text{AFR}}{(\text{AFR}+1)} R_{air} + \frac{1}{(\text{AFR}+1)} R_{fuel} \tag{C.47}$$

When neglecting the error on the specific gas constant for air and the fuel, the error can be calculated as:

$$AE_{R_{inlet}} = \sqrt{(R_{air} - R_{fuel})^2 \, AE_{\text{AFR}}} \tag{C.48}$$

Because of the presence of residual gases, the value of the specific gas constant of the in-cylinder mixture is slightly different from the incoming mixture. However, the contribution to the absolute error is negligible. It is allowed to assume:

$$AE_{R_{mixture}} = AE_{R_{inlet}} \tag{C.49}$$

Gas temperature

The gas temperature of the mixture can be calculated using the ideal gas law:

$$T_{gas} = \frac{p_{cyl} V_{cyl}}{R_{mixture} m_{mixture}} \tag{C.50}$$

The error on the cylinder volume is negligible with respect to the other errors. The relative error on the gas temperature can be determined as:

$$RE_{T_{gas}} = \sqrt{RE^2_{p_{cyl}} + RE^2_{R_{mixture}} + RE^2_{m_{mixture}}} \tag{C.51}$$

Heat release rate

The calculation of the heat release rate is described above. The absolute error can be calculated as follows:

$$AE_{HRR} = \sqrt{(\frac{AE_p \gamma \frac{dV}{d\theta}}{\gamma - 1})^2 + (\frac{AE_V \frac{dp}{d\theta}}{\gamma - 1})^2 + AE_\gamma^2 (\frac{p\frac{dV}{d\theta}}{\gamma - 1} - \frac{\gamma p \frac{dV}{d\theta}}{(\gamma-1)^2} - \frac{V\frac{dp}{d\theta}}{(\gamma-1)^2})^2} \quad \text{(C.52)}$$

C.2.3 Heat flux measurements

A single layer TFG heat flux sensor is used to perform heat flux measurements.

Wall heat flux

The wall temperature has to be calculated from the signal coming from the TFG sensor. This can be done using following equation:

$$T_w = T_{TFGS} = \frac{V_{TFGS}}{G_{TFGS} \cdot \alpha_0 \cdot V_0} + T_{atm} \quad \text{(C.53)}$$

with V_{TFGS} the measured voltage, V_0 the reference voltage, G_{TFGS} the gain and α_0 the coefficient which characterizes the change in resistance of the RTD as a function of temperature:

$$R = R_0 \cdot [1 + \alpha_0 (T - T_0)] \quad \text{(C.54)}$$

The absolute error on the wall temperature is:

$$AE_{T_w} = \sqrt{\left(\frac{AE_{V_{TFGS}}}{V_{TFGS}}\right)^2 + \left(\frac{AE_{G_{TFGS}}}{G_{TFGS}}\right)^2 + \left(\frac{AE_{\alpha_0}}{\alpha_0}\right)^2 + \left(\frac{AE_{V_0}}{V_0}\right)^2 + \left(AE_{T_{atm}} \frac{G_{TFGS} \cdot \alpha_0 \cdot V_0}{V_{TFGS}}\right)^2} \frac{V_{TFGS}}{G_{TFGS} \cdot \alpha_0 \cdot V_0} \quad \text{(C.55)}$$

Take note that in this equation the error on the amplification of the signal coming from the TFG sensor is also taken into account.
In table C.2.3 the absolute and relative errors can be found.
The error on α_0 can be calculated with:

$$AE_{\alpha_0} = \sqrt{\frac{b^2 (AE_a)^2 + a^2 (AE_b)^2 + a^4 (AE_{T_0})^2}{(b + a\ T_0)^4}} \quad \text{(C.56)}$$

Table C.8: Absolute and relative errors for heat flux measurements

Variable X	RE_X [%]	AE_X	Unity
V_0	-	10.10^{-3}	V
G_{TFGS}	1	-	-
V_{TFGS}	-	$2,5.10^{-3}$	V

with a and b the coefficients in $R = aT + b$, which can be determined from calibrating the TFG sensor, and T_0 the reference temperature.

Next, the errors coming from the different wall heat flux calculation methods need to be examined. The method to determine these errors is rather complex, since a sensitivity analysis needs to be carried out. In the master thesis of *S. Broekaert and T. De Cuyper* [6] a thorough explanation about the determination of these errors can be found.

Convection coefficient

The convection coefficient can be determined with:

$$h_c = \frac{q}{T_{gas} - T_{wall}} \tag{C.57}$$

The error on the temperature difference between the gas and wall ΔT can be written as:

$$AE_{\Delta T} = \sqrt{AE_{T_{gas}}^2 + AE_{T_{wall}}^2} \tag{C.58}$$

The error on the convection coefficient follows:

$$RE_h = \sqrt{RE_q^2 + RE_{\Delta T}^2} \tag{C.59}$$

Convection coefficient from heat flux correlations

The convection coefficient of the heat flux correlations can be calculated as:

$$h_c(t) = \alpha_s L(t)^{-j} P(t)^k T(t)^{-l} v(t)^m \tag{C.60}$$

This results in the following error:

$$RE_{h_c} = \sqrt{(k \cdot RE_P)^2 + (l \cdot RE_T)^2} \tag{C.61}$$

when it is assumed that the error on $alpha_s$, L and v are negligible. Take note that using this equation to calculate the convection coefficient h_c already is an approximation, since simplifications are being used in obtaining this equation.

C.3 Acquiring and processing data

The data from a measurement is acquired and stored using LabView. For each measurement an Excel file is made. This file contains the various operating conditions and a file path to the voltages of the pressure and heat flux sensors. The processing of this data is done using Matlab. The following scripts are used:

measurements_2014.m

This is the main file, it is the backbone of the processing. First, the initialization is done. This means: reading the operating conditions for each measurement (CR, λ, EGR, mass flows, atmospheric conditions, inlet temperature, outlet temperature, oil temperature coolant temperature), initializing the gas properties and defining the engine characteristics (geometry, speed, valve timing). Next, two other scripts are addressed: measurements_calculation_2014.m and error_analysis_2014.m. These two scripts are used to do the calculations and error analysis as described above. Finally, the measured and calculated data is stored.

measurements_calculation_2014.m

This script is used to read the voltages of the pressure and heat flux sensors. These voltages are converted to the right values for pressure and wall temperature. Once these values are known, all the necessary calculations can be done.

error_analysis_2014.m

In this script, the error analysis calculations are done, as described above.

Heat_Release_Analysis.m

After the measured and calculated data is stored, this script can be used to perform a heat release analysis on a specific measurement (or more measurements). The output of this script is a graph, which shows the net CHR, total CHR and wall heat losses as a function of crank angle. It is also possible to show the total CHR making use of the various heat flux correlations (as discussed in this thesis) instead of the heat flux from the TFG sensor. Take note that the heat fluxes resulting from the correlations first need to be calculated using the script Heat_flux_corr.m.

Heat_flux_corr.m

This script can be used on the stored data. In this script, the heat flux and the convection coefficient for the heat transfer correlation of Woschni, Assanis, Annand and Hohenberg are calculated. The output of this script are two graphs showing the results. Take note that a pressure measurement in motored condition needs to be loaded as well (aside the stored data), since the Woschni correlation makes use of such a pressure measurement.

Heat_flux_corr_best_a.m

This script is used to calculate the optimal scaling factor for the various heat transfer correlations. The correlations are optimized using the minimum mean square method. The output of this script is the optimal scaling factor of each correlation and the mean error of each correlation with respect to the measured heat flux.

T_ivc_calculation.m

This script is used to generate a plot of the required inlet temperature as a function of CR to achieve HCCI combustion, assuming the compression stroke is a polytropic process. The polytropic index, which is equal to the specific heat ratio for an isentropic proces, is taken constant (but can be changed if necessary).

LabView

Some changes were made to the LabView interface. The temperature of the EGR can be read from the temperature block. Second, a block is added to operate the EGR valve and to account for the amount of EGR that is applied. The frequency and duty cycle of the EGR valve can be adjusted. It is recommended not to go above 6 Hz. The dry volume percentages of CO and CO_2 at the inlet and outlet can be read from the emission analyzer and filled out in the EGR block of the LabView interface. LabView calculates the percentage EGR from these dry volume concentrations and displays it on the LabView interface.

Third, the maximum pressure rise rate in $bar/°ca$ is calculated and displayed on the interface. This is to have an idea of the upper load limit for HCCI combustion. As already said, we took 5 $bar/°ca$ as the criterion for the upper load limit. A print screen of the LabView interface can be found in the new 'Operations manual' of the CFR engine.

Appendix D

Measurements

The operating conditions and results of the most important measurements can be found in this chapter of the appendix.

D.1 Operating conditions for the first measurement on HCCI

Measurement 1

Inlet temperature		Lambda		Outlet gas composition				CR
T_heater [°C]	255	lambda sensor	-	O2 [vol%]	CO2 [vol%]	CO [vol%]	NOx/NO[ppm]	13
T_in [°C]	170	lambda grav	-	17,02	3,01	0,171	-7	
Mass flows		lambda O2	4,622605	Inlet gas composition				
air flow [kg/h]	8,17	EGR % dry		O2 [vol%]	CO2 [vol%]	CO [vol%]	Nox [ppm]	
fuel flow [kg/h]	0,120231401	EGR %	0	-	-	-	-	
EGR flow [kg/h]	0							
Totaal	8,290231401							

Figure D.1: Operating conditions for the first measurement on HCCI

D.2 Measurements on the effects of EGR on HCCI

Measurement 1

Inlet temperature		Lambda		Outlet gas composition				CR
T_heater [°C]	253	lambda sensor	-	O2 [vol%]	CO2 [vol%]	CO [vol%]	Nox [ppm]	13
T_in [°C]	170	lambda grav	-	17,33	-	-	-	
Mass flows		lambda O2	4,937382	Inlet gas composition				
air flow [kg/h]	8,05	EGR % dry		O2 [vol%]	CO2 [vol%]	CO [vol%]	Nox [ppm]	
fuel flow [kg/h]	0,110913	EGR %	0	-	-	-	-	
EGR flow [kg/h]	0							
Total [kg/h]	8,160913							

Measurement 2

Inlet temperature		Lambda		Outlet gas composition				CR
T_heater [°C]	253	lambda sensor	-	O2 [vol%]	CO2 [vol%]	CO [vol%]	Nox [ppm]	13
T_in [°C]	170	lambda grav	-	16,77	-	-	-	
Mass flows		lambda O2	4,40457	Inlet gas composition				
air flow [kg/h]	7,3	EGR % dry		O2 [vol%]	CO2 [vol%]	CO [vol%]	Nox [ppm]	
fuel flow [kg/h]	0,112746	EGR %	9,98	-	-	-	-	
EGR flow [kg/h]	0,821809							
Total [kg/h]	8,234555							

Measurement 3

Inlet temperature		Lambda		Outlet gas composition				CR
T_heater [°C]	253	lambda sensor	-	O2 [vol%]	CO2 [vol%]	CO [vol%]	Nox [ppm]	13
T_in [°C]	170	lambda grav	-	15,88	-	-	-	
Mass flows		lambda O2	3,757402	Inlet gas composition				
air flow [kg/h]	6,03	EGR % dry		O2 [vol%]	CO2 [vol%]	CO [vol%]	Nox [ppm]	
fuel flow [kg/h]	0,109172	EGR %	24,4	-	-	-	-	
EGR flow [kg/h]	1,981426							
Total [kg/h]	8,120598							

Measurement 4

Inlet temperature		Lambda		Outlet gas composition				CR
T_heater [°C]	253	lambda sensor	-	O2 [vol%]	CO2 [vol%]	CO [vol%]	Nox [ppm]	13
T_in [°C]	170	lambda grav	-	13,62	-	-	-	
Mass flows		lambda O2	2,729503	Inlet gas composition				
air flow [kg/h]	4,56	EGR % dry		O2 [vol%]	CO2 [vol%]	CO [vol%]	Nox [ppm]	
fuel flow [kg/h]	0,113649	EGR %	42,97	-	-	-	-	
EGR flow [kg/h]	3,521422							
Total [kg/h]	8,19507							

Figure D.2: Operating conditions for the determination of the effects of EGR on HCCI

D.3 Measurements on the effects of air preheating on HCCI

Measurement 1

Inlet temperature		Lambda		Outlet gas composition				CR
T_heater [°C]	195,5	lambda sensor	4,8	O2 [vol%]	CO2 [vol%]	CO [vol%]	Nox [ppm]	14,75
T_in [°C]	140	lambda grav	-	17,800	2,400	0,187	0	
Mass flows		lambda O2	5,657059	Inlet gas composition				
air flow [kg/h]	8,5	EGR % dry		O2 [vol%]	CO2 [vol%]	CO [vol%]	Nox [ppm]	
fuel flow [kg/h]	0,102214124	EGR %	0	-	-	-	-	
EGR flow [kg/h]	0							
Totaal	8,602214124							

Measurement 2

Inlet temperature		Lambda		Outlet gas composition				CR
T_heater [°C]	172	lambda sensor	4,9	O2 [vol%]	CO2 [vol%]	CO [vol%]	Nox [ppm]	14,75
T_in [°C]	130	lambda grav	-	17,900	2,310	0,210	0	
Mass flows		lambda O2	5,803865	Inlet gas composition				
air flow [kg/h]	8	EGR % dry		O2 [vol%]	CO2 [vol%]	CO [vol%]	Nox [ppm]	
fuel flow [kg/h]	0,093768144	EGR %	0	-	-	-	-	
EGR flow [kg/h]	0							
Totaal	8,093768144							

Measurement 3

Inlet temperature		Lambda		Outlet gas composition				CR
T_heater [°C]	145	lambda sensor	5,1	O2 [vol%]	CO2 [vol%]	CO [vol%]	Nox [ppm]	14,75
T_in [°C]	120	lambda grav	-	18,060	2,100	0,340	0	
Mass flows		lambda O2	5,982145	Inlet gas composition				
air flow [kg/h]	8,87	EGR % dry		O2 [vol%]	CO2 [vol%]	CO [vol%]	Nox [ppm]	
fuel flow [kg/h]	0,10086706	EGR %	0	-	-	-	-	
EGR flow [kg/h]	0							
Totaal	8,97086706							

Measurement 4

Inlet temperature		Lambda		Outlet gas composition				CR
T_heater [°C]	137	lambda sensor	5,2	O2 [vol%]	CO2 [vol%]	CO [vol%]	Nox [ppm]	14,75
T_in [°C]	110	lambda grav	-	18,270	1,750	0,535	0	
Mass flows		lambda O2	6,343101	Inlet gas composition				
air flow [kg/h]	9,06	EGR % dry		O2 [vol%]	CO2 [vol%]	CO [vol%]	Nox [ppm]	
fuel flow [kg/h]	0,097164855	EGR %	0	-	-	-	-	
EGR flow [kg/h]	0							
Totaal	9,157164855							

Figure D.3: Operating conditions for the determination of the effects of air preheating on HCCI

D.4 Measurements on the effects of CR on HCCI

Measurement 1

Inlet temperature		Lambda		Outlet gas composition				CR
T_heater [°C]	276	lambda sensor	4,5	O2 [vol%]	CO2 [vol%]	CO [vol%]	NOx/NO[ppm]	12
T_in [°C]	180	lambda grav	-	17,670	2,395	0,388	-15	
Mass flows		lambda O2	5,26499	Inlet gas composition				
air flow [kg/h]	8	EGR % dry		O2 [vol%]	CO2 [vol%]	CO [vol%]	Nox [ppm]	
fuel flow [kg/h]	0,103365382	EGR %	0	-	-	-	-	
EGR flow [kg/h]	0							
Totaal	8,103365382							

Measurement 2

Inlet temperature		Lambda		Outlet gas composition				CR
T_heater [°C]	276	lambda sensor	4,5	O2 [vol%]	CO2 [vol%]	CO [vol%]	NOx/NO[ppm]	13
T_in [°C]	180	lambda grav	-	17,490	2,680	0,157	-18	
Mass flows		lambda O2	5,176897	Inlet gas composition				
air flow [kg/h]	8	EGR % dry		O2 [vol%]	CO2 [vol%]	CO [vol%]	Nox [ppm]	
fuel flow [kg/h]	0,105124296	EGR %	0	-	-	-	-	
EGR flow [kg/h]	0							
Totaal	8,105124296							

Measurement 3

Inlet temperature		Lambda		Outlet gas composition				CR
T_heater [°C]	278	lambda sensor	4,5	O2 [vol%]	CO2 [vol%]	CO [vol%]	NOx/NO[ppm]	14
T_in [°C]	180	lambda grav	-	17,440	2,750	0,127	-12	
Mass flows		lambda O2	5,111557	Inlet gas composition				
air flow [kg/h]	8	EGR % dry		O2 [vol%]	CO2 [vol%]	CO [vol%]	Nox [ppm]	
fuel flow [kg/h]	0,106468082	EGR %	0	-	-	-	-	
EGR flow [kg/h]	0							
Totaal	8,106468082							

Figure D.4: Operating conditions for the determination of the effects of CR on HCCI

D.5 Measurements on the operating limits of HCCI

Measurement 1

Inlet temperature		Lambda		Outlet gas composition				CR
T_heater [°C]	253	lambda sensor	5,15	O2 [vol%]	CO2 [vol%]	CO [vol%]	Nox [ppm]	13
T_in [°C]	170	lambda grav	3,47	18,12	1,943	0,506	-16,1	
Mass flows		lambda O2	5,949407	Inlet gas composition				
air flow [kg/h]	8,164	EGR % dry		O2 [vol%]	CO2 [vol%]	CO [vol%]	Nox [ppm]	
fuel flow [kg/h]	0,093349	EGR %	0	-	-	-	-	
EGR flow [kg/h]	0							
Total [kg/h]	8,257349							

Measurement 2

Inlet temperature		Lambda		Outlet gas composition				CR
T_heater [°C]	253	lambda sensor	3,5	O2 [vol%]	CO2 [vol%]	CO [vol%]	Nox [ppm]	13
T_in [°C]	170	lambda grav	2,52	16,4	3,518	0,131	-18,1	
Mass flows		lambda O2	4,047026	Inlet gas composition				
air flow [kg/h]	8,164	EGR % dry		O2 [vol%]	CO2 [vol%]	CO [vol%]	Nox [ppm]	
fuel flow [kg/h]	0,13723	EGR %	0	-	-	-	-	
EGR flow [kg/h]	0							
Total [kg/h]	8,30123							

Measurement 3

Inlet temperature		Lambda		Outlet gas composition				CR
T_heater [°C]	211	lambda sensor	4,2	O2 [vol%]	CO2 [vol%]	CO [vol%]	Nox [ppm]	13
T_in [°C]	150	lambda grav	3,2	17,21	2,741	0,319	-19,4	
Mass flows		lambda O2	4,786722	Inlet gas composition				
air flow [kg/h]	8,5	EGR % dry		O2 [vol%]	CO2 [vol%]	CO [vol%]	Nox [ppm]	
fuel flow [kg/h]	0,120799	EGR %	0	-	-	-	-	
EGR flow [kg/h]	0							
Total [kg/h]	8,620799							

Measurement 4

Inlet temperature		Lambda		Outlet gas composition				CR
T_heater [°C]	211	lambda sensor	3,6	O2 [vol%]	CO2 [vol%]	CO [vol%]	Nox [ppm]	13
T_in [°C]	150	lambda grav	2,77	16,46	3,424	0,176	-20,8	
Mass flows		lambda O2	4,094386	Inlet gas composition				
air flow [kg/h]	8,5	EGR % dry		O2 [vol%]	CO2 [vol%]	CO [vol%]	Nox [ppm]	
fuel flow [kg/h]	0,141225	EGR %	0	-	-	-	-	
EGR flow [kg/h]	0							
Total [kg/h]	8,641225							

Measurement 5

Inlet temperature		Lambda		Outlet gas composition				CR
T_heater [°C]	195	lambda sensor	3,8	O2 [vol%]	CO2 [vol%]	CO [vol%]	Nox [ppm]	13
T_in [°C]	140	lambda grav	3,07	16,97	2,88	0,42	-32	
Mass flows		lambda O2	4,448101	Inlet gas composition				
air flow [kg/h]	8,6	EGR % dry		O2 [vol%]	CO2 [vol%]	CO [vol%]	Nox [ppm]	
fuel flow [kg/h]	0,131524	EGR %	0	-	-	-	-	
EGR flow [kg/h]	0							
Total [kg/h]	8,731524							

Measurement 6

Inlet temperature		Lambda		Outlet gas composition				CR
T_heater [°C]	195	lambda sensor	3,3	O2 [vol%]	CO2 [vol%]	CO [vol%]	Nox [ppm]	13
T_in [°C]	140	lambda grav	2,65	16,09	3,696	0,197	-18,8	
Mass flows		lambda O2	3,794375	Inlet gas composition				
air flow [kg/h]	8,6	EGR % dry		O2 [vol%]	CO2 [vol%]	CO [vol%]	Nox [ppm]	
fuel flow [kg/h]	0,154185	EGR %	0	-	-	-	-	
EGR flow [kg/h]	0							
Total [kg/h]	8,754185							

Measurement 7

Inlet temperature		Lambda		Outlet gas composition				CR
T_heater [°C]	297	lambda sensor	6,2	O2 [vol%]	CO2 [vol%]	CO [vol%]	Nox [ppm]	13
T_in [°C]	190	lambda grav	4,2	18,61	1,589	0,507	-17,5	
Mass flows		lambda O2	6,94127	Inlet gas composition				
air flow [kg/h]	7,9	EGR % dry		O2 [vol%]	CO2 [vol%]	CO [vol%]	Nox [ppm]	
fuel flow [kg/h]	0,077423	EGR %	0	-	-	-	-	
EGR flow [kg/h]	0							
Total [kg/h]	7,977423							

Figure D.5: Operating conditions for the experiments of the operating limits of HCCI

Measurement 8

Inlet temperature		Lambda		Outlet gas composition				CR
T_heater [°C]	296,5	lambda sensor	4	O2 [vol%]	CO2 [vol%]	CO [vol%]	Nox [ppm]	13
T_in [°C]	190	lambda grav	2,82	16,87	3,196	0,12	-20,8	
Mass flows		lambda O2	4,451038	Inlet gas composition				
air flow [kg/h]	7,9	EGR % dry		O2 [vol%]	CO2 [vol%]	CO [vol%]	Nox [ppm]	
fuel flow [kg/h]	0,120739	EGR %	0	-	-	-	-	
EGR flow [kg/h]	0							
Total [kg/h]	8,020739							

Measurement 9

Inlet temperature		Lambda		Outlet gas composition				CR
T_heater [°C]	311	lambda sensor	6,5	O2 [vol%]	CO2 [vol%]	CO [vol%]	Nox [ppm]	13
T_in [°C]	200	lambda grav	3,9	18,68	1,627	0,417	-12,1	
Mass flows		lambda O2	7,136313	Inlet gas composition				
air flow [kg/h]	7,8	EGR % dry		O2 [vol%]	CO2 [vol%]	CO [vol%]	Nox [ppm]	
fuel flow [kg/h]	0,074354	EGR %	0	-	-	-	-	
EGR flow [kg/h]	0							
Total [kg/h]	7,874354							

Measurement 10

Inlet temperature		Lambda		Outlet gas composition				CR
T_heater [°C]	311	lambda sensor	4,1	O2 [vol%]	CO2 [vol%]	CO [vol%]	Nox [ppm]	13
T_in [°C]	200	lambda grav	2,77	17	3,083	0,107	-13,4	
Mass flows		lambda O2	4,616894	Inlet gas composition				
air flow [kg/h]	7,8	EGR % dry		O2 [vol%]	CO2 [vol%]	CO [vol%]	Nox [ppm]	
fuel flow [kg/h]	0,114928	EGR %	0	-	-	-	-	
EGR flow [kg/h]	0							
Total [kg/h]	7,914928							

Measurement 11

Inlet temperature		Lambda		Outlet gas composition				CR
T_heater [°C]	286,5	lambda sensor	3,7	O2 [vol%]	CO2 [vol%]	CO [vol%]	Nox [ppm]	13
T_in [°C]	180	lambda grav	3,2	16,52	3,4	0,111	0	
Mass flows		lambda O2	4,192562	Inlet gas composition				
air flow [kg/h]	8	EGR % dry		O2 [vol%]	CO2 [vol%]	CO [vol%]	Nox [ppm]	
fuel flow [kg/h]	0,129806	EGR %	0	-	-	-	-	
EGR flow [kg/h]	0							
Total [kg/h]	8,129806							

Measurement 12

Inlet temperature		Lambda		Outlet gas composition				CR
T_heater [°C]	279,8	lambda sensor	5,6	O2 [vol%]	CO2 [vol%]	CO [vol%]	Nox [ppm]	13
T_in [°C]	180	lambda grav	/	18,36	1,749	0,515	-10,6	
Mass flows		lambda O2	6,423867	Inlet gas composition				
air flow [kg/h]	8	EGR % dry		O2 [vol%]	CO2 [vol%]	CO [vol%]	Nox [ppm]	
fuel flow [kg/h]	0,084718	EGR %	0	-	-	-	-	
EGR flow [kg/h]	0							
Total [kg/h]	8,084718							

Measurement 13

Inlet temperature		Lambda		Outlet gas composition				CR
T_heater [°C]	230	lambda sensor	4,75	O2 [vol%]	CO2 [vol%]	CO [vol%]	Nox [ppm]	13
T_in [°C]	160	lambda grav	/	17,8	2,199	0,47	-13,3	
Mass flows		lambda O2	5,466243	Inlet gas composition				
air flow [kg/h]	8,25	EGR % dry		O2 [vol%]	CO2 [vol%]	CO [vol%]	Nox [ppm]	
fuel flow [kg/h]	0,102671	EGR %	0	-	-	-	-	
EGR flow [kg/h]	0							
Total [kg/h]	8,352671							

Measurement 14

Inlet temperature		Lambda		Outlet gas composition				CR
T_heater [°C]	231	lambda sensor	3,53	O2 [vol%]	CO2 [vol%]	CO [vol%]	Nox [ppm]	13
T_in [°C]	160	lambda grav	/	16,33	3,552	0,121	0	
Mass flows		lambda O2	4,015318	Inlet gas composition				
air flow [kg/h]	8,25	EGR % dry		O2 [vol%]	CO2 [vol%]	CO [vol%]	Nox [ppm]	
fuel flow [kg/h]	0,139771	EGR %	0	-	-	-	-	
EGR flow [kg/h]	0							
Total [kg/h]	8,389771							

Figure D.6: Operating conditions for the experiments of the operating limits of HCCI

Measurement 15

Inlet temperature		Lambda		Outlet gas composition				CR
T_heater [°C]	248	lambda sensor	2,2	O2 [vol%]	CO2 [vol%]	CO [vol%]	Nox [ppm]	13
T_in [°C]	170	lambda grav	-	12,92	6,004	0,151	-4,7	
Mass flows		lambda O2	2,419765	Inlet gas composition				
air flow [kg/h]	5,15	EGR % dry		O2 [vol%]	CO2 [vol%]	CO [vol%]	Nox [ppm]	
fuel flow [kg/h]	0,144783	EGR %	34,4	19,45	1,3	0,035	-28,5	
EGR flow [kg/h]	2,776532							
Total [kg/h]	8,071315							

Measurement 16

Inlet temperature		Lambda		Outlet gas composition				CR
T_heater [°C]	270	lambda sensor	2,35	O2 [vol%]	CO2 [vol%]	CO [vol%]	Nox [ppm]	13
T_in [°C]	180	lambda grav	-	13,410	5,664	0,132	-34,5	
Mass flows		lambda O2	2,566736	Inlet gas composition				
air flow [kg/h]	4,98	EGR % dry		O2 [vol%]	CO2 [vol%]	CO [vol%]	Nox [ppm]	
fuel flow [kg/h]	0,131987	EGR %	37,5	19,43	1,315	0,056	-39,7	
EGR flow [kg/h]	3,067192							
Total [kg/h]	8,179179							

Measurement 17

Inlet temperature		Lambda		Outlet gas composition				CR
T_heater [°C]	291	lambda sensor	2,45	O2 [vol%]	CO2 [vol%]	CO [vol%]	Nox [ppm]	13
T_in [°C]	190	lambda grav	-	13,650	5,490	0,120	-5,3	
Mass flows		lambda O2	2,648762	Inlet gas composition				
air flow [kg/h]	4,9	EGR % dry		O2 [vol%]	CO2 [vol%]	CO [vol%]	Nox [ppm]	
fuel flow [kg/h]	0,125845	EGR %	36,3	19,45	1,305	0,035	-13,3	
EGR flow [kg/h]	2,864022							
Total [kg/h]	7,889866							

Measurement 18

Inlet temperature		Lambda		Outlet gas composition				CR
T_heater [°C]	306	lambda sensor	2,6	O2 [vol%]	CO2 [vol%]	CO [vol%]	Nox [ppm]	13
T_in [°C]	200	lambda grav	-	13,900	5,300	0,123	-14,6	
Mass flows		lambda O2	2,736788	Inlet gas composition				
air flow [kg/h]	4,85	EGR % dry		O2 [vol%]	CO2 [vol%]	CO [vol%]	Nox [ppm]	
fuel flow [kg/h]	0,120554	EGR %	36,3	19,5	1,29	0,044	-9,3	
EGR flow [kg/h]	2,832514							
Total [kg/h]	7,803068							

Measurement 19

Inlet temperature		Lambda		Outlet gas composition				CR
T_heater [°C]	226	lambda sensor	2,15	O2 [vol%]	CO2 [vol%]	CO [vol%]	Nox [ppm]	13
T_in [°C]	160	lambda grav	-	13,120	5,820	0,156	-15	
Mass flows		lambda O2	2,484731	Inlet gas composition				
air flow [kg/h]	5,35	EGR % dry		O2 [vol%]	CO2 [vol%]	CO [vol%]	Nox [ppm]	
fuel flow [kg/h]	0,146473	EGR %	34,6	19,55	1,25	0,043	-10	
EGR flow [kg/h]	2,90792							
Total [kg/h]	8,404393							

Measurement 20

Inlet temperature		Lambda		Outlet gas composition				CR
T_heater [°C]	208	lambda sensor	1,9	O2 [vol%]	CO2 [vol%]	CO [vol%]	Nox [ppm]	13
T_in [°C]	150	lambda grav	-	11,900	6,740	0,198	-28,4	
Mass flows		lambda O2	2,15641	Inlet gas composition				
air flow [kg/h]	5,5	EGR % dry		O2 [vol%]	CO2 [vol%]	CO [vol%]	Nox [ppm]	
fuel flow [kg/h]	0,173506	EGR %	33,8	19,46	1,31	0,057	-18,5	
EGR flow [kg/h]	2,896745							
Total [kg/h]	8,570251							

Figure D.7: Operating conditions for the experiments of the operating limits of HCCI

D.6 Operating conditions for the heat flux measurements on HCCI

Take note that these measurements are also used to study the effect of the excess air ratio on HCCI combustion.

Measurement 1

Inlet temperature		Lambda		Outlet gas composition				CR
T_heater [°C]	288	lambda sensor	3,75	O2 [vol%]	CO2 [vol%]	CO [vol%]	Nox [ppm]	13
T_in [°C]	180	lambda grav	3,6	16,740	3,266	0,127	8,500	
Mass flows		lambda O2	4,345714	Inlet gas composition				
air flow [kg/h]	8	EGR % dry		O2 [vol%]	CO2 [vol%]	CO [vol%]	Nox [ppm]	
fuel flow [kg/h]	0,125230907	EGR %	0	-	-	-	-	
EGR flow [kg/h]	0							
Totaal	8,125230907							

Measurement 2

Inlet temperature		Lambda		Outlet gas composition				CR
T_heater [°C]	288	lambda sensor	4,1	O2 [vol%]	CO2 [vol%]	CO [vol%]	Nox [ppm]	13
T_in [°C]	180	lambda grav	3,79	17,000	3,077	0,177	10,500	
Mass flows		lambda O2	4,536343	Inlet gas composition				
air flow [kg/h]	8	EGR % dry		O2 [vol%]	CO2 [vol%]	CO [vol%]	Nox [ppm]	
fuel flow [kg/h]	0,119968384	EGR %	0	-	-	-	-	
EGR flow [kg/h]	0							
Totaal	8,119968384							

Measurement 3

Inlet temperature		Lambda		Outlet gas composition				CR
T_heater [°C]	288	lambda sensor	4,4	O2 [vol%]	CO2 [vol%]	CO [vol%]	Nox [ppm]	13
T_in [°C]	180	lambda grav	4,06	17,430	2,734	0,153	5,200	
Mass flows		lambda O2	5,091008	Inlet gas composition				
air flow [kg/h]	8	EGR % dry		O2 [vol%]	CO2 [vol%]	CO [vol%]	Nox [ppm]	
fuel flow [kg/h]	0,106897834	EGR %	0	-	-	-	-	
EGR flow [kg/h]	0							
Totaal	8,106897834							

Measurement 4

Inlet temperature		Lambda		Outlet gas composition				CR
T_heater [°C]	288	lambda sensor	5,05	O2 [vol%]	CO2 [vol%]	CO [vol%]	Nox [ppm]	13
T_in [°C]	180	lambda grav	4,57	17,990	2,268	0,234	-10,000	
Mass flows		lambda O2	5,85867	Inlet gas composition				
air flow [kg/h]	8	EGR % dry		O2 [vol%]	CO2 [vol%]	CO [vol%]	Nox [ppm]	
fuel flow [kg/h]	0,092890991	EGR %	0	-	-	-	-	
EGR flow [kg/h]	0							
Totaal	8,092890991							

Figure D.8: Operating conditions for the heat flux measurements on HCCI for an inlet temperature of $180°C$

Measurement 1

Inlet temperature		Lambda		Outlet gas composition				CR
T_heater [°C]	196,4	lambda sensor	3,9	O2 [vol%]	CO2 [vol%]	CO [vol%]	NOx/NO[ppm]	13
T_in [°C]	150	lambda grav	3,7	16,960	3,066	0,181	-10	
Mass flows		lambda O2	4,53503	Inlet gas composition				
air flow [kg/h]	8,32	EGR % dry		O2 [vol%]	CO2 [vol%]	CO [vol%]	Nox [ppm]	
fuel flow [kg/h]	0,124803229	EGR %	0	-	-	-	-	
EGR flow [kg/h]	0							
Totaal	8,444803229							

Measurement 2

Inlet temperature		Lambda		Outlet gas composition				CR
T_heater [°C]	190	lambda sensor	3,65	O2 [vol%]	CO2 [vol%]	CO [vol%]	NOx/NO[ppm]	13
T_in [°C]	150	lambda grav	3,32	16,610	3,310	0,158	-10	
Mass flows		lambda O2	4,243907	Inlet gas composition				
air flow [kg/h]	8,32	EGR % dry		O2 [vol%]	CO2 [vol%]	CO [vol%]	Nox [ppm]	
fuel flow [kg/h]	0,133364452	EGR %	0	-	-	-	-	
EGR flow [kg/h]	0							
Totaal	8,453364452							

Figure D.9: Operating conditions for the heat flux measurements on HCCI for an inlet temperature of $150°C$

Appendix E

Operations manual: CFR engine

Operations manual: CFR engine

Room 0.01, Block IV, Technicum
Sint-Pietersnieuwstraat 41, Ghent

Last modified: *31/05/2014*
Author: *Joachim Demuynck*
Modified by: Leroy De Ruijsscher and Anthony Eelbode

This file gives a detailed description of the CFR engine setup.

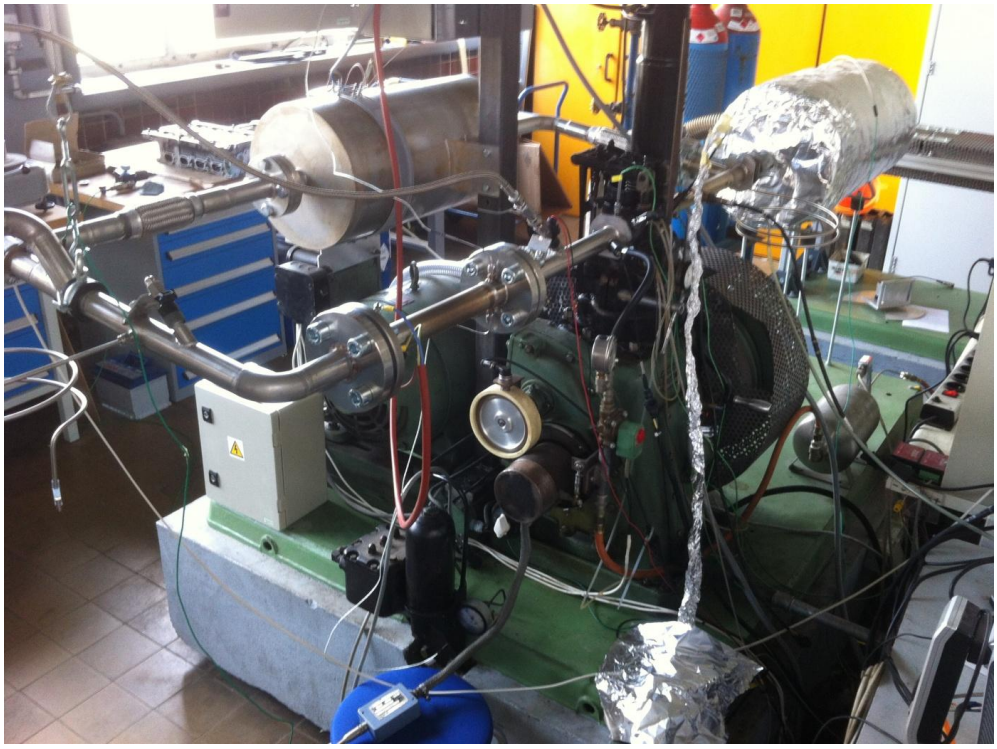

Contents

1. Setup description

1.1.Description and history

The CFR engine is a single cylinder research engine, which was designed to measure the octane number of fuels. It has been revised in 2011 and converted to a flex-fuel engine (both liquid and gaseous fuels). In 2013-2014 the engine setup has been rebuild and extended with an air preheater and EGR loop in order to perform measurements in HCCI operation.

1.2.Engine Properties

A summary of the engine properties is given in Table 1. A cross section of the engine is shown in Figure 1, which shows that there are 4 possible mounting positions for sensors to monitor the combustion process. One of those positions is used by the spark plug (P1).

Table 1: CFR engine properties after the revision of 2011

Bore	83.06 mm
Stroke	114.2 mm
Connecting rod length	254 mm
Swept Volume	618.8 cm^3
IVO	10 °CA ATDC
IVC	29 °CA ABDC
EVO	39 °CA BBDC
EVC	12 °CA ATDC

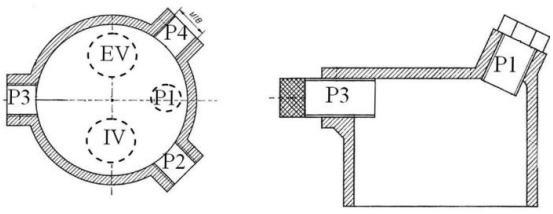

Figure 1: Cross section of the CFR engine,
P1: spark plug position, P2-P4: possible sensor positions, IV: intake valve, EV: exhaust valve

1.3.Part List

The engine set up consists out of the following parts, which are shown in Figure 2 to Figure 5.

1. Air intake with filter
2. Air flow rate sensor
3. Gravimetric measurement system for liquid fuels (separate closets for alcohols and gasoline)
4. Surge tank for intake air flow which buffers the oscillating flow to have a constant air flow at the flow sensor (2), there is also one for the exhaust and gaseous fuel flow (both are not visible).
5. CFR engine (see Figure 4)
   5.1. Cooling water connection

5.2. Electric switch box
5.3. Electric motor which drives CFR engine under motored operation and operates as load under fired operation. It has a constant speed of 1500 rpm.
5.4. Transformer which separates the electrical oil heating circuit from the rest because there is some leakage in that circuit.
5.5. Cooling tower where the coolant condensates because of the cold external cooling flow. The coolant reaches the tower as vapour because it evaporates at the cylinder liner during fired operation. This system enables a constant coolant temperature of around 100°C.
5.6. Cylinder head (see Figure 5)
    5.6.1. Fuel injectors (one for liquid and one for gaseous fuels)
    5.6.2. Indicator for the pressure of the gaseous fuel
    5.6.3. Indicator for the distance between the head of the cylinder and the crankcase (for the determination of the compression ratio)
    5.6.4. Handle to change the compression ratio of the engine (changes the distance between the head and the crankcase)
    5.6.5. Exhaust with λ-sensor
5.7. Toothed wheel connected to the camshaft which delivers a pulsed signal to the ECU. One revolution of the camshaft is equal to one engine cycle or two revolutions of the crankshaft. There is one missing tooth which can be used to reference the TDC in the fired cycle.

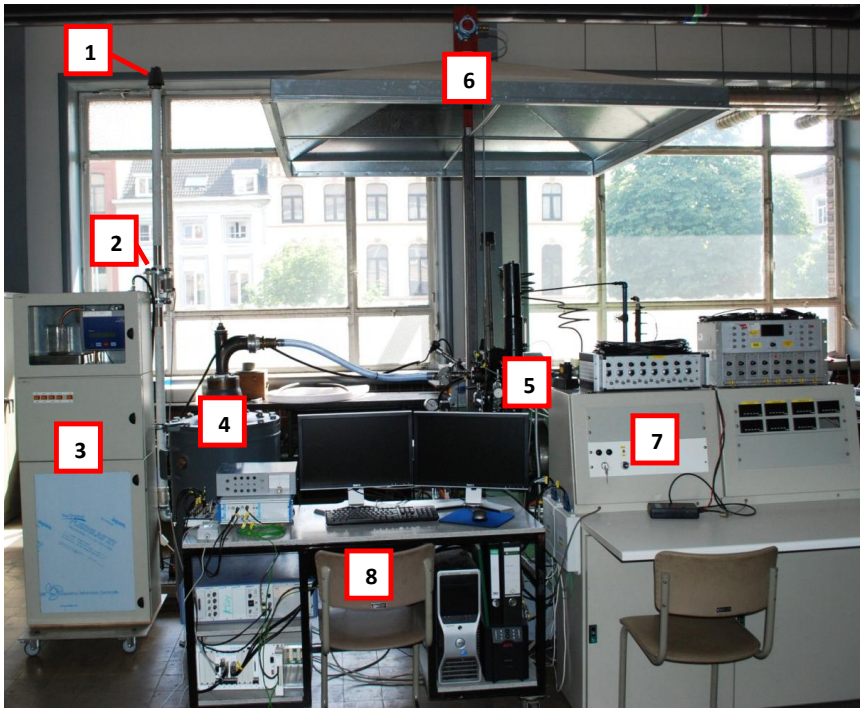

Figure 2: Overview of the CFR set up (1)

5.8. Crankcase
5.9. Switch to operate the oil heating circuit, with 4 options: off, low, medium and high.
5.10. Oil pump and filter
5.11. Encoder connected to the crankshaft which delivers the TRIG (one pulse per revolution) and CAM (360 pulses per revolution) signal for the triggering of the data acquisition. This does not allow a distinction between the fired or unfired cycle in contrast to the pulsed signal which is connected to the ECU.
5.12. Gaseous fuel flow valve which can be shut down by the safety system in the case of operation on hydrogen.

6. Hydrogen detection sensor which is connected to a safety system (see manual safety system)
7. Test bench where the battery and Motec ECU are located.
8. PC and data acquisition system
9. Exhaust surge tank
10. Exhaust pipe to basement (with water slot in basement to increase the back pressure)
11. Valves which control the external cooling water flow. The left pipe goes to the pressure sensors, the right one to the engine cooling tower.
12. Gaseous fuel surge tank
13. Gaseous fuel flow rate sensor
14. Exhaust pipe
15. Protection case for belt which connects the CFR engine and the electrical motor)
16. Air preheater
17. EGR surge vessel
18. Band heater
19. EGR valve
20. Fusebox of band heater, thyristor power supply and PID control
    20.1. Fuse band heater
    20.2. Fuse thyristor power supply
    20.3. Fuse PID control
    20.4. PID set temperature
    20.5. PID measured temperature
    20.6. Potentiometer
    20.7. Band heater thermostat
21. Backpressure valve
22. Emission analyser branch point at the inlet
23. Second injector

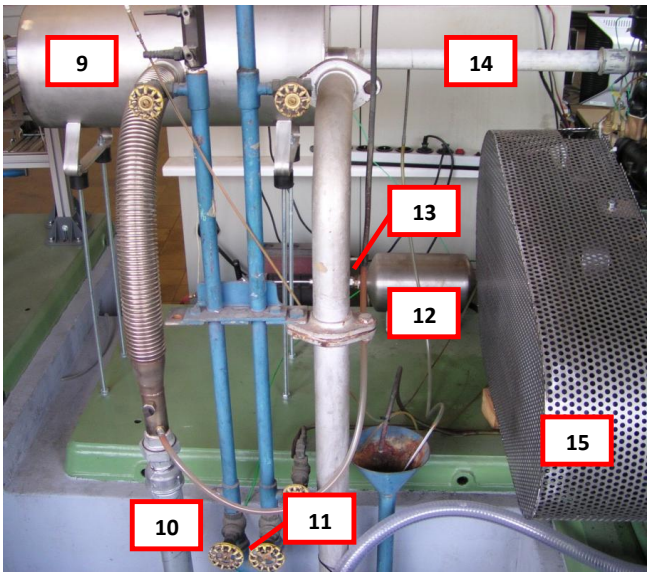

Figure 3: Back side of the CFR test bench

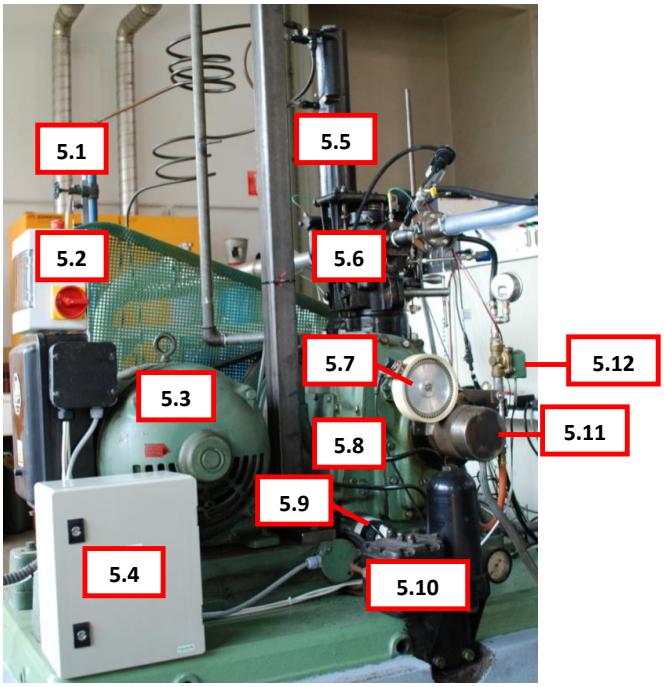

Figure 4: Overview of the CFR engine (5 in Figure 2)

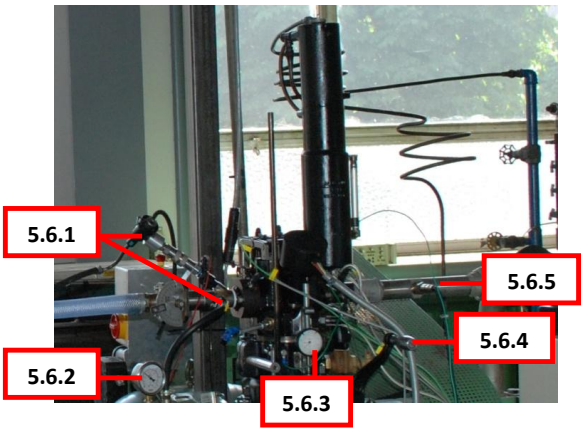

Figure 5: Overview of the cylinder head (5.6 in Figure 4)

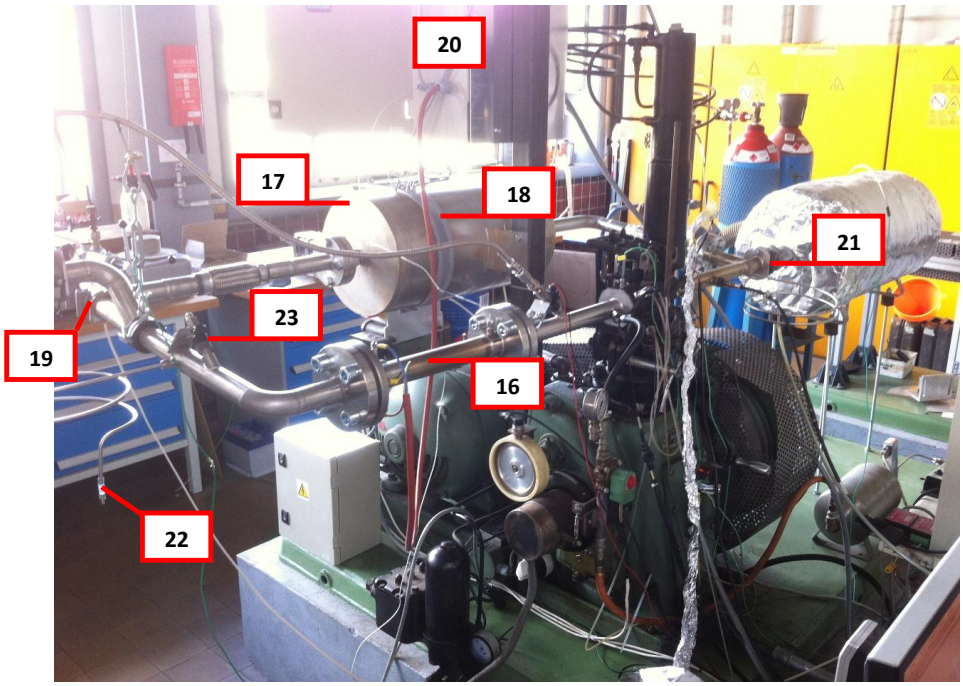

Figure 6: Overview of the new engine setup (2013-2014)

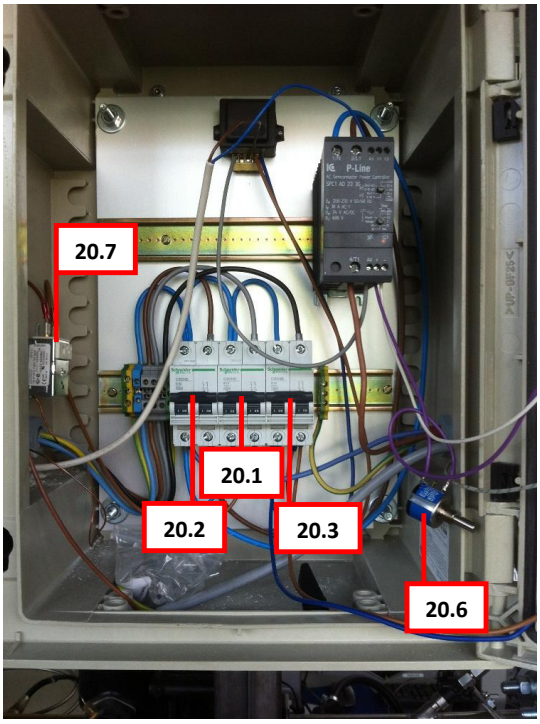

Figure 7: Fuse box

Figure 8: Band heater and air preheater temperature control

2. Measurements

2.1.Measured parameters

The following parameters are measured on the engine with a PXI data acquisition system (see section 3). Details on the used sensors can be found in section 2.

1. temperatures (thermocouples type K)
   1.1. intake
   1.2. exhaust
   1.3. exhaust surge tank
   1.4. coolant
   1.5. oil
   1.6. EGR after EGR valve
2. pressures
   2.1. intake (Kistler type 4075A10)
   2.2. cylinder (Kistler type 701A)
   2.3. exhaust (Kistler type 4075A10)
3. heat flux and cylinder wall temperature (Vatell HFM, Nanmac Eroding ribbon or Oxford TFG)
4. flow rates
   4.1. air (Bronkhorst type F-106BZ)
   4.2. gaseous fuel (Bronkhorst type F-201AC)
   4.3. liquid fuel (own designed gravimetric system)
5. exhaust emissions
   5.1. CO_2, CO and NO_x (Maihak Multor 610)
   5.2. O_2 (Maihak Unor S710)
   5.3. H_2 (Maihak Thermor 615)
   5.4. HC (Signal 3000)
6. atmospheric conditions in lab (ATAL type TRP232)
   6.1. temperature
   6.2. pressure
   6.3. humidity

2.2.Calculations

The following matlab files have to be used to convert the raw measured signals and to calculate additional indicated parameters (work, power, imep) or to plot figures.

1. 'measurements_2014.m', which results in a summary file of each measurement set. It uses the following additional matlab files:
   1.1. 'measurements_calculations_2014.m'
   1.2. 'error_analysis_2014.m'
2. Additional files are 'Heat_release_analysis.m' and 'Heat_flux_corr.m' which are used to perform a heat release analysis and to calculate various heat flux correlations respectively.

3. DAQ system

A PXI-SCXI DAQ system is used to acquire the signals. It consists out of the following cards:

1. PXI-e8160 (connection between PC and PXI)
2. PXI-8432 (2 serial ports)
3. PXI-6143 S-series with BNC connection block (synchronised acquisition triggered by crank encoder)
4. PXI-6224 M-series with two connection blocks (multiplexed acquisition of signals that can be averaged over time)
5. PXI-6259 M-series (multiplexed acquisition of signals of SCXI-1102, synchronised with 3)
6. SCXI-1102 conditioning module for fast thermocouples (high bandwith)

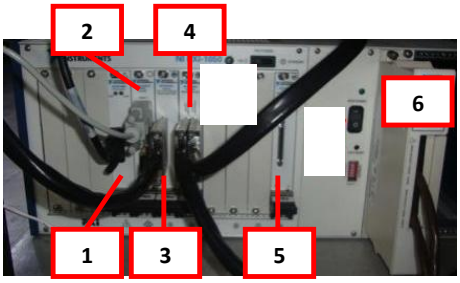

Figure 9: PXI DAQ system

An electrical connection scheme of the signals can be found below.

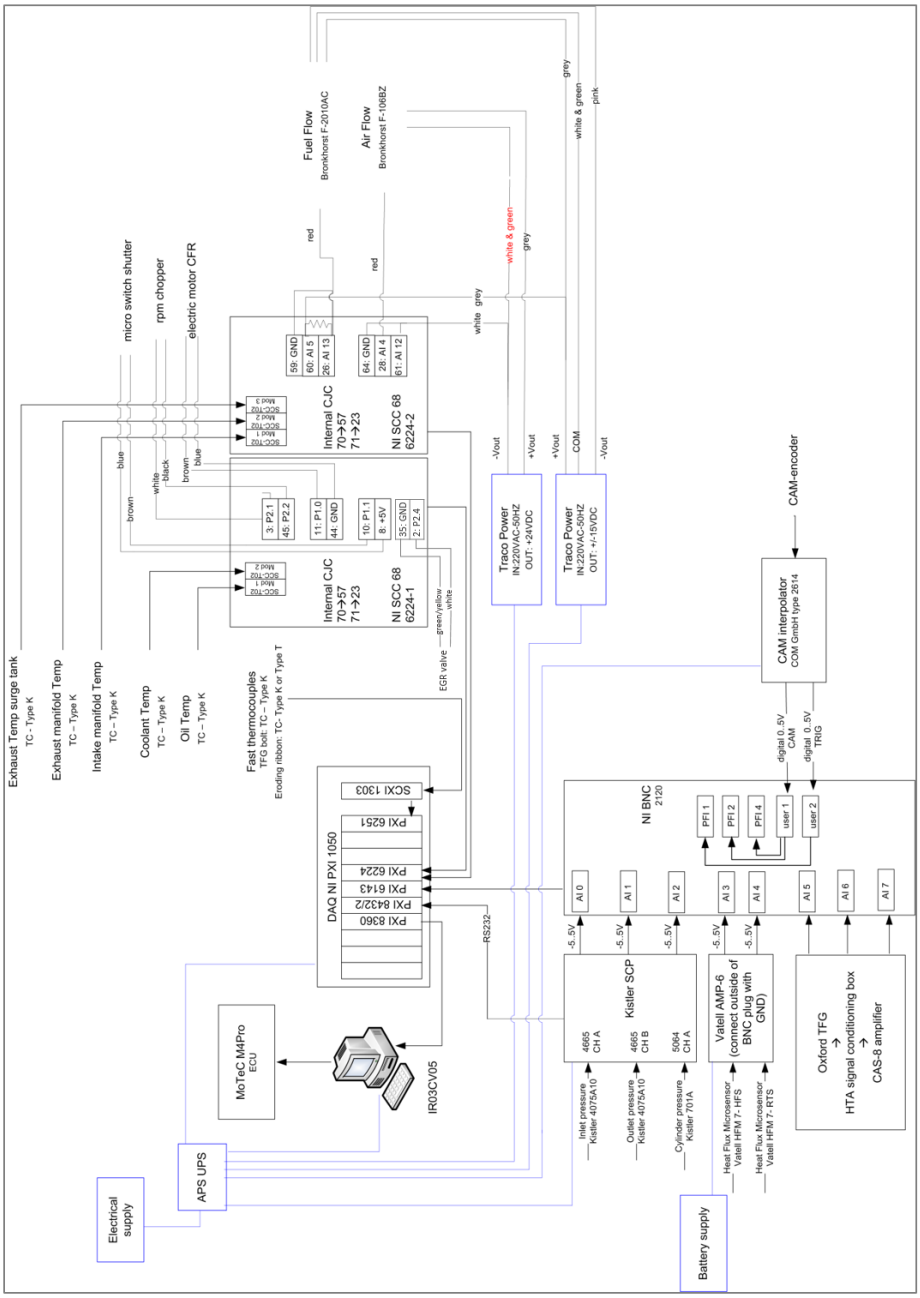

Figure 10: Connection diagram of PXI system

4. Operation Manual

4.1.Start-up procedure

4.1.1. summary of equipment that needs to heat up before the engine can be started

- emission analysers: 2 hours
- Oxford amplifiers: 1 hour
- oil preheating: 1 hour
- Vatell amplifier: 10 min

4.1.2. PC and data acquisition

- Turn on the main switch

Figure 11: Main switch

- Activate the smart-UPS 1500 and wait until it is fully charged. When it is fully charged, the led [1] will stop blinking.

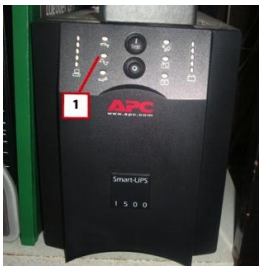

Figure 12: Smart-ups 1500

- Activate the NI PXI-1050 by turning on the SCXI power switch [2] followed by the PXI power switch [3].

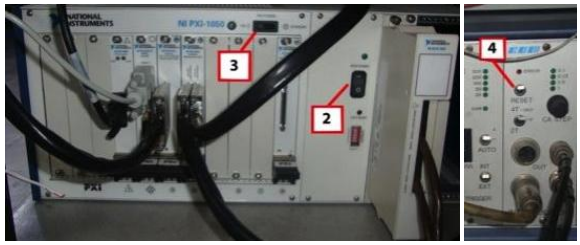

Figure 63: NI PXI 1050 chassis (left) and interpolator for the crank angle encoder (right)

- Turn on the PC
- In order to measure the pressures in the intake, cylinder and exhaust, the communications with the Kistler SCP chassis have to be established. Open the program by double-clicking on 'Kistler SCP' on the desktop. You will get the following error screen:

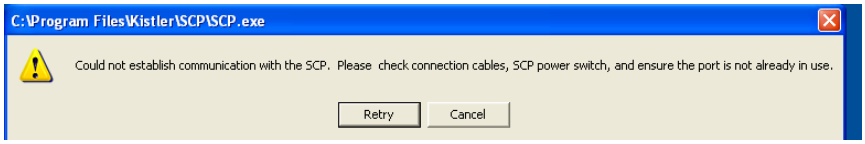

Figure 74: error screen

- Next, click retry, change COM1 to COM3 and click close.

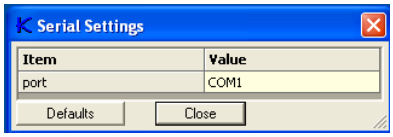

Figure 85: Settings

- Finally, click measure on the following screen and close it

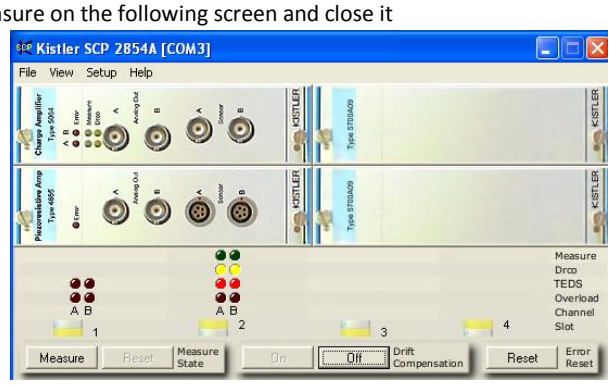

Figure 96: Settings

4.1.3. Vatell HFM-sensor

- For the use of the HFM-sensor, turn on the Vatell Corporation AMP-6 and let it heat up for **10 min**. Then select the desired gain [5]. The RTS- and HFS-signal have to be calibrated at atmospheric conditions, with the zero calibration screws (at the beginning of the Labview program, see below) [6].

Figure 107: Vatell corporation amp-6

4.1.4. Oxford Thin Film Gage sensors

- For the Oxford TFG sensors, turn on the Oxford Heat Transfer Analogous Box (HTA-1) [7] and the Oxford Amplifier [8] and let both heat up **for 1 hour**.

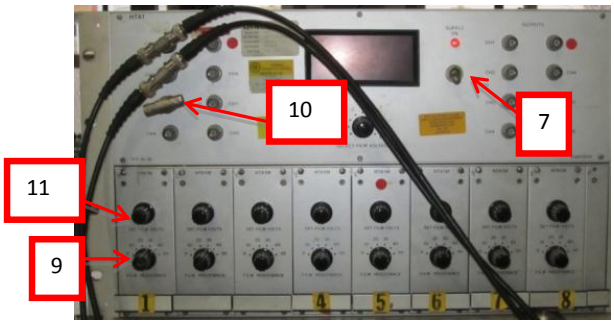

Figure 118: oxford film voltage box

Figure 129: Oxford amplifier

- The following settings of the HTA-1 have to be set: select the Resistance of the sensor at atmospheric conditions [9], closest to the one measured with a multimeter. Next, measure the voltage at the output [10] and turn the knob [11] to set it at 250 mV (sets the constant current which is sent through the sensor).
- Connect the sensor to the amplifier, HTA-1 and data acquisition system. The cable runs from the sensor to the HTA-1 (left input of the plug at [10]), HTA-1 (right output of the plug at [10]) to amplifier input and amplifier output to data acquisition (Figure 10).

Figure 20: BNC Connection box

- Next, the sensor has to be calibrated at atmospheric conditions using the knob [12] on the amplifier (at the beginning of the Labview program, see below).

4.1.5. Engine Auxiliaries

- For the cooling circuit of the CFR-engine and pressure sensors, open the valves [13] (a little bit is sufficient) and wait until water flows through the hoses [14] (the exit of the cooling circuit of the engine flows into the exhaust pipe of the engine to fill the water slot in the basement).

Figure 21: Cooling circuit of the cfr-engine

- When working in fired operation, turn on the exhaust ventilation by pushing on the green button (switch is mounted near the Volvo test bench).

Figure 22: operating buttons of the exhaust ventilation

- Make sure that nothing blocks the flywheel. Turn on the main switch of the synchronous motor [15], the emergency button is located at [16]. Make sure that the brokers [17] are positioned upwards.

Figure 23: controls of the synchronous motor

- Turn on the oil heater (Figure 1324). There are two different settings:
  - Medium: use this setting when performing measurements on fired operation
  - High: use this setting to heat the oil before performing measurements (around **1 hour** in advance), measurements can be started when the oil temperature has reached about 80°C. This temperature can be monitored with the Labview vi 'oil T check.vi'. Also use this setting when performing measurements on motored operation.
  - **Be sure not to overheat the engine oil.** If this happens the engine may not be started until the oil temperature has dropped to 80°C.
  - **Put the switch in the 'off' position when you start the synchronous motor**, in order to limit the amount of electricity that has to be delivered. Otherwise the brokers of the engine can fail.

Figure 134: oil heater switch in the OFF position

4.1.6. Band heater and Air preheater

- Turn on the fuse of the band heater and set the thermostat on 120°C. This is done to prevent the exhaust gases to condensate in the EGR piping.
- When you need the air preheater, turn the potentiometer completely to the right (clockwise). Then turn on the fuses of the thyristor power supply and the PID controller.

DO NOT RAISE TEMPERATURE OF THE AIR PREHEATER WITH THE PID CONTROLLER AS LONG AS THE ENGINE IS NOT RUNNUNG! BEFORE YOU SET A TEMPERATURE, MAKE SURE THE COOLING CIRCUIT IS WORKING AND THAT AIR IS FLOWING TROUGH THE HEATER

When the engine is running, determine the set temperature by tapping the up-arrow. Then turn the potentiometer anti-clockwise to adapt the voltage of the preheater power supply. The potentiometer is used to limit the temperature overshoot. Make sure you don't heat up the mixture above the auto-ignition temperature of your fuel. When using the air preheater for the first time, please ask your supervisor to assist you.

4.1.7. Emission analyzers

The emission analyser must be turned on at **least 2 hours before** the measuring time:

- Turn on switch [1]: the NO/NOx analyser [2] will heat up till 380°C.

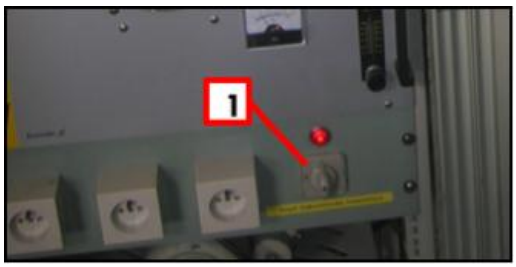

Figure 145: Main switch of the emissions analyzers

- The analyser for NO [3], NO/NOx, CO, CO_2 [4], for H_2 [5] and for O_2 [6] should always be turned on. (otherwise the calibration values will be lost because the devices don't have a backup battery)

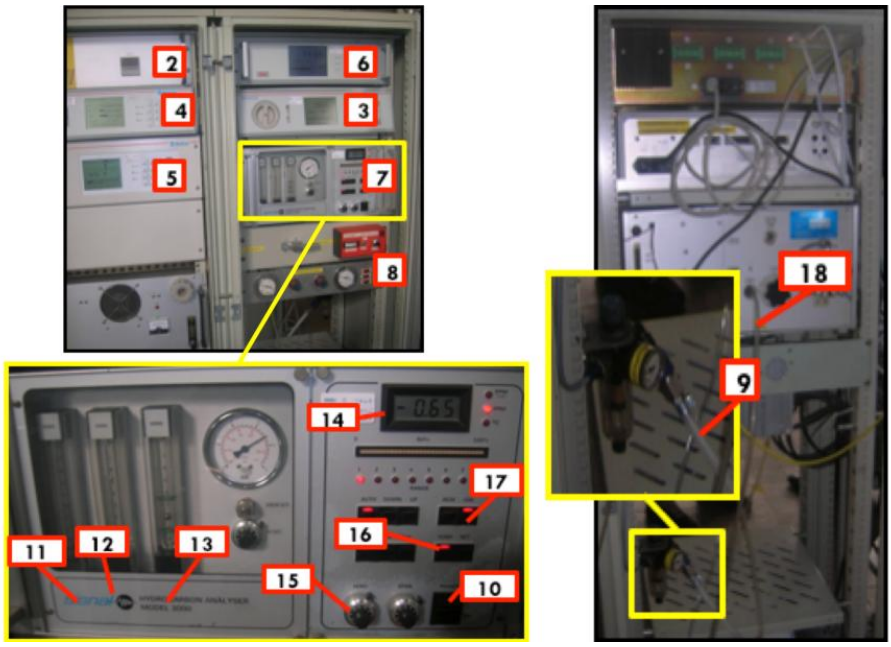

Figure 156: Emission analyzers

- For the HC analyser [7]:
  - You should connect the compressed air [9] and turn open the H_2 which operates as the fuel for the analyser.
  - Turn on the device [10] and the switches for the fuel (H_2) [11], air [12] and sample [13].
  - Reset the value on the screen [14] to 0 by the left knob [15].
  - The device will heat up till 180°C. The temperature can be seen on the screen [14] by pressing the button "TEMP" [16].
  - When the light of "TEMP" turns out, you are able to turn on by pressing "IGN" [17] a first time. As a result the valves inside the device will open and the flow of the three inputs (sample, bypass air and hydrogen fuel) should be within the specified limits (see flow rate sensors on the front of the device)
  - After some seconds you need to press the "IGN" button a second time. If the device starts properly, the HC range reading (below [16]) should go from left to right on the screen. After that it will settle down and the device is ready.
- Connect the **pipe "CFR"** to measure point 1 at the back of the orange box [8].
- Connect the **pipe "CFRHC"** to the pipe "sample" [18] at the back of the HC analyser (not yet present).

4.1.8. Motec software

The injection of fuel and ignition is controlled with a Motec ECU (Engine Control Unit). Before you turn on the synchronous motor, you have to load the proper Motec file.

- Turn on the motec switch
- Open the Motec software
- Click on load file
- Load the proper file and send the data to the Motec. When you want to run in HCCI operation, make sure you select an HCCI file. Otherwise the engine will start to knock heavily because too much fuel is injected with Motec files for SI operation.

4.1.9. LabView software

Engine measurements are performed with LabView software. The .vi file is located in D:\Labview\vis_nieuw. A screenshot of the GUI is shown in Figure 16. Before measurements can be performed, the following steps have to be completed:

- Choose settings
  - Fuel selection: for fired operation choose one of the four fuels, for motored operation choose Air
  - File path: this is the directory where the Excel file generated during the zeroing procedure (see below) will be saved
  - Filename: the name of the Excel file
  - Gains:
    - Pressure sensors: Gain P_in: inlet pressure sensor, Gain P_uit: outlet pressure sensor, Gain P_cyl: cylinder pressure sensor
    - HFM sensor: Gain HFS: HFS gain setting on Vatell amplifier, Gain RTS: RTS gain setting on Vatell amplifier
    - TFG sensor: Gain TFG1 & Gain TFG2: gain setting on Oxford amplifier. **Attention: the gain is minus the inverse value of that given on the amplifier (e.g. amplifier setting: 1/100 ➔ gain value: -100).**
  - CR: compression ratio (use calibration curve and reading from clock)
  - Position: here the position of the sensors in P2 to P4 are filled in
  - # cycles: number of engine cycles to be measured (standard: 100)
  - Resolution: number of samples per degree crank angle set with the interpolator (e.g. a resolution of 2 results in 1440 sample points per engine cycle)
- Zeroing procedure
  - If the zeroing procedure has already been performed on the measurement day, do not push the button 'Include zeroing'. If it has not yet been performed, go to the next step. Enter the number of the measurement you want to perform in 'measurement number @ program start' (**Attention**: do not overwrite existing measurement). If all settings are checked, press 'Check all settings before clicking' to go on to performing measurements.
  - The zeroing procedure enables the users to bring the signals of the HFM sensor and TFG sensor to zero prior to performing measurements. After entering all settings, press 'Include zeroing?' and then 'Check all settings before clicking'. In the graph on the bottom-right the signals of both

sensors are shown, and these can be brought to zero using the dials on both sensors. At the same time, the atmospheric conditions are measured by the ATAL sensors. This generates an Excel file where the atmospheric conditions and some general information on the engine settings are stored. Next, press 'Zeroing control'.

- Start the synchronous motor by pressing 'Start' under 'Electrical engine'.

The following items can be monitored in the GUI:

- At the left, always visible
  - measured parameters
    - temperatures of intake, exhaust (2), oil, cooling water and EGR
    - atmospheric conditions
    - air and fuel flow rate
  - calculated parameters
    - air-to-fuel equivalence ratio
    - indicated work per cycle
    - indicated mean effective pressure
    - coefficient of variation
    - maximum pressure rise rate
    - %EGR
- Toggle screens
  - 'pressure plots', allows to view
    - the inlet, outlet and cylinder pressure
    - the temperatures measured by the HFM and TFG sensors
    - the flux measured by the HFM and TFG sensors
  - 'PV diagrams', allows to view a normal and a logarithmic pressure-volume diagram. A theoretic compression and expansion line can be switched on to check the correct operation of the engine (or settings).

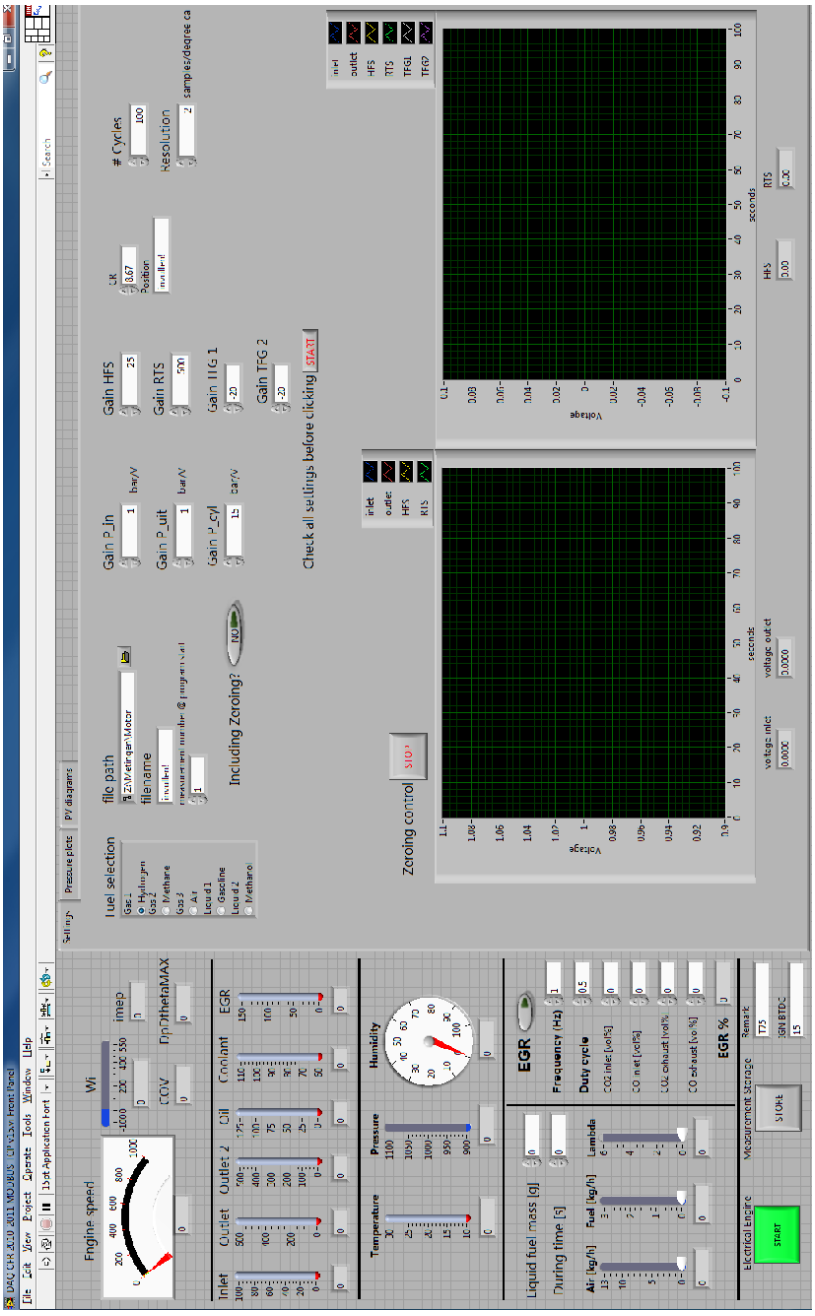

Figure 167: LabView program for engine measurement

4.2.Emergency procedure

In the case something is not working properly, immediately switch off the Motec switch and hit the emergency button. In the case an error occurs in LabView, a screen will pop up. **Switch off the Motec switch before clicking 'OK' or the engine will accelerate! When using the air preheater, first set the temperature to zero and wait until the temperature shown on the PID display drops below 65°C before clicking 'OK'.**

4.3.Measurements procedure

4.3.1. Setting an operating point

- The position of the air throttle can be adjusted by moving the handle [1]

The compression ratio can be adjusted by turning the handle [2]. The value of the compression ration can be determined by the value of clock [3] according to

- Table 2.
- The ignition and amount of injected fuel have to be regulated with the Motec software.

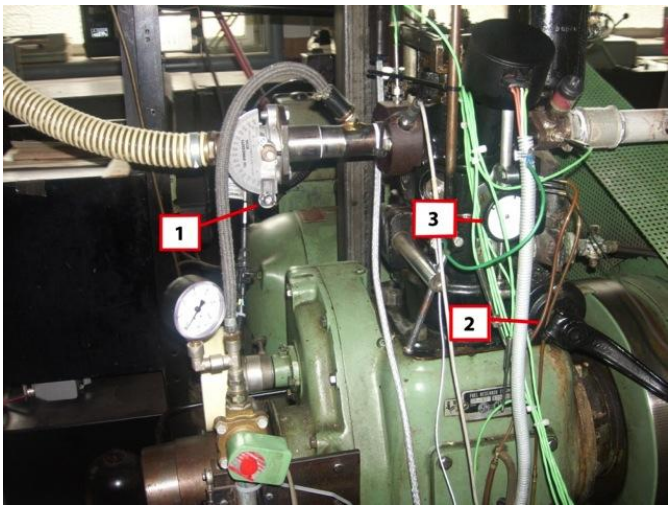

Figure 178: overview of items that can be varied to change the operation point

Table 2: Latest calibration of compression ratio of CFR (31/03/2011)

clock	CR
23.44	6
27.16	7
29.97	8
31.05	8.5
31.97	9
32.79	9.5
33.52	10
34.78	11
35.86	12
36.8	13
37.65	14
38.41	15

4.3.2. Emissions

The emissions can be read from the emission analysers (see Figure 15). Before writing down the values, make sure they have stabilized (this can take several minutes):

- O, CO, CO_2, H_2 can be read immediately from the screens [4], [5], [6]
- NO is displayed on 2 screens ([3] & [4]). On screen [3], the range is limited to 1000ppm. For higher values, the accuracy is not reliable anymore for screen [3]. Due to the measurement limit, this device is almost never useful for the CFR engine.
- Pushing the button on [2], the change can be done between measuring NOx and NO on the gas analyser [4]. Pay attention: when the NOx is activated on [4], the gas analyser [2] will still display NO however you will measure actually NOx (NO + NO_2). Due to the conversion time it is better to just measure NOx and no NO (mostly NOx is the most important for calculations)

4.3.3. Storing signals with the PXI chassis

The following steps need to be followed to store a measurement.

- Make sure the engine is in a stable operation point. The most critical values are the measured wall temperature and oil temperature.
- Make sure the settings in 'Remark' and 'IGN BTDC' are correctly adjusted
- Press 'Store' under 'Measurement storage'
- After the measurement is completed, a dialog window will pop up to determine where the measurements have to be saved. To be able to use the measurements with the Matlab software, save the measurements as a .prn file. Also, a new line in the Excel file is generated with the file name, engine settings and engine parameters given on the left side of the GUI.

4.4.Stopping procedure

- In the case of fired operation, make sure no fuel is being injected anymore by switching off the Motec switch.
- When using the air preheater, set the temperature of the PID control to zero and wait until the temperature of the PID display drops under 65°C.
- Turn on the EGR valve. This causes the EGR pipes to be flushed. The exhaust gases that are heated with the band heater will evaporate condensed water in the pipes. After 5 minutes turn off the EGR valve.
- Stop the synchronous motor by pressing 'Stop' under 'Electrical Engine' in the LabView GUI. This will also save the Excel file.
- Turn off the switch of the synchronous motor ([15] on Figure 23)
- Turn off all the measurement equipment.
- Turn off the fuses of the thyristor power supply, PID control and band heater.
- Turn off the PC
- Deactivate the NI PXI-1050 by turning off the PXI power switch [3] and SCXI power switch [2].

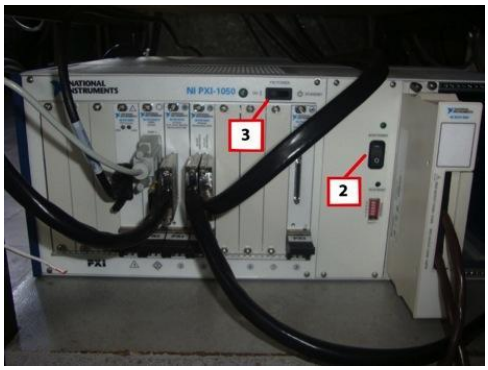

Figure 29 : NI PXI-1050

- Deactivate the smart-UPS 15007
- Turn off the main switch
- When working in fired operation, turn off the ventilation by pushing on the red button in Figure30.

Figure 30: operating buttons of the exhaust ventilation

- Shut down the cooling circuit of the CFR-engine by closing the valves.
- Turn off the oil heater.

Fill in the logbook. It's important to have an overview of what happened on the test setup. In the future this can be handy to trace back any changes or errors that were made.

4.5.Remarks

- Always double check the starting procedure. Failing to switch on certain equipment (e.g. engine cooling) can lead to engine failure.
- Always report if something is not working properly. Not reporting it can lead to even bigger problems.
- When in doubt, ask a technician or your supervisor for help.
- Always be very careful with switching on the air preheater. When in doubt, ask your supervisor for help.

Bibliography

[1] Verhelst, S., T. Wallner, H. Eichlseder, and K. Naganuma et al.: *Electricity powering combustion: Hydrogen engines.* Proceedings of the IEEE 100 (2), pages 427–439, 2012.

[2] Onishi, S., S. Jo, K. Shoda, and P. Jo et al.: *Active thermo-atmosphere combustion (ATAC) - a new combustion process for internal combustion engines.* SAE Technical Paper 790501, 1979.

[3] Soyhan, H. S., H. Yasar, H. Walmsley, B. Head, G. T. Kalghatgi, and C. Sorusbay: *Evaluation of heat transfer correlations for HCCI engine modeling.* Applied Thermal Engineering 23 (2-3), pages 541–549, 2009.

[4] Najt, P.M. and D.E. Foster: *Compression-ignited homogeneous charge combustion.* SAE Technical Paper 830264, 1983.

[5] Oldfield, M.L.G.: *Impulse response processing of transient heat tranfer gauge signals.* Journal of Turbomachinery, 2008.

[6] Broekaert, S. and T. De Cuyper: *Alcoholen als alternatieve brandstof voor vonkontstekingsmotoren: Experimentele studie naar het klopgedrag en de warmteafgifte naar de cilinderwanden.* Master's dissertation, Ghent University, 2012-2013.

[7] Maurya, R. K. and A. K. Agarwa: *Experimental study of combustion and emission characteristics of ethanol fuelled port injected homogeneous charge compression ignition (HCCI) combustion engine.* Applied Energy 88 (4), pages 1169–1180, 2011.

[8] Fuller, H.: *Spark of an idea for future cars*, June 2014. `http://www.zdnet.com/blog/green/spark-of-an-idea-for-future-cars/109`.

[9] Christensen, M. and B. Johansson: *Influence of mixture quality on homogeneous charge compression ignition.* SAE Technical Paper 982454, 1998.

[10] Ceviz, M. A. and İ. Kaymaz: *Temperature and air-fuel ratio dependent specific heat ratio functions for lean burned and unburned mixture.* Energy Conversion and Management 46 (15-16), pages 2387–2404, 2005.

[11] Stockinger, M., H. Schäpertöns, and P. Kuhlmann: *Versuche an einem gemischansugenden verbrennungsmotor mit selbstzündung.* MTZ, Motertechnisches Zeitschrift 53, pages 80–85, 1992.

[12] Christensen, M., A. Hultqvist, and B. Johansson: *Demonstrating the multi fuel capability of a homogeneous charge compression ignition engine with variable compression ratio.* SAE Technical Paper 1999-01-3679, 1999.

[13] Johansson, B.: *Cycle to cycle variations in s.i. engines - the effects of fluid flow and gas composition in the vicinity of the spark plug on early combustion.* SAE Technical Paper 962084, 1996.

[14] Iida, M., M. Hayashi, D.E. Foster, and J.K. Martin: *Characteristics of homogeneous charge compression ignition (HCCI) engine operation for variations in compression ratio, speed, and intake temperature while using n-butane as a fuel.* Journal of Engineering for Gas Turbines and Power 125 (2), page 472, 2003.

[15] Aroonsrisopon, T., V. Sohm, P. Werner, and D. E. Foster et al.: *An investigation into the effect of fuel composition on hcci combustion characteristics.* SAE Technical Paper 2002-01-2830, 2002.

[16] Fathi, M., R. K. Saray, and M.D. Checkel: *The influence of exhaust gas recirculation (EGR) on combustion and emissions of n-heptane/natural gas fueled homogeneous charge compression ignition (HCCI) engines.* Applied Energy 88 (12), pages 4719–4724, 2011.

[17] U.S. Department of Energy: *Homogeneous charge compression ignition (HCCI) technology - A report to the U.S. congress.* 2001.

[18] Johansson, T.: *Turbocharged HCCI engine: Improving efficiency and operating range.* Doctoral dissertation, 2010.

[19] Charalambides, A. G.: *Homogenous charge compression ignition (HCCI) engines, advances in internal combustion engines and fuel technologies.* 2013.

[20] Assanis, D., Z. Filipi, O. Guralp, and J. Chang: *New heat transfer correlation for an HCCI engine derived from measurements of instantaneous surface heat flux.* SAE Technical Paper 2004-01-2996, 2004.

[21] Woschni, G.: *A universally applicable equation for the instantaneous heat transfer coefficient in the internal combustion engine.* SAE Technical paper 670931, 1967.

[22] Hohenberg, G.: *dvanced approaches for heat transfer calculations.* SAE Technical Paper 790825, 1979.

[23] Brettschneider, J.: *Berechung des luftverhaeltnisses λ von luftkraftstoff-gemsichen und des einflusses on messfehlern auf λ.* Bosch Technische Berichte 4, pages 177–186, 1984.

[24] Taylor, C. F.: *The Internal Combustion Engine in Theory and Practice: Combustion, fuels, materials, design.* MIT, 1985.

[25] Truedsson, I.: *Measuring and describing autoignition for HCCI combustion engines.* Doctoral dissertation, 2014.

[26] Komninos, N. P. and G.M. Kosmadakis: *Heat transfer in HCCI multi-zone modeling: Validation of a new wall heat flux correlation under motoring conditions.* Applied Energy 88, pages 1635–1648, 2011.

[27] Heywood, J. B.: *Internal Combustion Engine Fundamentals.* McGraw-Hill, 1988.

[28] Perry, R. H.: *Perry's Chemical Engineer's Handbook, 7th edition.* McGraw-Hill, 1997.

[29] Klein, M. and L. Eriksson: *A comparison of specific heat ratio models for cylinder pressure modeling.* SAE Technical paper 2004-01-1464, 2004.

[30] Gatowski, J., E. Balles, K. Chun, and F. Nelson et al.: *Heat release analysis of engine pressure data.* SAE Technical Paper 841359, 1984.

[31] Brunt, M., H. Rai and A. Emtage: *The calculation of heat release energy from engine cylinder pressure data.* SAE Technical Paper 981052, 1998.

[32] Egnell, R.: *Combustion diagnostics by means of multizone heat release analysis and NO calculation.* SAE Technical Paper 981424, 1998.

[33] Ebrahimi, R.: *Effect of specific heat ratio on heat release analysis in a spark ignition engine.* Scientia Iranica 18 (6), pages 1231–1236, 2011.

[34] Demuynck, J.: *A fuel independent heat transfer correlation for premixed spark ignition engines.* Doctoral dissertation, Ghent University, 2012-2013.

[35] Annand, W.J.D.: *Heat transfer in the cylinders of reciprocating internal combustion engines.* Proceedings of the Institution of Mechanical Engineers 177, pages 973–996, 1963.

[36] Stone, R.: *Introduction to Internal Combustion Engines, 4th edition.* Palgrave Macmillan, 2012.

[37] Dierickx, J. and Y. Huyghebaert: *Alternatieve brandstoffen voor vonkontstekingsmotoren: optimalisatie van waterstofmotoren en opbouw van een methanolmotorproefstand.* Master's dissertation, Ghent University, 2009-2010.